

Cooperative MIMO techniques for outdoor optical wireless communication systems

Mohamed Abaza

▶ **To cite this version:**

Mohamed Abaza. Cooperative MIMO techniques for outdoor optical wireless communication systems. Other. Université de Bretagne occidentale - Brest, 2015. English. NNT : 2015BRES0073 . tel-02013947

HAL Id: tel-02013947
https://theses.hal.science/tel-02013947

Submitted on 11 Feb 2019

HAL is a multi-disciplinary open access archive for the deposit and dissemination of scientific research documents, whether they are published or not. The documents may come from teaching and research institutions in France or abroad, or from public or private research centers.

L'archive ouverte pluridisciplinaire **HAL**, est destinée au dépôt et à la diffusion de documents scientifiques de niveau recherche, publiés ou non, émanant des établissements d'enseignement et de recherche français ou étrangers, des laboratoires publics ou privés.

université de bretagne occidentale

THÈSE / UNIVERSITÉ DE BRETAGNE OCCIDENTALE

sous le sceau de l'Université européenne de Bretagne

pour obtenir le titre de

DOCTEUR DE L'UNIVERSITÉ DE BRETAGNE OCCIDENTALE

Mention : Sciences et Technologies de l'Information et de la Communication - Spécialité Communication Numérique

École Doctorale SICMA

Presented by

Mohamed Abaza

Prepared at Sensor Networks and Cellular Systems (SNCS) Research Center, and ENSTA Bretagne

Cooperative MIMO Techniques For Outdoor Optical Wireless Communication Systems

Thesis defended on 1 December 2015 at ENSTA Bretagne
In front of the following committee:

M. Christian JUTTEN
Professor, University of Grenoble, Institut Universitaire de France / President

M. Karim ABED-MERAIM
Professor, Polytech Orléans / Rapporteur

M. Denis HAMAD
Professor, University of Littoral Côte d'Opale / Rapporteur

M. Gilles BUREL
Professor, Lab-STICC, Université de Bretagne Occidentale / Examiner

M. Moustafa HUSSEIN
Professor, Arab Academy for Science, Technology and Maritime Transport, Egypt / Examiner

M. Ali MANSOUR
Professor, ENSTA Bretagne / Director of the thesis

M. Raed MESLEH
Associate Professor, University of Tabuk, Saudi Arabia / Supervisor of the thesis

Résumé

Au cours de la dernière décennie, les communications optiques en espace libre (FSO) ont pris de l'ampleur dans les deux domaines académiques et industriels. L'importance de FSO s'appuie sur la possibilité de faire un système de transmission économique et écologique avec un débit élevé et sans licence à l'opposition des systèmes de transmission radiofréquences (RF).
Dans la plupart des travaux antécédents sur les systèmes multi-émetteurs, seulement les canaux décorrélés ont été considérés. Un canal décorrélé nécessite un espace suffisant entre les émetteurs. Cette condition devient difficile et non-réalisable dans certaines applications. Pour cette raison, nos études se focalisent sur les performances des codes à répétition RC (Repitition Codes) et les codes OSTBC (Orthogonal Space-Time Block Codes) dans des canaux log-normaux corrélés en utilisant une modulation d'intensité et une détection directe (IM/DD). En addition, les effets des différentes conditions météorologiques sur le taux d'erreur moyen (ABER) sont étudiés.
Les systèmes FSO à multi-entrées/ multi-sorties MIMO (Multiple-Input Multiple-Output) avec une modulation SSK (Space Shift Keying) ont été abordés. Les résultats obtenus montrent que la SSK est supérieure aux RC avec une modulation d'impulsion (Multiple Pulse Amplitude Modulation) pour toute efficacité spectrale égale ou supérieure à 4 bit/s/Hz.
Nous avons aussi analysé les performances d'un système à sauts multiples (Multi-Hop) et des relais à transmission directe (forward relays). Nos simulations montrent que le système ainsi considéré est efficace pour atténuer les effets météorologiques et les pertes géométriques dans les systèmes de communication FSO. Nous avons montré qu'un tel système avec plusieurs entrées et une sortie (MISO, i.e. multiple-input single-output) à sauts multiples est supérieur à un système MISO avec un lien direct (direct link) avec une forte atténuation.
Pour satisfaire la demande croissante des réseaux de communication à débits élevés, la communauté scientifique s'intéresse de plus en plus aux systèmes FSO avec des relais full-duplex (FD). Pour ces derniers systèmes, nous avons étudié la probabilité d'erreur moyenne (ABER) et nous avons analysé leurs performances. En considérant des différentes conditions de transmission, les performances de relais FD ont été comparées à celles d'un système avec un lien direct ou des relais half-duplex. Les résultats obtenus montrent que les relais FD ont le minimum ABER. En conséquence, les résultats obtenus dans cette thèse sont très prometteurs pour la prochaine génération de FSO.

Abstract

Free-space optical (FSO) communication has been the subject of ongoing research activities and commercial attention in the past few years. Such attention is driven by the promise of high data rate, license-free operation, and cheap and ecological friendly means of communications alternative to congested radio frequency communications.
In most previous work considering multiple transmitters, uncorrelated channel conditions have been considered. An uncorrelated channel requires sufficient spacing between transmitters. However, this can be difficult and may not be always feasible in some applications. Thereby, this thesis studies repetition codes (RCs) and orthogonal space-time block codes performance in correlated log-normal FSO channels using intensity modulation and direct detection (IM/DD). Furthermore, the effect of different weather conditions on the average bit error rate (ABER) performance of the FSO links is studied.
Multiple-input multiple-output (MIMO) FSO communication systems using space shift keying (SSK) modulation have been also analyzed. Obtained results show that SSK is a potential technique for spectral efficiencies equal or greater than 4 bits/s/Hz as compared to RCs with multiple pulse amplitude modulations.
The performance analysis of a multi-hop decode and forward relays for FSO communication system using IM/DD is also considered in this thesis. It is shown that multi-hop is an efficient technique to mitigate atmospheric turbulence and different weather attenuation effects and geometric losses in FSO communication systems. Our simulation results show that multiple-input single-output (MISO) multi-hop FSO systems are superior to direct link and MISO systems over links exhibiting high attenuation.
Meeting the growing demand for higher data rates communication networks, a system with full-duplex (FD) relays is considered. For such a system, the outage probability and the ABER performance are analyzed under different turbulence conditions, misalignment error and path loss effects. FD relays are compared with the direct link and half-duplex relays. Obtained results show that FD relays have the lowest ABER and the outage probability as compared to the two other systems. Finally, the obtained results in this thesis are very promising towards the next generation of FSO systems.

Acknowledgement

I am very grateful to ALLAH *Subhanahu Wa Ta'ala* for all His blessing. I would also like to thank my parents, wife and son for what they have contributed towards my education. Their unconditional love, constant support, great advice and prayers over the past years are something that I cannot thank them for enough. Additionally, knowing that my success in completing my Ph.D. would be a source of happiness for them, I was further motivated to work hard. I am deeply indebted to my director of my thesis Prof. Ali MANSOUR for his valuable comments, discussions, encouragement and timely guidance along supervising my doctoral thesis. I thank him for always being available and helpful. I must also thank my supervisor Dr. Raed MESLEH for the time he took to evaluate my contributions, the problems he noticed, and the discussions we had, which helped me progress in my work and results.

I want to thank Prof. Christian JUTTEN from the University of Grenoble for being the president of my Ph.D. committee. I also would like to thank Prof. Karim ABED-MERAIM from the University of Polytech Orléans and Prof. Denis HAMAD from the University of Littoral Côte d'Opale for honoring me by accepting to be rapporteurs of my dissertation. I also want to thank Prof. Gilles BUREL from Université de Bretagne Occidentale and Prof. Moustafa HUSSEIN from Arab Academy for Science, Technology and Maritime Transport (AASTMT), Egypt for accepting to be examiners of my dissertation.

This work has been carried out at Sensor Networks and Cellular Systems (SNCS) Research Center, University of Tabuk. The financial support provided by SNCS is gratefully acknowledged. I would also like to thank Prof. el-Hadi M. AGGOUNE. The director of SNCS for all his support during my Ph.D. thesis. Moreover, I would like to express my hearty thanks to my friends especially Eng. Mohamed ABBAS and Eng. Mohamed El KHOREBY. They always encouraged me in this challenge.

Finally, I would like to thanks my colleagues that we have fruitful discussion during the preparation of my thesis : Prof. Murat UYSAL from the Özyeğin University, Turkey, Prof. Ayman ALFALOU from ISEN Brest, France, Dr. Chi Fai LO from the Chinese University of Hong Kong, Hong Kong, Dr. Kostas PEPPAS from the University of Peloponnese, Greece, Dr. Chadi ABOU-RJEILY from the Lebanese American University, Lebanon, Dr. Majid SAFARI from the University of Edinburgh, UK, Dr. Ismail BEN MABROUK from the University of Tabuk, Saudi Arabia, Dr. Hassan MORADI from the University of Oklahoma, USA, Eng. Ismail EL-BADAWY from AASTMT, Egypt, Eng. Yasser FOUAD from Carleton University, Canada and Eng. Mohammadreza AMINI from the Özyeğin University, Turkey.

Table of Contents

List of Figures 1

List of Tables 5

Abbreviations 7

Symbols 11

Mathematical Notation 15

1 Introduction 17
- 1.1 Background . . . 17
- 1.2 Thesis Contributions . . . 18
- 1.3 Thesis Organization . . . 20

2 State of the Art 23
- 2.1 Introduction . . . 23
- 2.2 Key Technologies . . . 23
  - 2.2.1 Indoor wireless optical communications . . . 24
  - 2.2.2 Underwater wireless optical communications . . . 25
  - 2.2.3 Space wireless optical communications . . . 25
  - 2.2.4 Free-space optical communications . . . 26
- 2.3 Motivation . . . 26
- 2.4 Major Challenges . . . 27
  - 2.4.1 Geometric loss . . . 27
  - 2.4.2 Misalignment loss . . . 27
  - 2.4.3 Weather attenuation loss . . . 27
  - 2.4.4 Background noise . . . 28
  - 2.4.5 Atmospheric turbulence . . . 28
- 2.5 Atmospheric Turbulence Channels . . . 28
  - 2.5.1 Experimental results . . . 28
  - 2.5.2 Simulation results . . . 29
  - 2.5.3 Proposed analytical models . . . 29
- 2.6 Suggested Solutions . . . 30
  - 2.6.1 Modulation techniques . . . 30
    - 2.6.1.1 Coherent and non-coherent detection . . . 30
    - 2.6.1.2 Energy and spectral efficiencies . . . 30
    - 2.6.1.3 Modulations suitable for IM/DD systems . . . 30
    - 2.6.1.4 Subcarrier intensity modulation . . . 31
    - 2.6.1.5 Polarization modulation . . . 31
    - 2.6.1.6 Coherent modulation . . . 32
  - 2.6.2 Forward error correction techniques . . . 32
    - 2.6.2.1 Reed-Solomon (RS) codes . . . 32

2.6.2.2 Concatenated Reed-Solomon codes . . . 33
2.6.2.3 Turbo codes and low-density parity-check codes . . . 33
2.6.2.4 FEC drawbacks for FSO . . . 33
2.6.3 Aperture averaging . . . 33
2.6.4 Spatial diversity . . . 33
2.6.4.1 Single-input multiple-output . . . 34
2.6.4.2 Multiple-input single-output . . . 34
2.6.4.3 Multiple-input multiple-output . . . 34
2.6.4.4 Correlation effects . . . 35
2.6.5 Multi-hop relay systems . . . 35
2.6.5.1 Conventional multi-hop relay systems . . . 35
2.6.5.2 All-optical multi-hop relay systems . . . 36
2.6.5.3 Coherent multi-hop relay systems . . . 36
2.6.5.4 Subcarrier intensity modulation multi-hop relay systems 37
2.6.5.5 Optimum placement for multi-hop relay systems . . . 37
2.6.5.6 Photon counting receiver for multi-hop relay systems . . 37
2.6.5.7 Beam size variation at the receiver for multi-hop relay systems . . . 37
2.6.5.8 Hybrid spatial diversity and multi-hop relay systems . . 37
2.6.5.9 Hybrid FSO and RF links for multi-hop relay systems . 38
2.6.6 Cooperative relay systems . . . 38
2.6.6.1 Transmission relays . . . 38
2.6.6.2 Types of DF cooperative relay systems . . . 38
2.6.6.3 Conventional cooperative relay systems . . . 39
2.6.6.4 All-optical cooperative relay systems . . . 39
2.6.6.5 Subcarrier intensity modulation cooperative relay systems 40
2.6.6.6 Selected relay for cooperative relay systems . . . 40
2.6.6.7 Power allocation for cooperative relay systems . . . 40
2.6.6.8 Multiple-source cooperation relaying . . . 41
2.6.6.9 Optimum placement for cooperative relay systems . . . 41
2.6.6.10 Multi-hop parallel relaying . . . 41
2.6.6.11 Mean time between failures for cooperative relay systems 41
2.6.6.12 Inter-relay cooperation of cooperative relay systems . . 41
2.6.6.13 Two-way relay systems . . . 42
2.7 Practical Results . . . 42
2.8 Summary . . . 42

3 Diversity Techniques for Correlated Log-normal Channels 45
3.1 Introduction . . . 45
3.2 System Model . . . 45
3.3 Performance Analysis . . . 47
3.3.1 Orthogonal Space-Time Block Codes . . . 47
3.3.2 Repetition Codes . . . 50
3.4 Numerical Results and Discussions . . . 51

3.5 Summary . . . 53

4 Performance Analysis of Space Shift Keying Over Turbulent Channels 61
4.1 Introduction . . . 61
4.2 System Model . . . 61
4.3 Performance Analysis . . . 63
4.4 Average BER Probability of SSK Over Turbulent Channels . . . 64
4.4.1 Negative exponential channels . . . 64
4.4.2 LN channels (moderate turbulence) . . . 66
4.4.3 LN channels (weak turbulence) . . . 67
4.5 Numerical Results and Discussions . . . 67
4.6 Summary . . . 70

5 Performance Analysis of MISO Multi-hop Over Log-normal Channels 73
5.1 Introduction . . . 73
5.2 System Description . . . 73
5.2.1 Single-Input Single-Output . . . 73
5.2.2 MISO Using Repetition Codes . . . 76
5.2.3 Multi-Hop DF Relaying . . . 77
5.2.4 MISO Multi-Hop DF Relaying . . . 79
5.3 Numerical Results and Discussions . . . 80
5.4 Summary . . . 84

6 Relay Selection For Full-Duplex FSO Relays Over Turbulent Channels 87
6.1 Introduction . . . 87
6.2 System And Channel Models . . . 87
6.2.1 System Model . . . 87
6.2.2 LN Channels . . . 89
6.2.3 G-G Channels . . . 90
6.3 Outage Performance Analysis . . . 90
6.3.1 LN Channels . . . 90
6.3.2 G-G Channels . . . 91
6.4 Performance Analysis . . . 92
6.5 Numerical Results and Discussions . . . 93
6.6 Summary . . . 96

7 Conclusions and Future Work 99
7.1 Conclusions . . . 99
7.2 Recommendations for Future Work . . . 101

Appendix A 103
A.1 List of Publications . . . 103

Appendix B **105**
B.1 Approximation of Equation (3.27) 105
B.2 Matlab Code of Equation (3.27) 106
B.2.1 Introduction 106
B.2.2 The Matlab code 108
B.3 Proof of Equation (5.7) 109
B.4 Proof of Equation (5.15) 110

Appendix C **111**
C.1 The error function 111
C.2 The complementary error function 111
C.3 Meijer's G-function 111

References **113**

List of Figures

1.1 Summary of thesis contributions. 19
1.2 The main axes of the research. 20

2.1 The main axes of the research. 23
2.2 Sale navigation using VLC technology in Korea. 24
2.3 Underwater robots using LED-based communications. 25
2.4 Wireless optical communication between satellites. 26
2.5 Free-space optical communication network. 27

3.1 The main axes of the research. 46
3.2 Synoptic diagram of the proposed model. 47
3.3 Correlation coefficient versus distance among transmit units for difference propagation distances. 53
3.4 Error due to the proposed approximation. 54
3.5 Correlated LN with $\sigma_x = 0.1$, $\mu_x = -\sigma_x^2$, $N_t = 2$ and $\alpha = 0$ dB. 54
3.6 Correlated LN with $\sigma_x = 0.1$, $\mu_x = -\sigma_x^2$, $N_t = 2$ and light fog. 55
3.7 Correlated LN with $\sigma_x = 0.1$, $\mu_x = -\sigma_x^2$, $N_t = 3$ and $\alpha = 0$ dB. 55
3.8 Correlated LN with $\sigma_x = 0.1$, $\mu_x = -\sigma_x^2$, $N_t = 3$ and light fog. 56
3.9 Correlated LN with $\sigma_x = 0.374$, $\mu_x = -\sigma_x^2$, $N_t = 2$, and $\alpha = 0$ dB. . . . 56
3.10 Correlated LN with $\sigma_x = 0.3$, $\mu_x = -\sigma_x^2$, $N_t = 2$, and clear air. 57
3.11 Correlated LN with $\sigma_x = 0.374$, $\mu_x = -\sigma_x^2$, $N_t = 3$ and $\alpha = 0$ dB. 57
3.12 Correlated LN with $\sigma_x = 0.3$, $\mu_x = -\sigma_x^2$, $N_t = 3$ and clear air. 58
3.13 Correlated LN using repetition codes with $\sigma_x = 0.1$, $\mu_x = -\sigma_x^2$, $\rho = 0.25$, $N_t = 3$ for different weather conditions. 58
3.14 RCs over correlated LN with $\sigma_x = 0.3$, $\mu_x = -\sigma_x^2$, $N_t = 2$, and clear air for different correlation coefficients. 59

4.1 The main axes of the research. 62
4.2 Synoptic diagram of the proposed model. 63
4.3 Histogram of the absolute difference of the two NE RVs. 65
4.4 Histogram of the absolute difference of two LN RVs ($\sigma_x = 0.37$ and $\mu_x = -\sigma_x^2$). 67
4.5 Histogram of the absolute difference of two LN RVs ($\sigma_x = 0.1$ and $\mu_x = -\sigma_x^2$). 68
4.6 Comparison of space shift keying and repetition codes with spectral efficiency = 3 bits/s/Hz in a NE channel (strong turbulence) with $N_t = 8$ and the number of receivers $N_r \epsilon$ [8 10]. 69
4.7 Comparison of space shift keying and repetition codes with spectral efficiency = 4 bits/s/Hz in a NE channel (strong turbulence), $N_t = N_r = 16$. 70
4.8 Comparison of space shift keying and repetition codes with spectral efficiency = 4 bits/s/Hz in a LN channel with $\sigma_x = 0.37$ (moderate turbulence), $N_t = N_r = 16$. 71

4.9 Comparison of space shift keying and repetition codes with spectral efficiency = 4 bits/s/Hz in a LN channel with $\sigma_x = 0.1$ (weak turbulence), $N_t = N_r = 16$. 72
4.10 A comparison between upper bound SSK using Q-function and using the approximation of Q-function on space shift keying. 72

5.1 The main axes of the research. 74
5.2 FSO SISO system using OOK modulation. 74
5.3 MISO scheme using RCs. 77
5.4 Multi-hop DF relay scheme. 77
5.5 MISO Multi-hop DF relay scheme. 79
5.6 ABER of single-relay multi-hop using one or two transmitters with 4-PAM modulation, two transmitters MISO using RCs and OOK, and SISO using OOK modulation FSO systems in LN fading channel and clear air conditions ($C_n^2 = 5 \times 10^{-14}$ m$^{-2/3}, \alpha = 0.43$ dB/km). From Equation (3.8), ρ in Equations (3.29) and (5.20) can be approximated as zero when $d \gg d_o$. 81
5.7 ABER of single-relay multi-hop using one or two transmitters with 4-PAM modulation, two transmitters MISO using RCs and OOK, and SISO using OOK modulation FSO systems in LN fading channel and light fog ($C_n^2 = 1.7 \times 10^{-14}$ m$^{-2/3}, \alpha = 20$ dB/km). 82
5.8 ABER of two-relays multi-hop using one or three transmitters with 8-PAM modulation, three transmitters MISO using RCs and OOK, and SISO using OOK modulation FSO systems in LN fading channel and clear air ($C_n^2 = 5 \times 10^{-14}$ m$^{-2/3}, \alpha = 0.43$ dB/km). 83
5.9 ABER of two-relays multi-hop using one or three transmitters with 8-PAM modulation, three transmitters MISO using RCs and OOK, and SISO using OOK modulation FSO systems in LN fading channel and light fog ($C_n^2 = 1.7 \times 10^{-14}$ m$^{-2/3}, \alpha = 20$ dB/km). 84

6.1 The main axes of the research. 88
6.2 Block diagram of the proposed FD FSO communication system. 88
6.3 OP for FSO over weak fading channel and clear air conditions ($C_n^2 = 0.5 \times 10^{-14}$ m$^{-2/3}, \alpha = 0.43$ dB/km). 95
6.4 OP for FSO over moderate fading channel and clear air conditions ($C_n^2 = 2 \times 10^{-14}$ m$^{-2/3}, \alpha = 0.43$ dB/km). 95
6.5 OP for FSO over strong fading channel and clear air conditions ($C_n^2 = 5 \times 10^{-14}$ m$^{-2/3}, \alpha = 0.43$ dB/km). 96
6.6 ABER of FSO over weak fading channel and clear air conditions ($C_n^2 = 0.5 \times 10^{-14}$ m$^{-2/3}, \alpha = 0.43$ dB/km). 96
6.7 ABER of FSO over moderate fading channel and clear air conditions ($C_n^2 = 2 \times 10^{-14}$ m$^{-2/3}, \alpha = 0.43$ dB/km). 97

7.1 The main axes of the research. 99

B.2 Impact of the correlation coefficient on the proposed approximation. . . 107
B.3 Impact of Monte Carlo simulations realizations on the proposed approximation for $\rho = 0.5$ and $\sigma_x = 0.1$. 107

List of Tables

2.1 Weather attenuation coefficient of FSO 28

3.1 Comparison among our MISO scheme & the closed literature works . . . 46

4.1 Comparison between our SSK scheme & the closed literature works . . . 62

5.1 Comparison between our MISO multi-hop scheme & the closed literature works 74
5.2 System configuration 81
5.3 Summary of SNR gains of Figures 5.6-5.7 85
5.4 Summary of SNR gains of Figures 5.8-5.9 85

6.1 Comparison between our FD best relay selection & the closed literature works 89
6.2 System configuration 94
6.3 Atmospheric conditions 94

Abbreviations

ABDF	Adaptive bit detect-and-forward
ABER	Average bit error rate
ADF	Adaptive decode-and-forward
AF	Amplify-and-forward
APD	Avalanche photodiode
ARDO	Asymptotical relative diversity order
AWGN	Additive white Gaussian noise
BDF	Bit detect-and-forward
BEP	Bit error probability
BER	Bit error rate
BPSK	Binary phase shift keying
c.i.d.	Correlated and identically distributed
CDF	Cumulative distribution function
CF	Count-and-forward
CRs	Cooperative relays
CSI	Channel state information
DF	Decode-and-forward
Double GG	Double Generalized Gamma
DPIM	Digital pulse interval modulation
DPPM	Differential pulse position modulation
DPSK	Differential phase-shift keying
DWDM	Dense wavelength division multiplexing
EDFA	Erbium doped fiber amplifier
EGC	Equal gain combining
EW	Exponentiated Weibull
FD	Full-duplex
FEC	Forward error correction
FOV	Field of view
FSO	Free-space optical
G-G	Gamma-Gamma
HD	Half-duplex
i.i.d.	Independent and identically distributed
IADF	Improved adaptive decode-and-forward
IM/DD	Intensity modulation and direct detection
ITU-T	International telecommunication union - telecommunications
LDPC	Low-density parity-check
LEDs	Light-emitting diodes
LEO	Low Earth orbit

LN	Log-normal
LO	Local oscillator
LOS	Line-of-sight
LTE	long-term evolution
MGF	Moment generating function
MIMO	Multiple-input multiple-output
MISO	Multiple-input single-output
ML	Maximum-likelihood
MPPM	Multiple pulse position modulation
MPSK	M-ary phase shift keying
MRC	Maximal ratio combining
MTBF	Mean time between failures
OHL	Optical hard-limiter
OLEDs	Organic light emitting diodes
OOK	On-off keying
OP	Outage probability
OSTBCs	Orthogonal space-time block codes
PAM	Pulse amplitude modulation
PCR	Photon counting receiver
PDF	Probability density function
PIN	Positive-intrinsic-negative
PM	Polarization modulation
PPM	Pulse position modulation
PPMPWM	Pulse-position-pulse-width modulation
PWM	Pulse width modulation
rad	Radian
RCs	Repetition codes
R-D	Relay to destination
RF	Radio frequency
RS	Reed-Solomon
RVs	Random variables
SC	Selection combining
SER	Symbol error rate
SI	Scintillation index
SIM	Subcarrier intensity modulation
SIMO	Single-input multiple-output
SISO	Single-input single-output
SM	Spatial modulation
SMux	Spatial multiplexing

SNR	Signal-to-noise ratio
SPPAM	Spatial pulse position amplitude modulation
S-R	Source to relay
SSK	Space shift keying
TLS	Transmit laser selection
TWRs	Two-way relays
VLC	Visible light communications

Symbols

$c_{ij}^{'}$	$(i,j)^{\text{th}}$ coefficient of the square root spatial covariance matrix
$\bar{N}$	Average number of constellation points away from any point
$\hat{\boldsymbol{s}}$	Vector specifies the activated antenna
$\mathbf{H}$	Channel irradiance matrix
$\mathbf{n}$	Received AWGN vector
$\mathbf{r}$	Received signal vector
$\mathbf{S}$	Codeword matrix
$\mathbf{s}$	Transmitted signal vector
$\boldsymbol{I}$	Received light intensity vector
$\grave{w}_i$	Weights of the generalized Laguerre polynomial
$\grave{z}_i$	Roots of the generalized Laguerre polynomial
$\hat{g}$	Estimated active transmitter
$\hat{h}_{ji}$	Channel irradiance between the receiver j and the estimated active transmitter i
$\mathbf{G}$	Full rate real orthogonal matrices
$\mathbf{S}$	Linear transformation of $\mathbf{G}$ matrix to on-off keying matrix
$\mathbf{U}$	Matrix of ones with the same size as $\mathbf{G}$
$\mathrm{d_H}(b_g, b_i)$	Number of bit errors between received symbol and transmitted symbol
$\mathrm{K}_v(.)$	vth order modified Bessel function of the second kind
Pr(a)	Probability of an event a
$\overline{I}$	Average light intensity without turbulence effect
w_{zeq}	Equivalent beam width (in m)
a	Effective number of atmospheric turbulence large scale eddies
b	Effective number of atmospheric turbulence small scale eddies
b_g	Transmitted symbol
b_i	Received symbol
c	Constant
C_n^2	Refractive index constant ($\mathrm{m}^{-2/3}$)
d	Separation distance between each two successive transmitters
$d_{\min}$	Minimum Euclidean distance between two points in the signal constellation
d_o	Correlation length
D_R	Receiver aperture diameter (in m)
D_T	Transmitter aperture diameter (in m)
e	Constant
E_b	Average electrical energy of the transmitted pulse at each transmitter
$F(.)$	Cumulative distribution function
$f(.)$	Probability density function
g	Spatial location of the active transmitter
h	Channel irradiance from transmitter to the receiver

$h_{\mathrm{R}_i\mathrm{D}}$	Channel fading coefficients between ith relay and the destination
h_{SR_i}	Channel fading coefficients between the source and ith relay
h_{jg}	Channel irradiance between transmitter g and receiver j
h_a	Channel fading coefficients due to atmospheric turbulence
h_i	Channel irradiance from transmitter i to the receiver
h_p	Channel fading coefficients due to misalignment error
I	Received signal light intensity from the transmitter to the receiver
I_i	Received signal light intensity from the i^{th} transmitter to the receiver
I_i^{PAM}	Intensity levels of pulse amplitude modulation
K	Number of hops
k	Wave number
L	Link distance from source-destination
M	Modulation order
N	Order of the approximation
n	Total code length
$n(t)$	Additive white Gaussian noise at the receiver input
N_{re}	Number of relays
n_j	Received AWGN at receiver input
N_o	Noise spectral density
N_r	Number of receivers
N_t	Number of transmitters
p	Number of transmitted symbols
P	Optical power
P_{out}	Outage probability
P_M	Power margin
R	Data rate
r	Radial displacement which is modeled by Rayleigh distribution
$r(t)$	Received signal
r_j	Received signal at each branch
$r_k(t)$	Received signal at the kth hop
$s(t)$	Transmitted information symbol
t_1	First time slot
t_2	Second time slot
T_s	Symbol duration
u	Random variable
U	Subtraction of two independent random variables
V	Message length
w_{n_i}	Weights of N^{th} order Hermite polynomial
w_i	Weights of the Hermite polynomial

w_z	Beam waist (in m) (radius calculated at e^{-2})
x	Independent and identically distributed Gaussian random variables
X	Independent random variable
x_i	Spatially correlated identically distributed Gaussian random variable
Y	Independent random variable
z	Random variable
z_{nj}	Roots of N^{th} order Hermite polynomial
z_i	Roots of the Hermite polynomial

$\acute{\rho}$	Constant
α	Attenuation coefficient (in dB/km)
β	Path loss
β_{kn}	Normalized path loss for a hop
$\beta_d(\ell)$	Path loss of direct link in clear weather conditions
β_k	Path loss for a hop
β_n	Normalized path loss coefficient
$\boldsymbol{\gamma}$	Signal-to-noise ratio vector
δ	Relative estimation error percent
ℓ	Link distance for a hop
η	Optical-to-electrical conversion coefficient
$\Gamma(.)$	Gamma function
Γ_{ij}	Spatial covariance matrix coefficients
γ_{th}	Signal to noise ratio threshold
γ_i	Signal-to-noise ratio of transmitter i
λ	Wavelength of the transmitter
$\boldsymbol{\Gamma}$	Spatial covariance matrix
$\boldsymbol{\Gamma}_{\text{sq}}$	Square root spatial covariance matrix
μ_x	Mean of an independent and identically distributed Gaussian random variables
$\overline{\gamma_i}$	Average signal-to-noise ratio of transmitter i
$\Psi(.)$	Moment generating function
ρ	Correlation coefficient
σ_n^2	Variance of an additive white Gaussian noise
σ_k	Standard deviation for a hop
σ_R^2	Rytov variance
σ_s^2	Jitter variance at the receiver
σ_x^2	Variance of an independent and identically distributed Gaussian random variables
θ_f	Field of view of the receiver (in mrad)
θ_T	Optical beam divergence angle (in mrad)
ξ	Pointing error parameter

Mathematical Notation

$(\cdot)^{-1}$	Inverse of a matrix
$(\cdot)^{T}$	Transpose of a matrix
det[.]	Determinant of a matrix
$\forall$	For all
$\in$	Element of
$\lceil a \rceil$	Round a
$\mathbb{E}$[.]	Average over channel fading distributions
$\mathbb{R}$	Real numbers
$\mathbf{E}$[.]	Mean
erf(.)	Error function
erfc(.)	Complementary error function
$\lvert . \rvert$	Absolute value
$\lvert\lvert . \rvert\rvert_F$	Frobenius norm
$G_{p,w}^{m,o}[.]$	Meijer's G-function
$Q(.)$	Gaussian-Q function

1 Introduction

1.1 Background

Historically, free-space optical (FSO) communication was first invented by Alexander Graham Bell in 1880 [1]. He employed an experiment called "photophone" that converts voice sounds into telephone signals and transmits the signal through sunlight to an optical receiver at a distance of 213 m. Bell considered this optical technology the greatest invention he had ever made, greater than the telephone. However, it never came out as a commercial product, but it demonstrated the basic principle of FSO communications. After the invention of the laser, wireless optical commination has prompted great attention.

The fast growing demand for high data rates along with the scarcity of radio frequency (RF) spectrum necessitate the need to consider alternative wireless transmission technologies such as FSO. FSO, unlike fiber optic networks, does not require an expensive infrastructure. Due to this and other benefits FSO communication has become the leading subject for both research and commercial activities over the past years. Moreover, FSO utilizes an unlicensed spectrum and is a green communication technology, which constitutes a perfect solution for wide-range applications. FSO systems have typical applications such as backhaul for wireless cellular networks, fiber back up, disaster recovery for damaged landlines, connecting buildings with ultra-high data rate, broadcasting high-definition video and satellite communications [2, 3, 4, 5, 6, 7]. Employing dense wavelength division multiplexing (DWDM), FSO communication provides the world record transmission of 1.6 Tbps using 16 channels each operating at 100 Gbps over a link of 80 m [8].

However, practical deployment of FSO faces major challenges that degrade the performance significantly. High sensitivity to harsh weather conditions such as snow, haze, rain, smoke, fog and dust is shown to impact the performance significantly [9, 10]. In addition, background noise as a result of exposure to direct or indirect sunlight or artificial lights is another major issue to be considered. Background noise can be eliminated using optical filters [11]. Geometric losses caused by beam divergence is shown to degrade the performance of FSO systems as well [12]. An efficient solution is to narrow the transmitted beam [13]. However, such solution causes a misalignment problem, which can lead to a communication interruption and requires automatic pointing and tracking at the receiver [14]. Also, atmospheric turbulence-induced fading, which is the fluctua-

tion of the received signal due to inhomogeneity in temperature and pressure, leads to significant performance degradation [15].

These turbulences are the main reason for fading in FSO links. Such fading is caused by multipath propagation in RF systems [10, 16]. RF and FSO are affected differently by atmospheric and weather conditions. FSO links suffer from high attenuation in the presence of fog but are less affected by rain. In contrast, fog has practically no impact on RF systems while rain significantly increases link attenuation [16]. Many statistical models have been proposed to describe the atmospheric turbulence in FSO which give good agreement between theoretical and experimental data. The most widely used of are log-normal distribution (LN) for weak-moderate [11, 17], Gamma-Gamma (G-G) distribution for moderate-strong [14] and negative exponential distribution [15, 18] for strong saturated turbulence regimes. Moreover, generalized distributions such as exponentiated Weibull (EW) [19] and $\mathcal{M}$-distribution [20] can provide excellent agreement with the probability density function (PDF) of irradiance for both simulation and experiment data in weak-to-strong turbulence regimes.

1.2 Thesis Contributions

The main objective of this thesis is to propose reliable solutions for the previously mentioned challenges of FSO. In summary, the main contributions of this thesis are:

1. Showing that correlation among multiple transmitters leads to signal-to-noise ratio (SNR) losses. Separating the transmitters by few centimeters can decrease the correlation. However, the required separation may be difficult in practice as available space for the transmitters may not be sufficient for this requirement [21]. For this reason, correlated LN channels, as well as path loss due to weather effects using intensity modulation and direct detection schemes, have been also studied. Additionally, an approximated average bit error rate (ABER) expressions for repetition codes (RCs) and orthogonal space-time block codes (OSTBCs) are derived. Under the considered scenarios, results show that RCs outperform OSTBCs.

2. Meeting the growing demand for higher data rate communication networks, space shift keying (SSK) is proposed for high spectral efficiency FSO links. In comparison among SSK, single-input single-output (SISO), and RC multiple pulse amplitude modulations (M-PAM) techniques, our results are in favor of SSK FSO links for high spectral efficiency applications or channel high turbulence effects. Moreover, the ABER performance of FSO links with SSK over negative exponential and LN atmospheric turbulence channels are investigated. Tight upper and lower bounds for ABER expressions corresponding to negative exponential and LN channels, respectively are obtained.

3. Mitigating turbulence and path losses effects, the multi-hop system is investigated due to its advantage of shorter hops that yields significant performance improvements. Decode and forward (DF) multiple-input single-output (MISO) multi-hop FSO systems are proposed and the obtained results show the superiority of the

proposed system over a direct link and MISO systems considering correlation effects at the transmitter.

4. Analyzing full-duplex (FD) relays under different turbulence conditions, misalignment error and path loss effects. FD relays are compared with the direct link and half-duplex (HD) relays. Our results show that FD relays have the lowest ABER and the outage probability (OP).

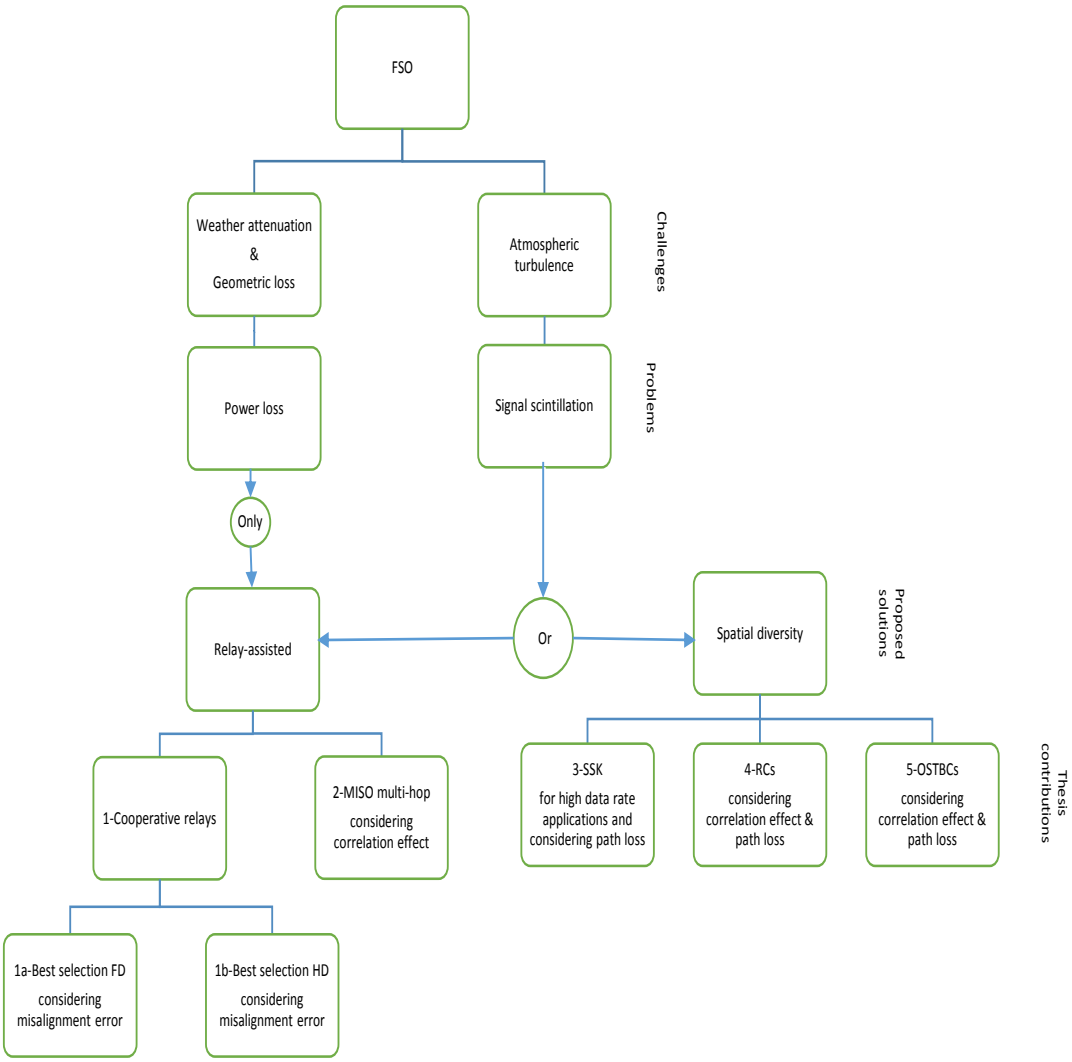


FIGURE 1.1 – Summary of thesis contributions.

These contributions are summarised in Figure 1.1. We consider two challenges facing FSO: weather attenuation and geometric loss, and atmospheric turbulence. In the case of weather attenuation and geometric loss, these challenges lead to power loss and relay-assisted FSO systems can mitigate these effects. Two schemes are employed as follows:

(a) cooperative relays where best relay selection for full-duplex and half suplex systems are considered considering misalignment error.

(b) MISO multi-hop system considering correlation effects among the transmitters.

In the case of atmospheric turbulence, which leads to signal scintillation, spatial diversity and/or relay-assisted can mitigate signal scintillation. Three schemes are employed as follows:

(c) space shift keying for high data rate application especially for moderate-to-strong turbulence regimes and different path loss effects are considered.

(d) RCs considering correlation effects among transmitters and different path loss effects.

(e) OSTBCs considering correlation effects among transmitters and different path loss effects.

1.3 Thesis Organization

Figure 1.2 shows the main three axes considered in the thesis to mitigate various challenges facing FSO. Firstly, the existing works in the three axes are discussed in Subsections 2.6.4-2.6.6. Secondly, the obtained contribution of the first axis, multiple-input multiple-output (MIMO), is considered in Chapter 3. Thirdly, the achieved contribution of the second axis, spatial modulation, is considered where a special case of spatial modulation called space shift keying is employed in Chapter 4. Finally, the third axis, relay assisted is considered in its two schemes: multi-hop and cooperative relays in Chapter 5 and Chapter 6, respectively.

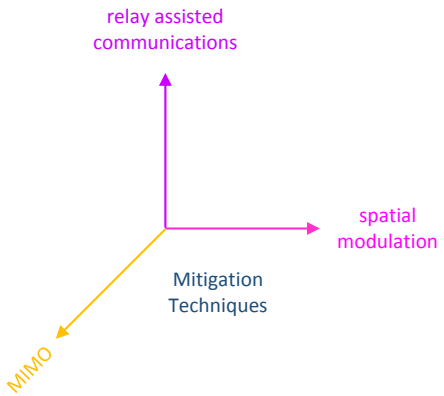


FIGURE 1.2 – The main axes of the research.

This thesis is organized as follows:

Chapter 2 reviews the state of art of FSO communication systems. The key technologies, the motivation, the major challenges, the potential solutions and the practical

results are discussed. This chapter considers suggested solutions such as different modulation techniques, channel models, forward error correction techniques, spatial diversity, aperture averaging and multi-hop relays as well as cooperative relays for FSO communication systems.

Chapter 3 gives the effects of both correlated LN channels and path loss due to different conditions under OSTBCs and RCs. In addition, approximated ABER expressions using non-coherent FSO systems for the two schemes are derived.

Chapter 4 covers a high spectral efficient FSO links based on SSK system and compared to the state of the art of RC-M-PAM.

Chapter 5 presents the superiority of MISO multi-hop DF FSO system, considering different turbulence conditions and path loss attenuations, compared to direct link and MISO systems.

Chapter 6 provides FD relays FSO communication systems are intensely alternative systems of communication between two indirect links or in the case of large distances.

Chapter 7 concludes this thesis and gives some prospects for further investigations in the same scope of the thesis.

2
State of the Art

2.1 Introduction

In this chapter, the key technologies, motivation, major challenges, channel models and the practical results of free-space optical (FSO) communication systems are discussed. This chapter also considers different modulation techniques, forward error correction techniques, spatial diversity, aperture averaging and multi-hop relays as well as cooperative relays to improve FSO communication systems. Figure 2.1 shows the main three axes considered in the thesis to mitigate various challenges facing FSO. The existing works in the three axes are discussed in Subsections 2.6.4-2.6.6.

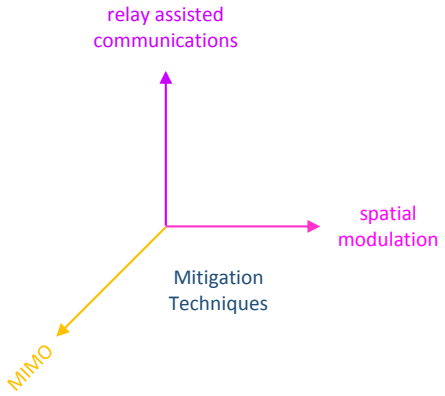


FIGURE 2.1 – The main axes of the research.

2.2 Key Technologies

Wireless optical communications transmit information through light. Light source converts the electrical signal to light signal which propagates through the optical channel till a photodetector. The photodetector converts again the light signal to electrical signal. Wireless optical can be classified into indoor wireless optical communications, underwater wireless optical communications, satellite wireless optical communications and free-space optical communications [2].

2.2.1 Indoor wireless optical communications

Indoor wireless optical communication can be classified into infrared and visible light communications (VLC). VLC has great attention nowadays due to its ability to communicate and illuminate simultaneously. White illumination using light-emitting diodes (LEDs) is preferred for VLC, due to their long lifetimes and energy efficiencies (at least 10 times greater than incandescent bulbs). In addition, by as early as 2018, majority of lighting installations are expected to be LED-based. This green technology can be used in places where radio frequency (RF) is prevented such as hospitals and airplanes [22, 23].

Moreover, it can be used for positioning of mobile devices in indoor environments as supermarkets, shopping malls, and museums (using the camera sensor as the receiver). The market for mobile indoor positioning in the retail sector is expected to reach \$5 billion by 2018 [24]. Also, sale navigation using VLC technology [25] is very interesting application as depicted in Figure 2.2. In addition, VLC can be used for smart automotive lighting using the already existing LEDs in the car to decrease the percentage of accidents [26].

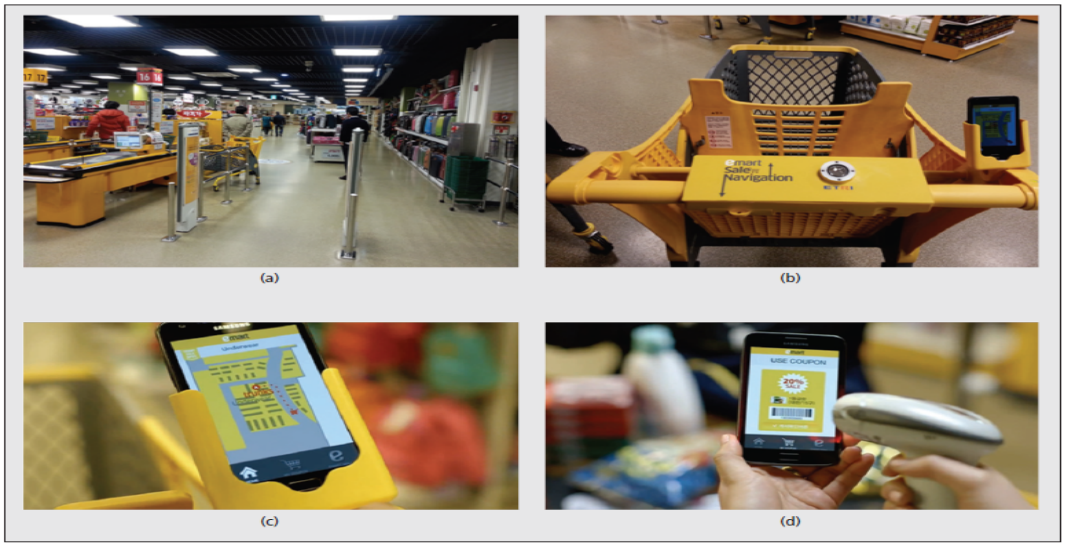


FIGURE 2.2 – Sale navigation using VLC technology in Korea [25].

In September 2011, IEEE ratified 802.15.7, a wireless personal area network standard for VLC at data rates ranging from 11 kbps to 96 Mbps [25]. VLC faces a lot of challenges such as increasing the temperature which reduces the LEDs lifetime, dimming of the light source for low data rates, path loss attenuation, sunlight and artificial light effects, fluctuation of the brightness of light and eye constrains safety and incorrect detection of LED color [27]. Different potential solutions are proposed in the literature to mitigate these challenges such as special filters for fluctuation of the brightness of the light, advanced modulation techniques for dimming of the light source and feedback correction for the incorrect detection of LED color [27].

High efficiency LEDs named organic light emitting diodes (OLEDs), contains multi-films such as carbon and hydrogen between two conductors, has been introduced since 1990 [28]. The advantages of OLEDs are low cost, no restriction on size, bright, power efficient and light weight. However, OLEDs have many challenges such as degradation of the organic layer and OLEDs have a capacitor-like behavior so huge bandwidth required small photoactive area while small OLEDs does not support the required illumination. These challenges limit the data rate being in the range of 2.7 Mbps [29]. Finally, OLEDs for VLC still needs a lot of developments to be commercialized.

2.2.2 Underwater wireless optical communications

Recently, wireless optical communication has been deployed for underwater robot [30], see Figure 2.3. LEDs are preferred than laser for robot communications as LEDs have a small size and low price. The authors achieved 20-30 meters propagation distance with average power consumption of 500 mW. The interesting thing is the cost of wireless optical communication devices is only 70 dollars. Different data rates between 9600 bps to 38400 bps were carried out to ensure the reliability of the system.



FIGURE 2.3 – Underwater robots using LED-based communications [30].

2.2.3 Space wireless optical communications

NASA employed wireless optical communications link between Moon and Earth for a propagation distance of 384600 km at 622 Mbps [31]. German Space Agency, named DLR-Space, employed wireless optical communications link between two low Earth orbit (LEO) satellites (TerraSAR-X and NFIRE) see Figure 2.4. This link is considered the

first coherent link for wireless optical satellite communication with BPSK and homodyne detection for about 8000 km and 5.6 Gbps is achieved [32].

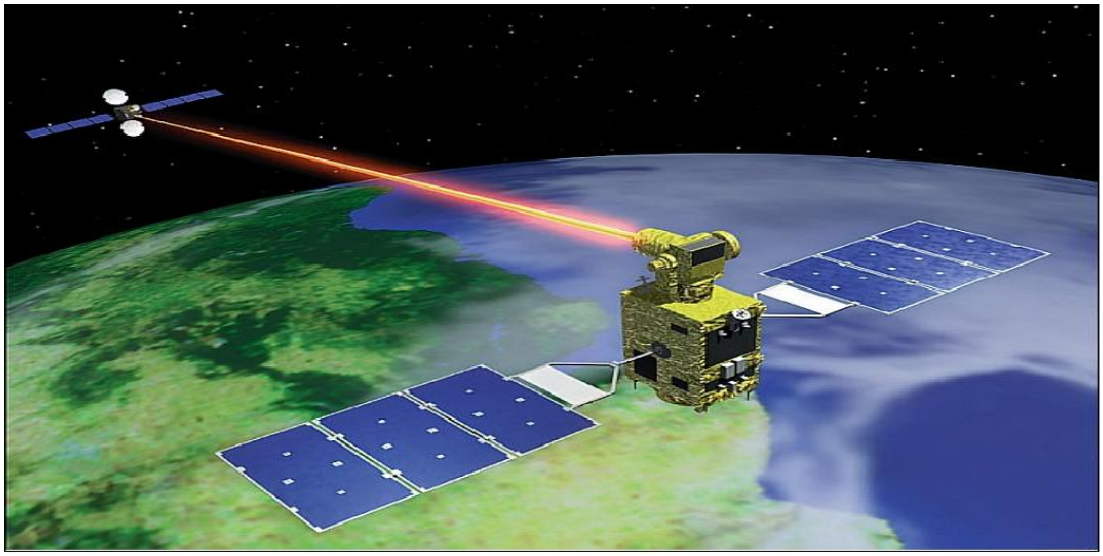


FIGURE 2.4 – Wireless optical communication between satellites [33].

2.2.4 Free-space optical communications

FSO communications or outdoor wireless optical usually referred to wireless optical communications among buildings see Figure 2.5. In this thesis, we focus on FSO using lasers.

2.3 Motivation

In fact, the information carrying capacity of a communication system increases by using higher carrier frequency. In RF systems, the allowable bandwidth can be up to 20% of the carrier frequency for a licensed system. Even 1% of the optical bandwidth for the carrier frequency of $\approx 10^{16}$ Hz can achieve a bandwidth of 100 THz. Therefore, optical systems can handle almost 10^5 times actual RF systems [34]. However, available electronics can not provide such huge bandwidth at the moment. Thus, techniques such as wavelength division multiplexing and spatial diversity should be used.

The fast growing demand for high data rates in conjunction with the scarcity of RF band necessitate considering alternative solutions. Fiber optic network can achieve these demands, however, it requires an expensive infrastructure. Therefore, FSO communication is a leading technology that has been at the forefront of both research and commercial activities over the past years.

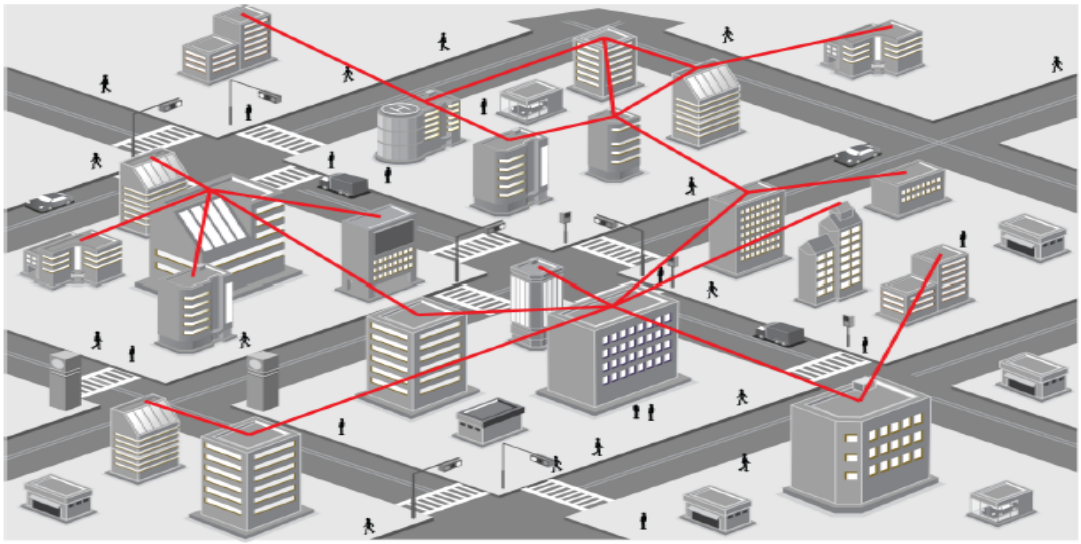


FIGURE 2.5 – Free-space optical communication network [2].

2.4 Major Challenges

FSO advantages did not come without cost. The transmitted optical signal is affected by several challenges such as geometric loss, misalignment loss, weather attenuation loss, and background noise and atmospheric turbulence.

2.4.1 Geometric loss

The geometric loss is due to the divergence of the optical beam through propagating which is affected by the divergence angle, the propagation distance, and the receiver aperture size [12].

2.4.2 Misalignment loss

Misalignment loss occurs due to an error in tracking system or building sway. The main reasons for building sway are the wind, a small earthquake, and vibrations [35]. For short range communications, a laser with a wide divergence angle can be used to reduce the effect of misalignment loss. However, for long-range communications (i.e. several kilometers), a laser with narrow divergence angle must be used to avoid severe geometric loss and automatic pointing and tracking adjustment must be employed [13].

2.4.3 Weather attenuation loss

Different weather attenuation losses such as haze, rain, snow, dust, and smoke and fog cause severe attenuation for the transmitted signal [9,10]. RF and FSO are differently affected by weather effects. FSO links suffer from the highest attenuation in the presence

of fog but are less affected by the rain. In contrast, RF links at 10 GHz aren't affected by the fog while the rain significantly increases the attenuation. This property leads to the design of hybrid RF/FSO systems [16] and mixed RF/FSO [35,36]. Hybrid RF/FSO uses FSO and RF parallel between two nodes [16]. However, in mixed RF/FSO, RF and FSO are deployed together for dual-hop communication systems [36]. The attenuation coefficient (α in dB/km) of different weather conditions are provided in Table 2.1.

TABLE 2.1 – Weather attenuation coefficient of FSO

Weather conditions	α **[dB/km]**
Clear air	0.43
Haze	4.2
Moderate rain (12.5 mm/h)	5.8
Heavy rain (25 mm/h)	9.2
Light fog	20
Moderate fog	42.2
Heavy fog	125

2.4.4 Background noise

Background noise, due to undesirable background radiations, results of exposure of the receiver to direct or indirect sunlight or artificial lights. This noise reduces the SNR gain but it can be eliminated using bandpass optical filter before photo-detection. Direct sunlight statistically occurs less than 1 hour per year [13,37].

2.4.5 Atmospheric turbulence

Atmospheric turbulence-induced fading can be defined as a random fluctuation in both amplitude and phase of the received signal due to the inhomogeneity in temperature and pressure. Such turbulence causes significant performance degradation in FSO [15]. The turbulence is the main reason for the fading in FSO. While in RF links, the fading is due to the multipath propagation [10,16]. The atmospheric turbulence has a severe effect on the performance of FSO systems especially for long distances [38]. The turbulence effect depends on the link distance, the wavelength of the light source and the refractive index constant, C_n^2 ($\mathrm{m}^{-2/3}$) [14]. C_n^2 is strongly affected by temperature so it has the peak value at noon and it has the minimum value at midnight [39].

2.5 Atmospheric Turbulence Channels

2.5.1 Experimental results

In [40], a FSO experiment was carried out using a 632.8 nm wavelength laser, a beam divergence of 1 mrad, a power of 15 mW and the distances were 183 m and

3 km. At the receiver, positive-intrinsic-negative (PIN) photodetector was used with a high gain amplifier and a filter. The experiment was conducted during the middle of March 1980 at air temperatures 23.8-26.6 °C, a cloudy sky, the wind speed up to 5.36 m/sec and low humidity. The same experiment was repeated on August 1980 at air temperatures 27.7-32.3 °C, a cloudy sky, the wind speed up to 2.68 m/sec but the humidity was high. Results show that log-normal (LN) channels have good agreement to experimental data for weak-moderate turbulence channels especially for short ranges and negative exponential channels have a good agreement for strong saturated turbulence regimes.

In [41], a FSO experiment was carried out in August 1985, with a laser of a wavelength 633 nm, beam divergence of 1 mrad, power of 4 mW, the height of the link was 2 m and the distance was 1 km. Results show that LN channels do not fit the experimental results for strong turbulence channels. Moreover, an analytical model is proposed named log-normally modulated exponential which has a good agreement with the experimental results.

2.5.2 Simulation results

Simulation results for FSO channels assuming plane wave [42] and spherical wave [43] are carried out. The simulations carried out by approximating a three-dimensional random medium as a collection of two-dimensional random phase screens that are transverse to the direction of wave propagation. These simulation results have excellent agreements with the FSO experiment carried out in [41].

2.5.3 Proposed analytical models

In [44], Gamma-Gamma (G-G) distribution is proposed as an efficiency model for moderate-strong turbulence and has a good agreement with simulation results for both plane wave [42] and spherical wave [43]. In G-G distribution, the received light intensity is the product of two independent Gamma random variables, where the irradiance fluctuations are the product of small-scale and large-scale fluctuations.

Double Weibull distribution is proved in [45] to be more accurate than G-G distribution for moderate-strong turbulence using the same set of measured data of [44]. However, G-G distribution has simpler calculation complexity. Additionally, Double Generalized Gamma (Double GG) model is proposed in [46], where the received light intensity is the product of two independent Generalized Gamma random variables. Compared with G-G and Double Weibull using the same set of measured data of [44] for the comparison, Double GG is more accurate in the strong turbulence using spherical wave model and in moderate turbulence using plane wave model [2].

Moreover, generalized distributions such as exponentiated Weibull (EW) [19], $\mathcal{M}$-distribution [20] and Generalized homodyned K distribution [47] provide excellent agreements with the probability density function (PDF) of irradiance for both simulated and experimented data in weak-to-strong turbulence regimes.

2.6 Suggested Solutions

This section considers different techniques such as modulation techniques, forward error correction techniques, spatial diversity, aperture averaging and multi-hop relays as well as cooperative relays to enhance the performance of FSO communication systems.

2.6.1 Modulation techniques

Several advanced modulation schemes have been suggested in the literature to mitigate the challenges of FSO communication systems.

2.6.1.1 Coherent and non-coherent detection

FSO systems use coherent or non-coherent. In coherent systems, the information is encoded by the optical amplitude, frequency, or phase modulation. At the receiver side, the received field is optically mixed with a locally generated optical field. In non-coherent systems, intensity modulation [1] of the emitted light is employed to convey the information. At the receiver side, the photo-detector directly detects changes in light intensity without the need for a local oscillator. These systems are also known as intensity modulation and direct detection (IM/DD) systems.

2.6.1.2 Energy and spectral efficiencies

There are two important factors relative to the choice of a modulation scheme as energy efficiency and spectral efficiency. Energy efficiency refers to the minimum bit error rate (BER) at a target data rate for a given transmit energy irrespectively of the occupied bandwidth. However, it does not take into account the implementation complexity. Spectral efficiency, on the other hand, refers to the information transmission rate for a given bandwidth without taking the required transmit energy into account [2, 49].

2.6.1.3 Modulations suitable for IM/DD systems

On-off keying (OOK), a binary level modulation scheme, is the most commonly used IM technique due to its simple implementation. In OOK signaling, modulated data is represented by the presence ("on") or absence ("off") of a light pulse in each symbol interval. At the receiver side and for an optimal signal detection, the instantaneous channel fading coefficient should be estimated to perform dynamic thresholding [49]. In addition, OOK has relatively poor energy and spectral efficiency [50]. Another modulation technique is the pulse position modulation (PPM), which is an energy efficient modulation technique that does not require dynamic thresholds for optimal detection compared with OOK [51].

1. It is important to note that the intensity modulation and the amplitude modulation are not identical as the spectrum for intensity modulation contains harmonics of the modulation waveform [48].

In comparison with PPM, multiple PPM (MPPM) is proposed in [52] to achieve a higher spectral efficiency at the expense of demodulation complexity. It is important to note that although optical communications have a large bandwidth and high spectral efficiency modulation, it requires high-speed electronic circuits which are difficult to be designed and implemented. Under the constraint on peak transmiting power, MPPM outperforms PPM in signal-to-noise ratio (SNR) gain [51, 53]. Compared with PPM, pulse width modulation (PWM) has higher spectral efficiency at the expense of higher average power requirements [54].

Digital pulse interval modulation (DPIM) sends a pulse followed by a number of empty slots which depends on the information bits. To avoid the problem of consecutive "on" pulses, an additional guard slot is added to each symbol. The major drawback of DPIM is the inferior error performance compared with PPM and MPPM as they require symbol synchronization [55]. Other modulation techniques based on PWM and PPM are differential PPM (DPPM) and pulse-position-pulse-width modulation (PPMPWM). In DPPM, the slots after the "on" pulse are discarded so every DPPM symbol ends with a pulse which decreases the complexity of the synchronization at the receiver. Discarding the empty slots improves the spectral efficiency of the system. However, variable rate encoding and decoding have practical drawbacks [56, 57]. In PPMPWM, the energy efficiency and the spectral efficiency are in mid-way between PWM and PPM [54].

Multiple pulse amplitude modulation (M-PAM) can be used in FSO to obtain high spectral efficiency compared with OOK at the expense of energy efficiency and system complexity as it requires a laser with variable emission intensity [58].

2.6.1.4 Subcarrier intensity modulation

In subcarrier intensity modulation (SIM), the data is first modulated onto a RF signal then the signal is transmitted using the IM of an optical source. The concept of the SIM is to transmit parallel data streams through a number of non-orthogonal overlapping subcarriers [59]. Compared with coherent modulation at the same spectral efficiency, SIM has cost effective implementation at the expense of energy efficiency as a result of DC bias added to the signal to avoid negative amplitudes [2, 59]. The DC bias problem can be decreased by using a variable bias for each symbol [60].

2.6.1.5 Polarization modulation

Polarization modulation (PM) encodes the information as different states of the polarization of the laser source by an external modulator. At the receiver, based on the extraction of stoke parameters of received light, the signal can be recovered. PM has high mitigation to atmospheric turbulence as the polarization states are less affected by atmospheric turbulence compared with amplitude and phase. Moreover, PM has a high immunity to the phase noise and non-linearity of lasers. This advantage makes it a perfect solution for long-range FSO applications. However, PM requires perfect transmitter-receiver polarization alignment [61, 62, 63].

2.6.1.6 Coherent modulation

Compared with IM/DD systems, coherent systems can send the information in the amplitude, phase, or polarization of the optical signal which increases the spectral efficiency of the system. At the receiver, the signal is mixed with a local oscillator (LO) signal then the received signal is amplified. For this reason, coherent detection increases the receiver sensitivity and decreases the shot noise at the expense of the complexity of the system [64].

Commercial FSO systems are based on IM/DD due to its simplicity and low cost. However, the great evolution of digital signal processing of high-speed electronic circuits leads to turn into coherent systems [65].

The coherent detection can be divided into heterodyne and homodyne detection. In homodyne detection, the frequency of the LO is exactly the same as the incoming radiation which makes it very expensive. While in heterodyne detection, the incoming radiation, and the LO frequencies are different [49]. FSO link employing homodyne binary phase shift keying (BPSK) has been established between two of the Canary islands to transmit 5.625 Gbps over a distance of 142 km [66].

Finally, modulation techniques alone are not sufficient in enhancing the perofmrance of FSO communication systems. Other techniques must be considered such as forward error correction, spatial diversity, aperture averaging, multi-hop relay systems and cooperative relay systems.

2.6.2 Forward error correction techniques

One useful mitigation tool for atmospheric turbulence is forward error correction (FEC). Here, we discuss some FEC codes used for FSO communication systems.

2.6.2.1 Reed-Solomon (RS) codes

The total code length of RS (n, V) is defined by n and the message length is defined by V. In [67], the authors employed 256-ary PPM using different RS codes in the presence of atmospheric turbulence to keep the average bit error rate (ABER) below 10^{-9}. The authors used RS codes due to its easily implemented decoder and its alphabet size is easily matched to M-ary PPM. The results are employed over a weak turbulence channel using PIN receivers and with a data rate of 1 Gbps. Results show that truncated RS (255, 223) and RS (255, 207) outperform the standard RS (255, 239).

M-ary PPM and RS (255, 127) are employed in the presence of ambient noise and moderate fog conditions [68]. Results show a significant mitigation for both challenges by increasing the modulation level of PPM. In [69], the authors have shown that increasing the modulation level of the M-ary PPM improves the power efficiency of FSO system at the expense of bandwidth and synchronization complexity.

2.6.2.2 Concatenated Reed-Solomon codes

Two concatenated codes, RS (255, 239) + RS (255, 239) and RS (255, 239) + RS (255, 223), are compared with the standard RS (255, 239) of international telecommunication union - telecommunications (ITU-T) for optical communications. The results show that the two concatenated codes outperform the standard RS (255, 239) at an average bit error rate (ABER) 10^{-8} [70]. Using 256-PPM with concatenated RS (255, 239) + RS (255, 223) helps to upgrade the existing uncoded 256-PPM FSO system to work on strong turbulence rather than being limited to weak turbulence at ABER of 10^{-9} [18]. The same results appear using avalanche photodetectors (APDs) or PIN receivers [18].

2.6.2.3 Turbo codes and low-density parity-check codes

In [69], the authors compared the performance of RS (255, 127) with different rates of Turbo codes. They found that RS coded PPM might still be the preferable choice for practical implementation due to the decoding complexity of Turbo codes. Other works have considered the use of low-density parity-check (LDPC) codes for FSO systems over atmospheric turbulence channels such as [71].

2.6.2.4 FEC drawbacks for FSO

Although FEC achieves good results in mitigating atmospheric turbulence, however, using them for high data rates are not practical. As for high data rates, the complexity of encoder and decoder and the delay will not be acceptable [72].

2.6.3 Aperture averaging

Aperture averaging is another simple solution to reduce the fading effect, which uses a relatively large aperture at the receiver side to average over intensity fluctuations. However, the data rate of the system decreases as large parasitic capacitance is required [73].

2.6.4 Spatial diversity

Spatial diversity is considered as a promising solution to combat atmospheric turbulences and maximize the data rate of the systems [74, 75]. By using multiple apertures at the transmitter and/or the receiver sides, spatial diversity has the potential to mitigate atmospheric turbulence effects, enhance the performance of the FSO links and overcome the limitations on the transmit optical power. Also, the possibility of laser beam blockage by obstacles (e.g., birds or moving vehicles) is further reduced and longer distances can be covered in harsh weather conditions [75, 76, 77, 78].

2.6.4.1 Single-input multiple-output

For single-input multiple-output (SIMO) systems, equal gain combing (EGC) has the same performance of the optimal maximal ratio combining (MRC) for weak turbulence channels [79]. Also, at moderate turbulence channels, EGC has only a lower SNR gain of 0.3 dB compared with MRC at ABER of 10^{-5} while having the advantage of lower implementation complexity and simple analytical model. Moreover, the ABER expression of multiple-input multiple-output (MIMO) FSO system using EGC in LN channel is similar to that of single-input single-output (SISO) link with the difference of dividing the variance of the LN channel by the number of sub-channels.

2.6.4.2 Multiple-input single-output

For the multiple-input single-output (MISO) systems, the conventional orthogonal space-time block codes (OSTBCs), as used in RF systems, should be modified to deal with IM/DD techniques because the output of the transmitter must be unipolar [80, 81]. To achieve this, the negative part of a modulated signal is represented by the 1's complement (i.e., bitwiseNot) of a positive signal [80]. However, it has been shown in [11] that if we are not limited by practical implementation considerations such as time synchronization, repetition codes (RCs) outperform their counterpart OSTBCs using IM/DD in uncorrelated LN channels.

In a RCs system, the same signal is transmitted simultaneously from available transmitters. Yet, coherent and differential OSTBCs FSO systems are shown to outperform their counterpart RCs systems at the expense of laborious receivers [82]. Moreover, transmit laser selection (TLS) system, which requires channel knowledge at the transmitter and at the receiver, outperforms the ABER performance of RCs and OSTBCs at the expense of increases system complexity [83].

2.6.4.3 Multiple-input multiple-output

Spatial modulation (SM) MIMO system for indoor optical wireless communication has been studied in [75]. In SM, a group of data bits modulate a symbol from certain constellation diagram and another group activates one of the transmitter beams. A line-of-sight (LOS) indoor wireless optical communication system using SM is proposed in [84]. According to [84], SM outperforms its counterpart RC system with $M-$PAM for spectral efficiencies larger than 4 bits/s/Hz.

Another system is space shift keying (SSK), which is a special case of SM where only the index of the active transmitter is transmitted rather than the data symbols. A study conducted in [85] shows that OOK RC outperforms OSTBCs, spatial multiplexing (SMux) and SSK for FSO communications using IM/DD over G-G channels. However, these results are given only for a spectral efficiency of 1 bit/s/Hz. A detailed survey of SM and SSK systems are discussed in [86].

In [87], spatial pulse position amplitude modulation (SPPAM) is proposed for FSO links. It is shown that SPPAM outperforms SSK for spectral efficiencies of 2 bits/s/Hz or less.

Tight upper bounds are derived for the error probability for coherent SM FSO systems over Generalized H-K distribution [47]. In [88], hybrid SIM and SM system are proposed and the results show that the proposed system outperforms SIM system at the spectral efficiency of 4 bits/s/Hz using less number of receivers.

2.6.4.4 Correlation effects

In the case of uncorrelated channels, the spacing among transmitters is assumed to be larger than the fading correlation length. In addition, the total length of the transmitters must not exceed the capture zone of the receiver. Which is equal to $\theta_f \ell$ m, where θ_f is the field of view (FOV) of the receiver (in rad) and ℓ is the link distance (in m) [80]. However, the last assumption might be difficult in practice as available space for the transmitters may not be sufficient for this requirement [21]. A correlation model called the exponential model [89], corresponds to the scenario of a multichannel transmission from linearly equispaced transmitters, can be considered to calculate the correlation [9,90]. A simple and general method to approximate the PDF of correlated and uncorrelated LN channels using moment generating function (MGF) is derived in [91].

A unified framework determining the spatial correlation for both transmit and receive units is presented in [92]. This framework is applicable to different wave types, turbulence conditions and aperture size.

In [93], for a SIMO system with two receive apertures, the sum of correlated G-G random variables is approximated by an $\alpha - \mu$ distribution [94] in order to evaluate the BER performance at the receiver. This idea is then generalized to the case of MIMO in [95]. The Padé's approximation method approximates a function in one variable [96] and it is used in [97] to obtain the PDF of the sum of correlated G-G random variables from their MGF, which is then used to evaluate the system performance analytically. However, due to the limitation of the Padé's approximation, this method cannot be used for very low BERs.

Finally, spatial diversity can mitigate turbulence effects, however, it can not mitigate the path loss effects. Other techniques such as multi-hop relay systems and cooperative relay systems must be considered for path loss effects.

Our contributions for spatial diversity are discussed in Chapter 3 and Chapter 4.

2.6.5 Multi-hop relay systems

To further mitigate turbulence and path losses effects, multi-hop system is used due to its advantage of shorter hops that yields significant performance improvements.

2.6.5.1 Conventional multi-hop relay systems

In [98], the authors introduce multi-hop relays for FSO. They showed that multi-hop relays are more efficient than single-hop at the same BER. However, their results only considered weather attenuation without atmospheric turbulence effects. The outage probability (OP) of multi-hop FSO systems using amplify-and-forward (AF) over strong

turbulent channels is investigated in [99]. In [100], the OP of multi-hop FSO systems using AF or decode-and-forward (DF) over G-G channels is investigated and the ABER of dual-hop DF systems is derived.

The physical layer of cooperative relays (CRs) FSO systems are proposed in [101]. The OP of both CRs and multi-hop systems using DF and AF systems are derived. In addition, atmospheric turbulence and path loss attenuation are considered. Moreover, the results of [101] show that multi-hop systems outperform CRs, however, CRs can create an artificial broadcasting. Asymptotical relative diversity order (ARDO) of DF FSO for multi-hop systems and CRs is derived in [102]. Results show that ARDO of multi-hop systems is greater than CRs.

In [103], the OP of DF multi-hop system considering weak turbulence, path loss, and misalignment error is derived. In [104], the OP of a multi-hop DF FSO system over a Poisson channel degraded by LN turbulence channel is calculated. The effect of different weather conditions on multi-hop FSO systems is studied [105]. By neglecting background radiation and dark currents, power allocation for multi-hop FSO system is discussed in [106]. The ABER of multi-hop FSO systems over G-G and misalignment fading channels is derived in [107] and the OP of the same system is derived in [108].

2.6.5.2 All-optical multi-hop relay systems

All-optical FSO relaying is proposed in [109], without the need for optical-to-electrical and electrical-to-optical conversions required in conventional FSO relays. In all-optical FSO systems [109], DF systems outperform AF systems. Moreover, it is shown in [9], that FSO systems with all-optical relays achieve a better performance compared with systems having conventional FSO relay.

All-optical AF FSO systems, using an erbium doped fiber amplifier (EDFA) combined with an optical hard-limiter (OHL) over G-G channels, are employed in [110]. OHL is used to remove accumulated background noise. Then, closed-form ABER expression is derived for the system. Moreover, results show that using OHL leads to achieve the same performance of many relays with fewer relays.

2.6.5.3 Coherent multi-hop relay systems

Multi-hop coherent FSO systems are employed over turbulent channels. Moreover, the diversity and multiplexing gains are derived [111]. The OP of employing APD receivers for CRs and multi-hop systems over LN channels using BPSK is derived in [112] for DF relays and in [113] for AF relays. In [114], approximated closed-form, upper bound and asymptotic expressions for the capacity of dual-hop AF FSO communication systems over G-G channels with pointing errors are derived.

Closed-form expressions for capacity and average symbol error rate (SER) of M-ary phase shift keying (MPSK) for dual-hop AF FSO systems over G-G channels are derived [115]. In [116], the OP and the average SER of multi-hop FSO communications over G-G channels with pointing errors, using heterodyne detection and differential phase-shift keying (DPSK) modulation are derived.

The ABER and the OP of a dual-hop DF relay using BPSK over G-G channels are derived in [117], using the series representation of MGF of G-G distribution which was originally proposed by [118]. The lower bound OP for dual-hop AF coherent FSO systems is derived in [119]. Moreover, the results show that the outage performance of AF is comparable with that of DF for coherent FSO systems. In [120], closed-form and asymptotic for ABER and ergodic capacity are derived for multi-hop AF heterodyne FSO system over atmospheric turbulence with pointing errors.

2.6.5.4 Subcarrier intensity modulation multi-hop relay systems

The ergodic capacity of SIM dual-hop FSO systems is derived over G-G channels with pointing error for DF systems [121] and in [122] for variable and fixed gains of AF systems.

2.6.5.5 Optimum placement for multi-hop relay systems

The optimum placement for multi-hop relays is determined being equidistance between the source and the destination while for CRs, it is found being closer to the source and it is also a function of link distance, number of relays and SNRs [123]. The optimum placement for multi-hop relays is determined in the presence of obstacles blocking the direct link [124].

2.6.5.6 Photon counting receiver for multi-hop relay systems

Multi-hop FSO system using count-and-forward (CF) relay with photon counting receiver (PCR), that counts the number of received photons, is proposed in [125]. The relay employs OOK and uses discrete power levels corresponding to the number of received photons. Results show that using CF with PCR outperforms the performance of the hard-decision forwarding scheme.

2.6.5.7 Beam size variation at the receiver for multi-hop relay systems

The effect of beam size variation at the receiver due to turbulence is calculated for multi-hop FSO systems using a spatially coherent Gaussian beam model [126].

2.6.5.8 Hybrid spatial diversity and multi-hop relay systems

The OP of SIMO multi-hop systems using EGC is proposed over correlated G-G channels [127]. Both AF and DF relays are considered for the proposed system. Results show that employing fewer relays with SIMO have higher SNR gain than employing many relays without SIMO. Extended results are proposed in [128] for MIMO multi-hop systems, where the OP, the diversity order and power allocation of DF relays are considered over G-G channels.

2.6.5.9 Hybrid FSO and RF links for multi-hop relay systems

Mixed dual-hop AF systems using RF link in the first hop represented by Nakagami-m channel and using FSO link represented by G-G channel with pointing error is proposed in [129], where SIM is used for FSO transmission. Moreover, CDF, PDF, MGF, OP, ABER and the capacity are derived for the proposed dual-hop AF RF-FSO communication system. The same system of dual-hop AF RF-FSO is employed in [130] with an extra direct RF link, where both IM/DD and coherent modulation techniques are employed, and MRC and selection combining (SC) are employed at the destination side.

In this subsection, the superiority of multi-hop relay systems in mitigating the effects of turbulence and path loss effects are discussed. Our contributions for multi-hop systems are discussed in Chapter 5.

2.6.6 Cooperative relay systems

Cooperative relays systems as a powerful mitigation tool for the atmospheric turbulence and path loss effects are discussed in this subsection. Moreover, artificial broadcasting can be obtained using cooperative relays [101]. In cooperative relays, perfect synchronization is required to ensure that all the signals arrive simultaneously at the destinations. In practice, perfect synchronization is a cumbersome task especially for a large number of relays [131].

2.6.6.1 Transmission relays

CRs can be classified into all-active transmission and selective transmission systems. In all-active transmission, relays forward received signals to the destination [101]. However, in selective transmission, a relay only forward the received message based on the max-min SNR [131]. The selective transmission is considered an asynchronous low complexity system and outperforms the performance of the OP of all-active transmission. The selection process, based on the max-min SNR, is achieved according to [132]:

$$\underset{i\epsilon\{1,\cdots,N_{re}\}}{j=\max(\min(h^2_{\mathrm{SR}_i},h^2_{\mathrm{R}_i\mathrm{D}}))}, \tag{2.1}$$

where N_{re} is the number of relays, j is the index of the best relay, i is a relay index, h_{SR_i} and $h_{\mathrm{R}_i\mathrm{D}}$ are the channel fading coefficients between the source and ith relay, R_i, and between R_i and the destination, respectively.

2.6.6.2 Types of DF cooperative relay systems

In [133], three CRs for FSO communication systems using direct link are discussed as bit detect and forward (BDF), adaptive bit detect and forward (ABDF) and adaptive decode and forward (ADF). At BDF, the relay forwards the received bit regardless its correctness. However, at ABDF both the relay and the direct link re-forward the received bit with low SNR. While in ADF, the relay corrects the false bit then re-forward it. If the relay fails to correct the bit, ADF will behave like ABDF. Results show that the proposed systems outperform both the direct link and MISO systems.

In the absence of background noise, BDF has the same performance of ABDF. While, in the presence of background noise, ABDF has more SNR gain compared to BDF [134]. Moreover, results show that using a single feedback bit of RF has significant SNR gain especially in low SNRs.

In [135], the author showed that the diversity order for N_{re} relay system using BDF and ABDF is equal to $\lceil \frac{N_{re}}{2} \rceil + 1$ and $N_{re} + 1$, respectively. Where the function $\lceil a \rceil$, rounds a to the smallest integer greater than a. A novel CRs FSO scheme, called, improved adaptive decode-and-forward (IADF) is proposed [136]. The proposed system transmits two frames into four time slots. In the first time slot, the source transmits the message to the relay. In the second time slot, the relay transmits the message to the destination. The same thing happens for the second frame in the third and fourth time slots. However, if the relay has failed to receive the message correctly in any case, the source performs an XOR operation on the first frame with the second frame and sends the resultant directly to the destination. In addition, the diversity order is derived for the proposed system as a function of the propagation distance.

2.6.6.3 Conventional cooperative relay systems

CRs for DF FSO communication system using a single relay IM/DD in the absence of background noise is employed. The considered system achieve the same ABER compared with direct and MISO systems, that suffers from correlation at low SNR [137]. Closed-form expressions of the outage performance for multi-hop and CRs FSO systems over $\mathcal{M}$-distribution with nonzero boresight pointing errors are derived [138]. The boresight is the displacement between the center of the detector and the center of the received beam.

Asymptotic expressions for OP are derived for DF IM/DD CRs FSO system using repetition coding over G-G channels with pointing error and weather attenuation effects [139]. Where the destination receives two copies of the message over three time slots. The considered system outperforms the OP of both MISO and conventional CRs systems.

2.6.6.4 All-optical cooperative relay systems

All-optical CRs systems employing AF relays using PCR over LN channels with path loss effects are considered [140]. The proposed system has less SNR at the same ABER as compared with the multiple-transmitter system especially for long distances and/or high attenuation factors.

All-optical CRs systems using PCR over LN channels with path loss effects are considered for full channel state information (CSI) and semi-blind CSI [141]. However, both cases have comparable performance, semi-blind CSI has lower complexity. The OP of all-optical relay selection FSO systems using PCR over G-G turbulent channels is derived for both full CSI and semi-blind relays [142]. All-optical relay selection FSO systems have SNR gain up to 11.5 dB compared with all-active relays for a system using four relays.

2.6.6.5 Subcarrier intensity modulation cooperative relay systems

CRs for SIM FSO communication systems using DF relays and differential modulation are employed over G-G channels [143]. Moreover, the ABER, the diversity order and coding gain are derived. The OP of CRs BPSK-SIM for FSO systems over G-G turbulent channels with pointing errors is derived [144].

2.6.6.6 Selected relay for cooperative relay systems

In [145], the OP of relay selection for FSO systems using DF relays over LN channels with path loss effects is discussed. At OP of 10^{-5}, a selected relay depend on the SNR of all the links, has less power by 6 dB than a selected relay depend on the SNR of relay to destination (R-D). DF CRs in a FSO IM/DD communications system is employed over G-G channels and MRC is used at the receiver [146]. Then the OP, diversity and coding gain are derived.

In [147], opportunistic CRs for FSO links are proposed, where the relay participate only if the source to relay (S-R) link is strong enough. In the case that S-R and R-D links has the same performance, opportunistic CRs has the same OP of conventional CRs. While if S-R link is weak, opportunistic CRs has better OP compared with conventional CRs.

The ABER for CRs for FSO communication systems using selective transmission is obtained for LN and Rayleigh channels [148]. Partial relay section according to the best S-R path is employed and an approximated ABER of G-G channels is derived [149].

The ABER and the diversity order of relaying selection of DF CRs FSO over G-G channels with pointing errors are derived [150]. The ABER performance of a single relay selection according to max-min criterion of SNR for dual-hop parallel DF FSO over G-G channels employing adaptive subcarrier quadrature amplitude modulation is obtained using a power series approximation method [151].

Closed-form ABER of selective CRs for DF FSO system using SIM for BPSK over generalized $\mathcal{M}$-distributed turbulent channel is derived [152]. Moreover, the diversity order for various distributions, as a special case of generalized $\mathcal{M}$-distributed turbulent channel, is derived. The ABER and the OP of selective transmission for multi-hop parallel DF relaying using BPSK are derived for EW fading channels using the Gauss-Laguerre quadrature rule [153].

2.6.6.7 Power allocation for cooperative relay systems

Power allocation for quantum-limited CRs FSO systems is discussed in [154]. In the absence of CSI, the ABER performance is better if the power is distributed among the links. While in the presence of CSI, the ABER performance can be significantly enhanced by allocating all the power to the strongest link.

2.6.6.8 Multiple-source cooperation relaying

Multiple-source cooperation relaying for FSO systems over strong turbulence is proposed [155]. Where many users send their information to a single relay then this relay forwards all the messages to the final destination. Compared with conventional CRs, the proposed system requires less equipment cost.

2.6.6.9 Optimum placement for cooperative relay systems

The optimum placement for CRs is found being closer to the source and function of link distance, the number of relays and SNRs [123]. Asymptotic ABER of CR for FSO communication system using EGC over G-G channels with pointing error is derived [156]. This also results in that the diversity order is independent on pointing error in some cases, however, the diversity order strongly depends on the placement of the relay.

The ABER and the diversity order of relay placement in ADF CRs for FSO systems over G-G channels with pointing errors are derived [157]. Unlike [123], in the presence of pointing errors, the authors [157] show that the diversity order is better when the relay nodes are closer to the destination node. Moreover, the authors demonstrate that ADF system based on S-R selection always outperforms ADF system based on R-D regardless the position and number of relays.

2.6.6.10 Multi-hop parallel relaying

In [158], OP and diversity gain of multi-hop parallel relaying over LN channels are derived. Multi-hop parallel relaying has less power compared with multi-hop and parallel relaying at the same OP. Multi-hop parallel relaying, where only one selected participating path (i.e. the strongest channel gain) is discussed [159]. In addition, the second and the third strongest paths are considered in a case where the first strongest path is not available due to scheduling and load balancing issues. This results of the OP of the second and the third strongest paths outperforms multi-hop system using the same number of relays per path.

2.6.6.11 Mean time between failures for cooperative relay systems

In [160], results of mean time between failures (MTBF) was 12 years for a SISO FSO system using low data rate RF back up, while MTBF was 20 years for CRs FSO system using low data rate RF back up.

2.6.6.12 Inter-relay cooperation of cooperative relay systems

The OP and the diversity of inter-relay cooperation for all-active and selection CRs FSO systems are introduced and derived [161]. The inter-relay cooperation has less power compared with conventional CRs for certain relay positions. Moreover, power allocation and BER of inter-relay cooperation are derived in [162].

2.6.6.13 Two-way relay systems

Two-way relays (TWRs) using DF for FSO systems is employed in [163] over G-G channels, where two users communicate using three time slots. Thus achieving higher data rate, TWR using two time slots to communicate is investigated in [164,165]. In the first time slot, the two sources send their information to the relay. The relay decodes the received signals and performs an XOR operation on the decoded signals. The resultant signal is then forwarded to each user in the second time slot. The user can obtain its intended received signal by performing an XOR operation with the received message. Moreover, the SER and the OP are derived over $\mathcal{M}$-channel [164] and LN channel [165].

In [166], TWR DF FSO is employed over $\mathcal{M}$-distribution FSO channels, in addition the ABER and the OP are derived in the presence of pointing errors. Multi-user TWR is proposed in [167], where the received signal is affected by atmospheric turbulence, path loss and building sway. Partial relay selection for TWR coherent FSO using AF is employed over G-G channels and affected by path losses and pointing errors [168].

Our contributions for cooperative relay systems are given in Chapter 6. The techniques discussed in this section, make FSO communication systems reliable means of providing wireless communications.

2.7 Practical Results

In this section, we selected some practical results for FSO communication systems:

1. FSONA, one of the leading FSO companies, provides Crédit Agricole French bank with FSO links of 10 Gbps. Four 2.5 Gbps links were deployed instead of a fiber optic link for their new building in Paris. This link provides service for more than 1600 employees [169].
2. FSONA provides a mobile backhaul connectivity for the fourth generation long-term evolution (LTE) services to customers in Lebanon of 1.25 Gbps without the delay of a laying cable [170].
3. Northern Storm, one of the leading FSO companies, installed a FSO link in California city of 10.31 Gbps with 1 Gbps RF backup for a distance of 238 m. For the considered system, an availability of 99.999% is achieved in all weather conditions [171].
4. In [172], experimental results are employed for an all-optical dual-hop FSO system and 10 Gbps is achieved for a link of 500 m.

According to these encouraging results, we suggests the market of FSO communication systems with will be increased in the coming years.

2.8 Summary

In this chapter, a review of the state of the art for FSO communication systems has been discussed. We can conclude that spatial diversity and relay-assisted FSO communication systems are potential candidates for the next-generation communications

networks ; as spatial diversity combats atmospheric turbulence and maximizes the data rate of the systems. In addition, relay-assisted systems mitigate turbulence and path losses effects due to its advantage of shorter hops that yields significant performance improvements. In Chapter 3, spatial diversity is considered and the correlation effects among transmitters are discussed for correlated LN channels for RCs and OSTBCs.

3

Diversity Techniques for Correlated Log-normal Channels

3.1 Introduction

Performance analysis of free-space optical (FSO) communication systems assuming uncorrelated channel conditions have gained significant attention in the literature [11]. This assumption, however, requires sufficient spacing among transmitters and can not be satisfied in some applications. Thereby, this chapter considers correlated log-normal (LN) FSO channels with weather attenuation effects. Approximate analytical expressions using moment generating function (MGF) of the joint probability density function (PDF) of correlated LN channels are developed.

Using MGF approximation, the average bit error rate (ABER) expressions for repetition codes (RCs) and orthogonal space-time block codes (OSTBCs) using intensity modulation and direct detection (IM/DD) schemes in correlated LN channels are derived. Results demonstrate that RCs have higher signal-to-noise ratio (SNR) gain than OSTBCs in correlated channel conditions. In addition, the effect of light fog and clear air conditions on the ABER performance of the FSO communication systems are studied. Our Monte Carlo simulations corroborate the validity of the derived mathematical analysis.

Table 3.1 summarizes the contribution of the most relevant works in the literature and our work by specifying the considered channel models. Figure 3.1 shows the main three axes considered in the thesis to mitigate various challenges facing FSO. In this chapter, the obtained contribution of the first axis, multiple-input multiple-output (MIMO), is considered where a special case of MIMO, when the receiver has a single aperture, called multiple-input single-output (MISO) is employed in this chapter.

3.2 System Model

The synoptic diagram of the considered system model is depicted in Figure 3.2. The investigated system has N_t transmitters and a single receiver. On-off keying (OOK) pulsed modulation is employed to modulate the source bits then a MISO encoder is used. In the RCs system, the encoder transmits the same signal simultaneously from the N_t transmitters. In OSTBCs system, the encoder considers full rate real orthogonal

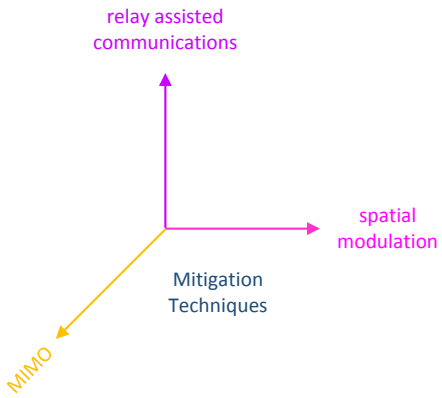


FIGURE 3.1 – The main axes of the research.

TABLE 3.1 – Comparison among our MISO scheme & the closed literature works

Reference	Channel Model	Contributions
[80]	negative-exponential	a modified version of Alamouti's code for IM/DD
[91]	correlated LN	derive approximated MGF for correlated LN
[11]	LN	RCs outperform OSTBCs using IM/DD
[83]	K distribution	transmit laser selection outperform RCs
Our work	correlated LN (to model correlation among transmitters)	impact of spatial correlation on RCs and OSTBCs

matrices, $\mathbf{G}$, for $N_t \leq 8$ for OSTBCs [173]. In [173], a linear transformation of $\mathbf{G}$ matrix to OOK matrix, $\mathbf{S} \in \mathbb{C}^{p \times N_t}$, through $\mathbf{S} = \frac{\mathbf{U}+\mathbf{G}}{2}$ is proposed, where $\mathbf{U}$ denotes a matrix of ones and p is the number of transmitted symbols.

The encoded real symbols modulate the synchronized laser diodes. The transmitted light is affected by a correlated LN channel and weather attenuation effects. Moreover, at the receiver side an additive white Gaussian noise (AWGN) is added.

For the OSTBC system, the received signal vector, $\mathbf{r} \in \mathbb{C}^{p \times 1}$, is given by

$$\mathbf{r} = \eta\, \mathbf{S}\, \mathbf{I} + \mathbf{n}, \tag{3.1}$$

where η, $\mathbf{S} \in \mathbb{C}^{p \times N_t}$, $\mathbf{I} \in \mathbb{C}^{N_t \times 1}$ and $\mathbf{n} \in \mathbb{C}^{p \times 1}$ are the optical-to-electrical conversion coefficient, the codeword matrix, the light intensity vector and AWGN vector, respectively.

The received signal for RC system is given by

$$r(t) = \eta \sum_{i=1}^{N_t} s(t) I_i + n(t), \tag{3.2}$$

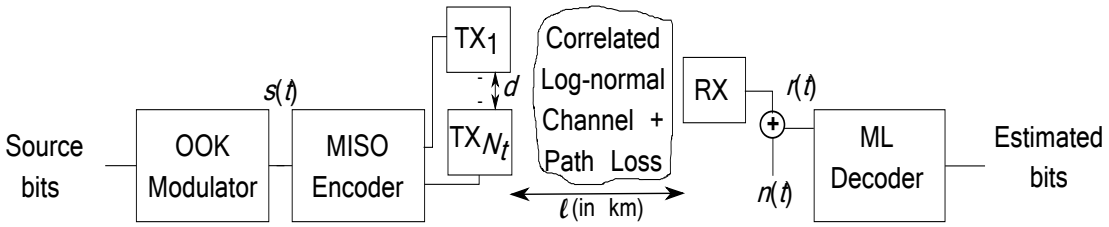


FIGURE 3.2 – Synoptic diagram of the proposed model.

where $s(t)$ denotes the transmitted symbols $\in \{0, 1\}$ and $n(t)$ is an AWGN with zero mean and variance σ_n^2. The shot noise, caused by background light, is assumed to dominate other noise sources such as thermal and dark noises [11]. I_i denotes the received signal light intensity from the i^{th} transmitter to the receiver after channel effect which can be evaluated according to [9, 79] as follows

$$I_i = \beta \, \overline{I} \, h_i, \tag{3.3}$$

with $\overline{I}$ being the received signal light intensity without considering the channel effect, $h_i = e^{2x_i}$ is the channel irradiance from transmitter i to the receiver with x_i being modeled as spatially correlated identically distributed (c.i.d.) Gaussian random variables (RVs) with mean μ_x and variance σ_x^2.

The path loss is modeled as [9]

$$\beta = 10^{-\alpha \ell / 10}, \tag{3.4}$$

where α is the weather-dependent attenuation coefficient (in dB/km) and ℓ is the link distance (in km). The values of α for different weather conditions are provided in Table 2.1.

Hence, h_i is a LN RVs with PDF given by [90]

$$f_{h_i}(h_i) = \frac{1}{h_i \sqrt{8\pi\sigma_x^2}} \times \exp\left(-\frac{(\ln(h_i) - 2\mu_x)^2}{8\sigma_x^2} \right). \tag{3.5}$$

To ensure that the fading channel does not attenuate or amplify the average power, the fading coefficients are normalized as $\mathbf{E}[h_i] = e^{2(\mu_x + \sigma_x^2)} = 1$. where $\mathbf{E}[.]$ is the mean.

At the receiver side, for RCs maximum-likelihood (ML) decoder is considered to decode the received signals. However, for OSTBCs the transpose of $\mathbf{I}$ vector must be multiplied by the received signal ($\mathbf{r}\mathbf{I}^T$) before using ML decoder [11].

3.3 Performance Analysis

3.3.1 Orthogonal Space-Time Block Codes

The PDF of the instantaneous SNR $\gamma_i, 1 \leq i \leq N_t$, of correlated jointly LN channels under path loss effect can be calculated as [9, 90]

$$f_{\gamma_i}(\gamma_1, \cdots, \gamma_{N_t}) = \frac{\exp\left(-\frac{1}{32} \, Z \, (\mathbf{\Gamma})^{-1} Z^T\right)}{4^{N_t} \sqrt{(2\pi)^{N_t} (\det[\mathbf{\Gamma}])} \Pi_{i=1}^{N_t} \gamma_i}, \tag{3.6}$$

where $Z = \left[\ln\left(\frac{\gamma_1}{\beta^2\overline{\gamma_1}}\right)\cdots\ln\left(\frac{\gamma_{N_t}}{\beta^2\overline{\gamma_{N_t}}}\right)\right] - 4\mu_x$, $\overline{\gamma_i}$ is the average SNR, $(\cdot)^{-1}$ is the inverse of a matrix, $(\cdot)^T$ is the transpose of a matrix and det[.] is the determinant of a matrix.

The spatial covariance matrix $\mathbf{\Gamma}$ coefficients, modeling the spatial correlation among transmitters, are given by [79]

$$\Gamma_{ij} = \sigma_x^2 \times \rho^{|i-j|}, \tag{3.7}$$

where |.| stands for the absolute value, ($\rho \leq 1$) is the correlation coefficient and i and j are the row and the column indices of the covariance matrix coefficients, respectively. According to [21], ρ is a function of the separation distance, d, between each two successive transmitters,

$$\rho = \exp\left[-\left(\frac{d}{d_o}\right)^{5/3}\right], \tag{3.8}$$

where the correlation length $d_o \approx \sqrt{\lambda\ell}$ with λ being the wavelength. This correlation model is called the exponential model [89] and corresponds to the scenario of a multi-channel transmission from linearly equispaced transmitters. From (3.8), the correlation of combined signals decays by increasing the spacing between the transmitters.

The instantaneous SNR γ_i in Equation (3.6) is given by [76],

$$\gamma_i = \frac{(\eta I_i)^2}{N_o}. \tag{3.9}$$

where N_o is the noise spectral density. The conditional bit error rate (BER) for FSO system using OSTBCs can be calculated as [9,11]

$$\Pr(e|h) = Q\left(\sqrt{\frac{E_b\ \beta^2}{2N_o}\sum_{i=1}^{N_t} h_i^2}\right) \tag{3.10}$$

The Gaussian-Q function is defined as [15]

$$\begin{aligned} Q(y) &= \frac{1}{\sqrt{2\pi}}\int_y^\infty \exp\left(-\frac{z^2}{2}\right)dz \\ &= \frac{1}{\pi}\int_0^{\frac{\pi}{2}} \exp\left(-\frac{y^2}{2\sin^2\theta}\right)d\theta. \end{aligned} \tag{3.11}$$

The average electrical energy E_b of the transmitted pulse at each transmitter is given by [11].

$$E_b = \frac{\eta^2\overline{I}^2}{N_t^2}. \tag{3.12}$$

To guarantee that the total power of the MISO system is equal to the power of a single-input single-output (SISO) system, N_t^2 is added to Equation (3.12) [1].

1. In FSO, the energy of the symbols is proportional to the square of the optical power [11].

Substituting Equation (3.12) into Equation (3.10) and using Equation (3.3) yields

$$\Pr(e|h) = Q\left(\sqrt{\frac{\eta^2}{2N_o(N_t)^2}\sum_{i=1}^{N_t} I_i^2}\right). \tag{3.13}$$

Using Equation (3.9), the conditional BER with respect to the SNR becomes

$$\Pr(e|h) = Q\left(\sqrt{\frac{\sum_{i=1}^{N_t}\gamma_i}{2(N_t)^2}}\right). \tag{3.14}$$

Using the PDF of the instantaneous SNR γ_i in Equation (3.6), the ABER of OSTBCs is given by

$$\text{ABER} = \int_0^\infty \cdots \int_0^\infty Q\left(\sqrt{\frac{\sum_{i=1}^{N_t}\gamma_i}{2(N_t)^2}}\right) \times \ f_{\gamma_i}(\gamma_1, \cdots, \gamma_{N_t})\, d\gamma_1 \cdots d\gamma_{N_t}. \tag{3.15}$$

According to [90], the MGF is defined by

$$\Psi_\gamma(-s) = \int_0^\infty \cdots \int_0^\infty \ f_{\gamma_i}(\gamma_1, \cdots, \gamma_{N_t}) \times \exp\left[-s\sum_{i=1}^{N_t}\gamma_i\right] d\gamma_1 \cdots d\gamma_{N_t}, s \in \mathbb{R}, \tag{3.16}$$

With the use of Equations (3.3), (3.5) and (3.9), and after few algebraic manipulations, the PDF of instantaneous branch SNR for the given branch i ,γ_i, becomes

$$f_{\gamma_i}(\gamma_i) = \frac{1}{\sqrt{32\pi\sigma_x^2\gamma_i}} \exp\left[-\frac{\left(\ln\left(\frac{\gamma_i}{\beta^2\overline{\gamma_i}}\right) + 4\sigma_x^2\right)^2}{32\sigma_x^2}\right] \tag{3.17}$$

The MGF of the RVs γ_i is then given by

$$\Psi_\gamma(-s) = \int_0^\infty \exp(-s\gamma_i)\frac{1}{\sqrt{32\pi\sigma_x^2\gamma_i}} \times \exp\left[-\frac{\left(\ln\left(\frac{\gamma_i}{\beta^2\overline{\gamma_i}}\right) + 4\sigma_x^2\right)^2}{32\sigma_x^2}\right] d\gamma_i. \tag{3.18}$$

Making the change of variable $z = \left(\frac{\ln\left(\frac{\gamma_i}{\beta^2\overline{\gamma_i}}\right)+4\sigma_x^2}{\sqrt{32\sigma_x^2}}\right)$ yields

$$\Psi_\gamma(-s) = \frac{1}{\sqrt{\pi}}\int_{-\infty}^\infty \exp(-z^2) \times \exp\left(-s\beta^2\overline{\gamma_i}\ \exp\left(\sqrt{32\sigma_x^2}z - 4\sigma_x^2\right)\right) dz. \tag{3.19}$$

Using Hermite's polynomial approximation, we can write [174, page 924]

$$\int_{-\infty}^\infty \exp(-z^2)g(z)dz \approx \sum_{i=1}^N w_i g(z_i), \tag{3.20}$$

where z_i and w_i are the roots and the weights of the Hermite's polynomial, respectively and N is the order of the approximation. It was shown in [15] that accurate results for LN channels can be obtained if $N \geq 20$.

Applying Equation (3.20) on Equation (3.19) yields

$$\Psi_\gamma(-s) \approx \frac{1}{\sqrt{\pi}} \sum_{i=1}^{N} w_i \exp\left(-s\beta^2 \overline{\gamma_i} \exp(\sqrt{32\sigma_x^2} z_i - 4\sigma_x^2)\right) \tag{3.21}$$

In [91], the authors found that $N = 12$ is sufficient for the approximation of Equation (3.21).

Using Equation (3.21) and substitute σ_x by $c_{ij}^{'}$ which is the $(i,j)^{\text{th}}$ coefficient of $\mathbf{\Gamma}_{\text{sq}} = \mathbf{\Gamma}^{1/2}$, the general form of the MGF in correlated LN channel under path loss effect becomes

$$\Psi_\gamma(-s) \approx \sum_{n_1=1}^{N} \cdots \sum_{n_{N_t}=1}^{N} \left[\prod_{i=1}^{N_t} \frac{w_{n_i}}{\sqrt{\pi}}\right] \times \exp\left(-s \sum_{i=1}^{N_t} \beta^2 \overline{\gamma_i} \left[\exp\left(\sqrt{32} \sum_{j=1}^{N_t} c_{ij}^{'} z_{n_j} - 4\sigma_x^2\right)\right]\right), \tag{3.22}$$

The values of w_{n_i} and z_{nj} of the N^{th} order Hermite's polynomial are tabulated in [174, Table 25.10].

Using the definition of the Q-function in Equation (3.11) on Equation (3.15), the ABER of OSTBCs system over correlated LN channel under path loss effect can be written as

$$\text{ABER} = \frac{1}{\pi} \int_0^\infty \cdots \int_0^\infty \int_0^{\frac{\pi}{2}} \exp\left(-\frac{\sum_{i=1}^{N_t} \gamma_i}{4N_t^2 \sin^2\theta}\right) \times \ f_{\gamma_i}(\gamma_1, \cdots, \gamma_{N_t})\, d\theta\, d\gamma_1 \cdots d\gamma_{N_t}. \tag{3.23}$$

The ABER in Equation (3.23) can be written using the MGF approach in Equation (3.16) as

$$\text{ABER} = \frac{1}{\pi} \int_0^{\frac{\pi}{2}} \Psi_\gamma\left(-\frac{1}{4N_t^2 \sin^2\theta}\right) d\theta. \tag{3.24}$$

Using Equation (3.22) and assuming that all the average SNR from the transmitters are equal, i.e., $\overline{\gamma_i} = \overline{\gamma}$, $\forall i = 1, \cdots, N_t$, an approximate novel expression of the ABER of OSTBCs over correlated LN channel under path loss effect is derived as

$$\text{ABER} \approx \sum_{n_1=1}^{N} \cdots \sum_{n_{N_t}=1}^{N} \left[\prod_{i=1}^{N_t} \frac{w_{n_i}}{\sqrt{\pi}}\right] \times Q\left(\sqrt{\frac{\beta^2 \overline{\gamma}}{2N_t^2} \sum_{i=1}^{N_t} \left[\exp\left(\sqrt{32} \sum_{j=1}^{N_t} c_{ij}^{'} z_{n_j} - 4\sigma_x^2\right)\right]}\right). \tag{3.25}$$

3.3.2 Repetition Codes

In the case of RCs, the conditional BER of MISO FSO system is given by [9, 11]

$$\Pr(e|h) = Q\left(\sqrt{\frac{E_b\ \beta^2}{2N_o}} \sum_{i=1}^{N_t} h_i\right). \tag{3.26}$$

Using the alternative definition of the Q-function in Equation (3.11), the ABER of RCs system over correlated LN channel under path loss effect is given by

$$\text{ABER} = \frac{1}{\pi}\int_0^{\infty}\cdots\int_0^{\infty}\int_0^{\frac{\pi}{2}} \exp\left(-\frac{\left(\sum_{i=1}^{N_t}\sqrt{\gamma_i}\right)^2}{4N_t^2\sin^2\theta}\right) \times f_{\gamma_i}(\gamma_1,\cdots,\gamma_{N_t})\, d\theta\, d\gamma_1\cdots d\gamma_{N_t}. \tag{3.27}$$

It is important to note that the MGF approach cannot be used to represent Equation (3.27), since it is directly proportional to $(\sqrt{\gamma_i}\ )^2$. However, under the condition that $\sigma_x^2 \ll 1$, the following approximation can be used

$$E_1 = \left(\sum_{i=1}^{N_t}\sqrt{\gamma_i}\right)^2 \approx E_2 = N_t\sum_{i=1}^{N_t}\gamma_i. \tag{3.28}$$

Extensive Monte Carlo simulations of 10^6 realizations of the random variables were generated to verify the accuracy of our approximation in Equation (3.28). The relative estimation error percent, $\delta = 100 \times \left(\frac{E_1-E_2}{E_1}\right) < 10\%$, is calculated for different σ_x values. The results are shown in Figure 3.14. Results clearly demonstrate that the proposed approximation is valid and leads to a negligible error ($< 10\%$) with practical σ_x values. For more details on the proposed approximation, see Appendices B.1 and B.2. Please note that the maximum value of σ_x for FSO LN channels corresponds to the maximum scintillation index (SI) value for LN channels, which is $\leq$ 0.75 [15]. The relation between SI and σ_x is defined in [90] as $\sigma_x = \left(\frac{\sqrt{\ln(\text{SI}+1)}}{2}\right)$. Hence, σ_x should be ≤ 0.374.

Hence, to obtain the ABER of RCs, substitute Equation (3.28) in Equation (3.27) and using Equation (3.16) yields

$$\text{ABER} \approx \frac{1}{\pi}\int_0^{\frac{\pi}{2}} \Psi\left(-\frac{1}{4N_t\sin^2\theta}\right) d\theta \tag{3.29}$$

From Equations (3.22) and (3.29), an approximate expression for the ABER of RCs systems over correlated LN channels under path loss effect is derived as

$$\text{ABER} \approx \sum_{n_1=1}^{N}\cdots\sum_{n_{N_t}=1}^{N}\left[\prod_{i=1}^{N_t}\frac{w_{n_i}}{\sqrt{\pi}}\right] \times Q\left(\sqrt{\frac{\beta^2\overline{\gamma}}{2N_t}\sum_{i=1}^{N_t}\left[\exp\left(\sqrt{32}\sum_{j=1}^{N_t}c_{ij}^{'}z_{n_j} - 4\sigma_x^2\right)\right]}\right). \tag{3.30}$$

It is important to note here that Equations (3.25) and (3.30) can also applied for uncorrelated LN channels by setting $\rho \approx 0$ in $c_{ij}^{'}$.

3.4 Numerical Results and Discussions

In this section, a typically ABER for IM/DD FSO system using OOK of 10^{-9} is targeted, $\lambda = 1550$ nm and $\ell = 1$ km. The transmitters branches are assumed to be

identically distributed, low and high correlation values are considered ($\rho = 0.25$ and 0.5). Analytical results with $N = 20$ are compared to Monte Carlo simulations. Results demonstrate close match for a wide range of SNR values.

In Figure 3.3, the relation between the correlation effect and the separation distance among the transmit units is studied. The selected wavelength is $\lambda = 1550$ nm and different propagating distances are considered. Simulation results show that if a correlation coefficient $\rho \leq 10^{-3}$ is to be maintained, the distance among the transmit units should be at least 3 times the correlation length.

In Figure 3.5, a correlated LN channel with $\sigma_x = 0.1$ and $N_t = 2$ is employed. It is revealed that RCs are more power efficient than OSTBCs by about 3 dB for the two considered cases, $\rho = 0.25$ and 0.5. In Figure 3.6, a light fog environment with $\sigma_x = 0.1$ and $\alpha = 20$ dB/km is considered. These parameters are chosen considering the inversely proportional relationship between the turbulence strength and attenuation. It is very unlikely that strong turbulence occurs during a fog event [175]. The light fog effects lead to a severe effect on the performance of SNR gain as depicted in Figure 3.6.

In Figures 3.7 and 3.8, results demonstrate that RCs with $N_t = 3$ has more SNR gain by 0.6 dB and 0.5 dB for $\rho = 0.25$ and 0.5 as compared with RCs with $N_t = 2$, respectively. On the other hand, increasing the number of transmitters from two to three, degrades the performance of OSTBCs by 1 dB and 1.3 dB for 0.25 and 0.5, respectively.

For LN channels with small σ_x, the LN channels behave like Gaussian channels. Moreover, in Gaussian channels there is no diversity gain due to the use of multiple transmitter. This is the reason of OSTBCs with $N_t = 2$, has better SNR gain than OSTBCs with $N_t = 3$.

In Figure 3.9, moderate turbulence represented by LN channel of $\sigma_x = 0.374$ with $N_t = 2$ is considered. This, in turn, results in degradation in the ABER performance of FSO system severely. The required SNR to achieve the target ABER increases by 18.9 dB and 21 dB for RCs and by 19.3 dB and 21.5 dB for OSTBCs codes with $\rho = 0.25$ and 0.5, respectively compared to $\sigma_x = 0.1$ with $N_t = 2$ and $\alpha = 0$ dB. This also results in RCs outperform OSTBCs by about 3 dB.

In Figure 3.10, a clear air environment of a LN channel $\sigma_x = 0.3$ and $\alpha = 0.43$ dB/km with $N_t = 2$ is considered. It can be seen that light fog effect in Figure 3.6 is higher than increasing the atmospheric turbulence on the ABER performance of the FSO system. The required SNR to achieve the target ABER decreases by 25.74 dB and 24.88 dB for RCs and by 25.94 dB and 24.34 dB for OSTBCs with $\rho = 0.25$ and 0.5, respectively.

Figure 3.11 shows results for $N_t = 3$, $\sigma_x = 0.374$ and $\alpha = 0$. An interesting observation is the behavior of OSTBCs results, where increasing the number of transmitters enhances the performance unlike weak turbulence case. As compared to the results in Figure 3.9, OSTBCs show a SNR gain of 1.95 dB and 2 dB for $\rho = 0.25$ and 0.5, respectively. The required SNR for moderate turbulence increases by 14.5 dB and 17.7 dB for RCs and 15.4 dB and 17.6 dB for OSTBCs codes with $\rho = 0.25$ and 0.5, respectively compared to $\sigma_x = 0.1$ with $N_t = 3$ and $\alpha = 0$ dB.

Figure 3.12 shows results for $N_t = 3$, $\sigma_x = 0.3$ and $\alpha = 0.43$ dB/km. As compared

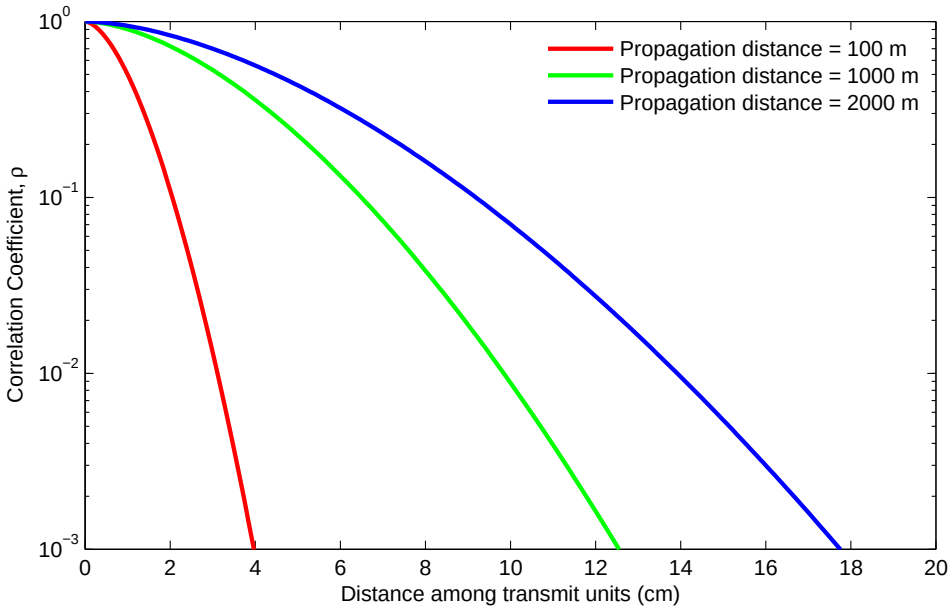


FIGURE 3.3 – Correlation coefficient versus distance among transmit units for difference propagation distances.

to the results of Figure 3.10, OSTBCs show a SNR gain of 1.4 dB and 0.8 dB with ρ = 0.25 and 0.5, respectively. However, the required SNR to achieve the target ABER decreases by 28.24 dB and 26.14 dB for RCs and 28.34 dB and 26.44 dB for OSTBCs with ρ = 0.25 and 0.5, respectively in the absence of light fog.

In Figure 3.13, the severe effect of different weather conditions on the FSO links using three transmitters are investigated using repetition codes with α = 0.1 dB/km and ρ = 0.25. Finally, the effect of increasing correlation on the ABER performance is depicted on Figure 3.14 using RCs for two transmitters with $\sigma_x = 0.3$ and by considering clear air condition.

3.5 Summary

In this chapter, MISO FSO systems with OOK modulation using IM/DD are considered. The effects of both correlated LN channels with different path loss effects are also considered. The PDF of correlated LN channels is expressed using the MGF approach. Based on the MGF approach, approximated ABER expressions for both OSTBCs and RCs in correlated LN channels are obtained. It is shown that increasing the number of transmitters always enhances the ABER performance of RCs, but it does not necessarily improve the SNR gain in OSTBCs.

Additionally, RCs are shown to always has higher SNR gain than OSTBCs approximately by 3 dB. Finally, the severe effects of different weather conditions on the FSO

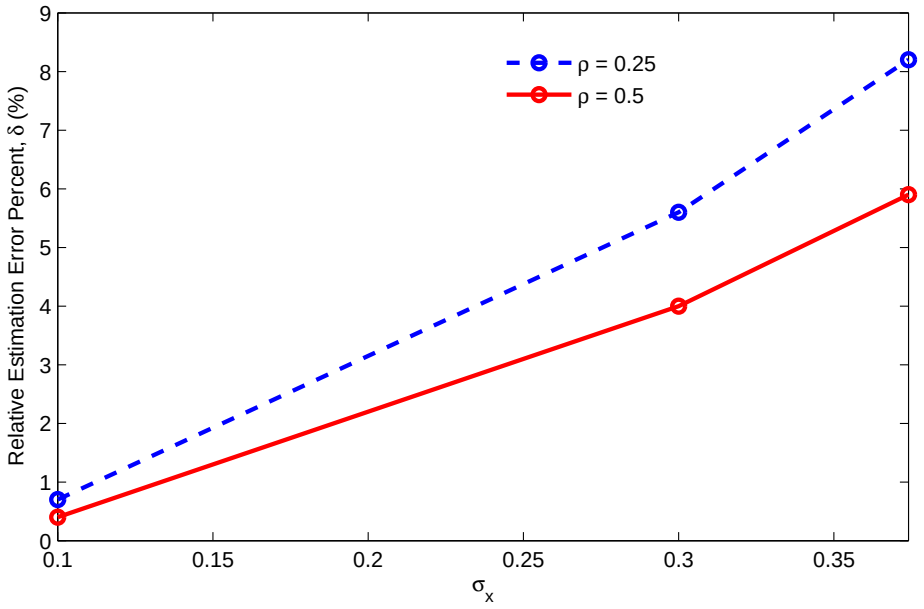


FIGURE 3.4 – Error due to the proposed approximation.

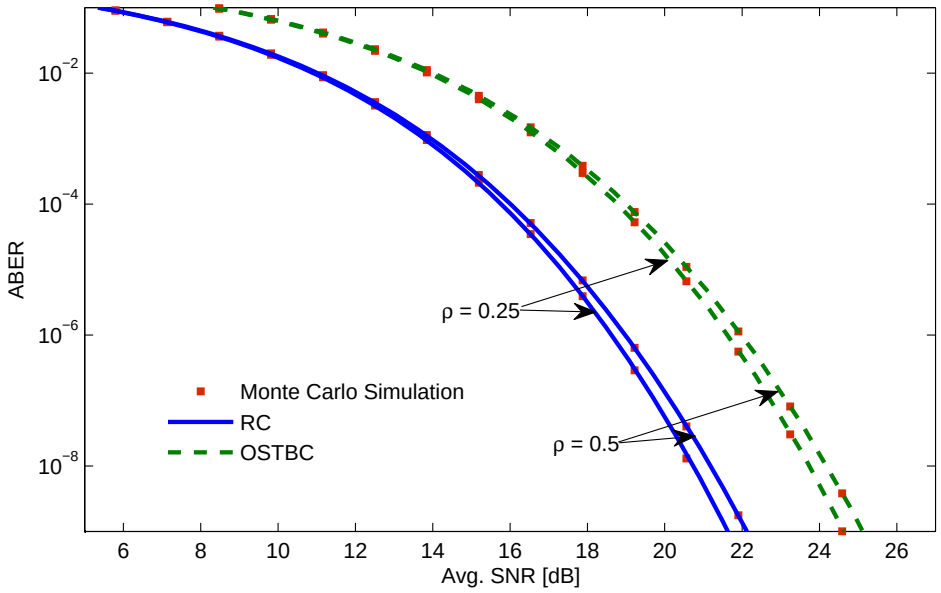


FIGURE 3.5 – Correlated LN with $\sigma_x = 0.1$, $\mu_x = -\sigma_x^2$, $N_t = 2$ and $\alpha = 0$ dB.

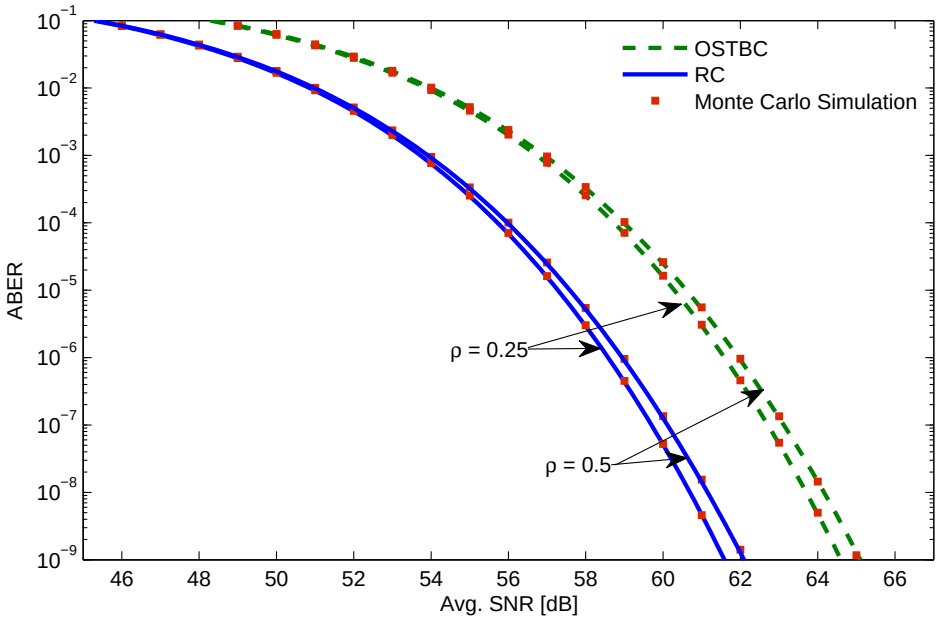


FIGURE 3.6 – Correlated LN with $\sigma_x = 0.1$, $\mu_x = -\sigma_x^2$, $N_t = 2$ and light fog.

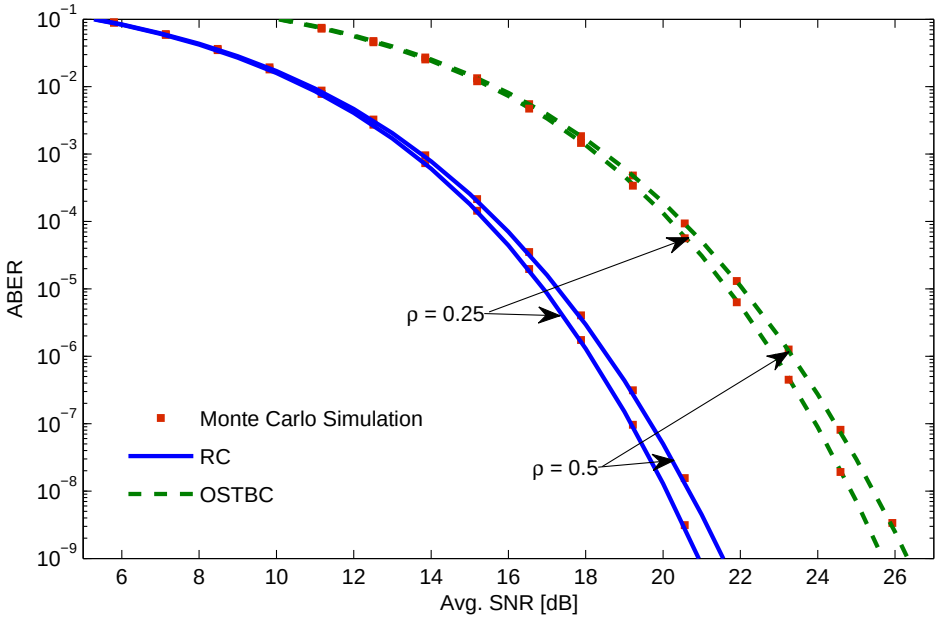


FIGURE 3.7 – Correlated LN with $\sigma_x = 0.1$, $\mu_x = -\sigma_x^2$, $N_t = 3$ and $\alpha = 0$ dB.

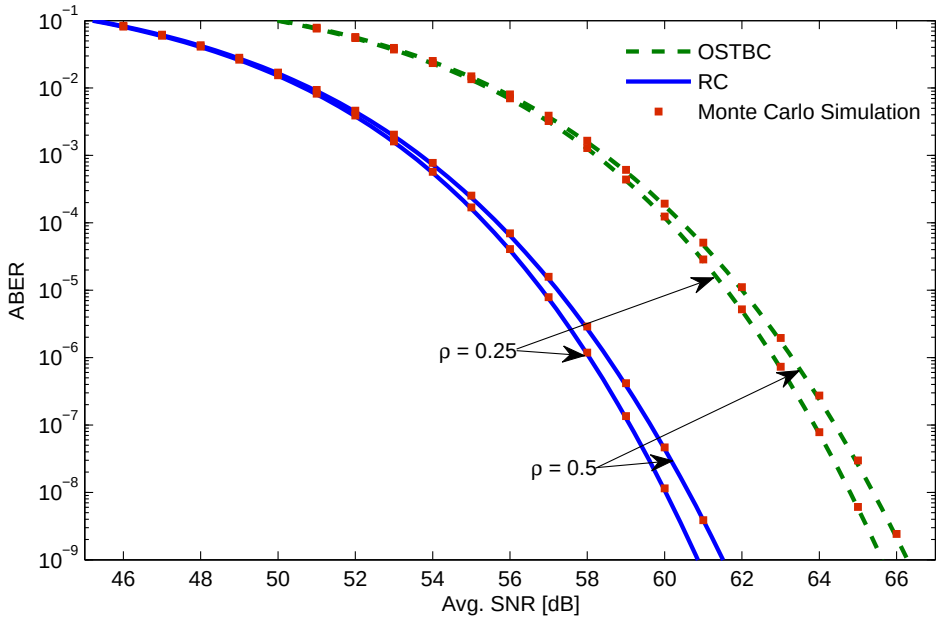


FIGURE 3.8 – Correlated LN with $\sigma_x = 0.1$, $\mu_x = -\sigma_x^2$, $N_t = 3$ and light fog.

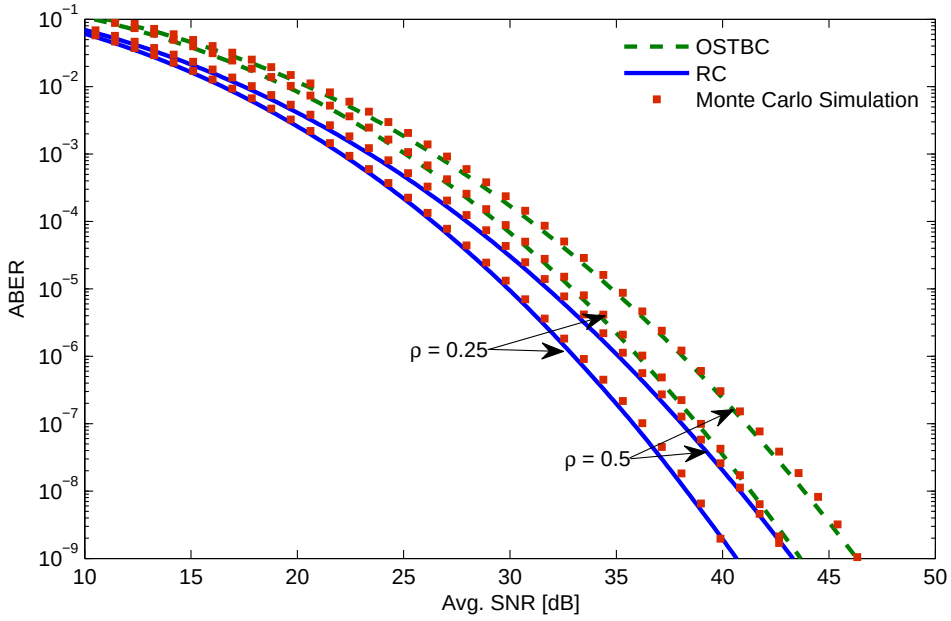


FIGURE 3.9 – Correlated LN with $\sigma_x = 0.374$, $\mu_x = -\sigma_x^2$, $N_t = 2$, and $\alpha = 0$ dB.

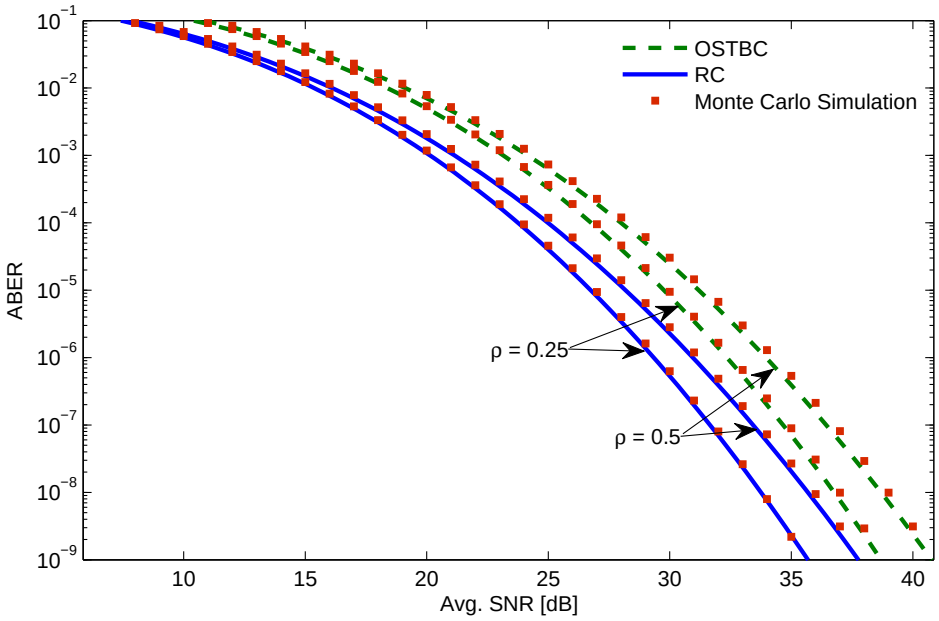


FIGURE 3.10 – Correlated LN with $\sigma_x = 0.3$, $\mu_x = -\sigma_x^2$, $N_t = 2$, and clear air.

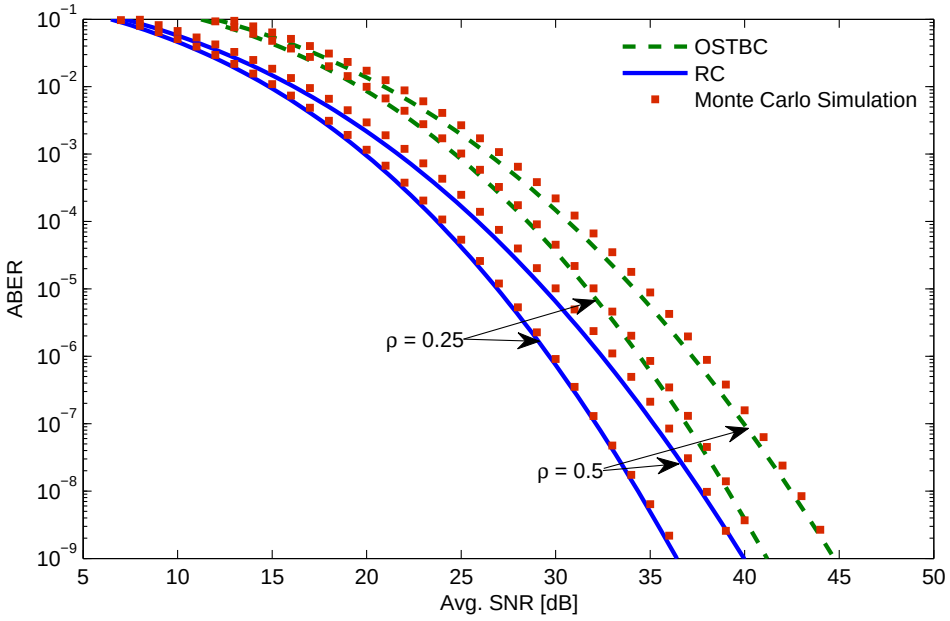


FIGURE 3.11 – Correlated LN with $\sigma_x = 0.374$, $\mu_x = -\sigma_x^2$, $N_t = 3$ and $\alpha = 0$ dB.

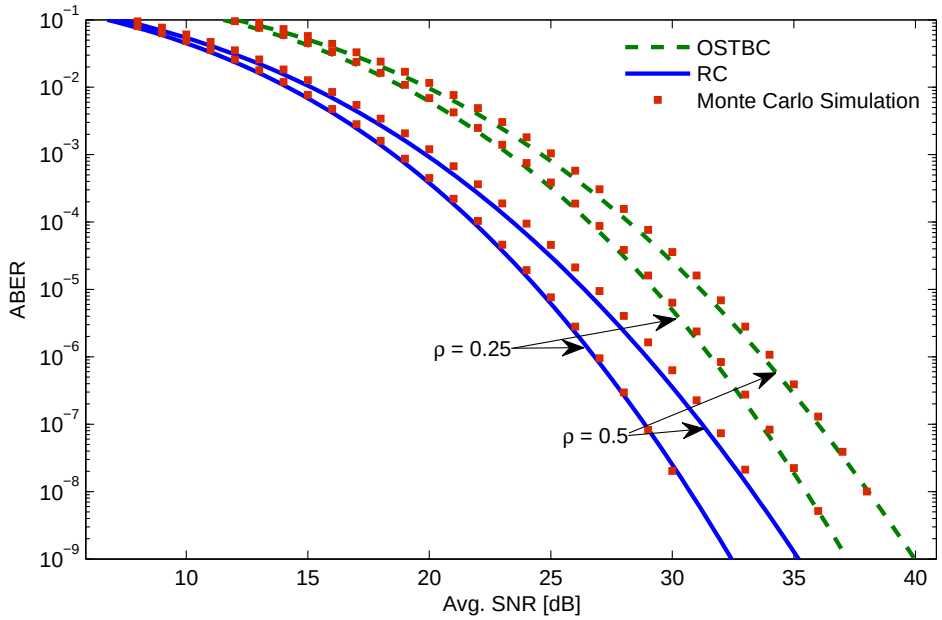


FIGURE 3.12 – Correlated LN with $\sigma_x = 0.3$, $\mu_x = -\sigma_x^2$, $N_t = 3$ and clear air.

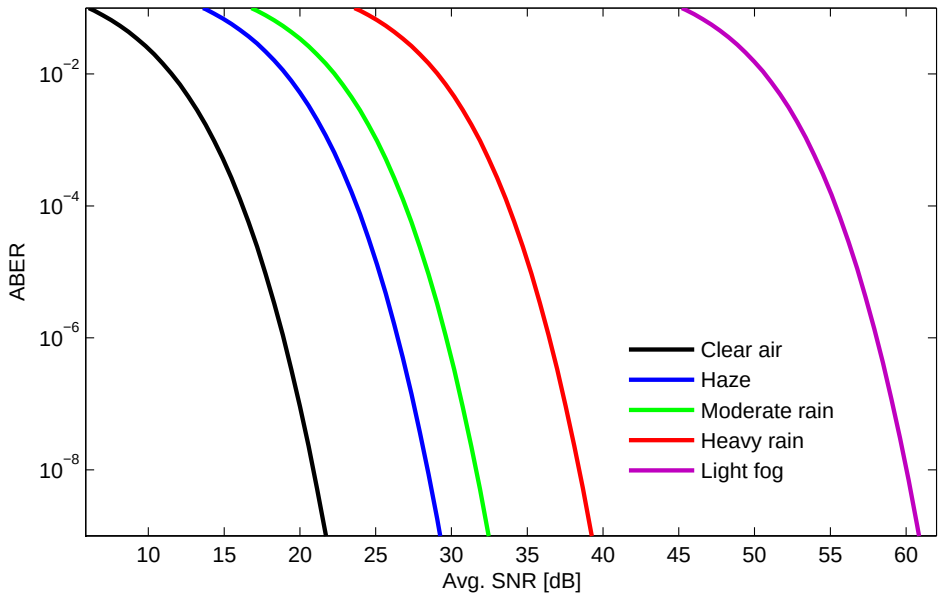


FIGURE 3.13 – Correlated LN using repetition codes with $\sigma_x = 0.1$, $\mu_x = -\sigma_x^2$, $\rho = 0.25$, $N_t = 3$ for different weather conditions.

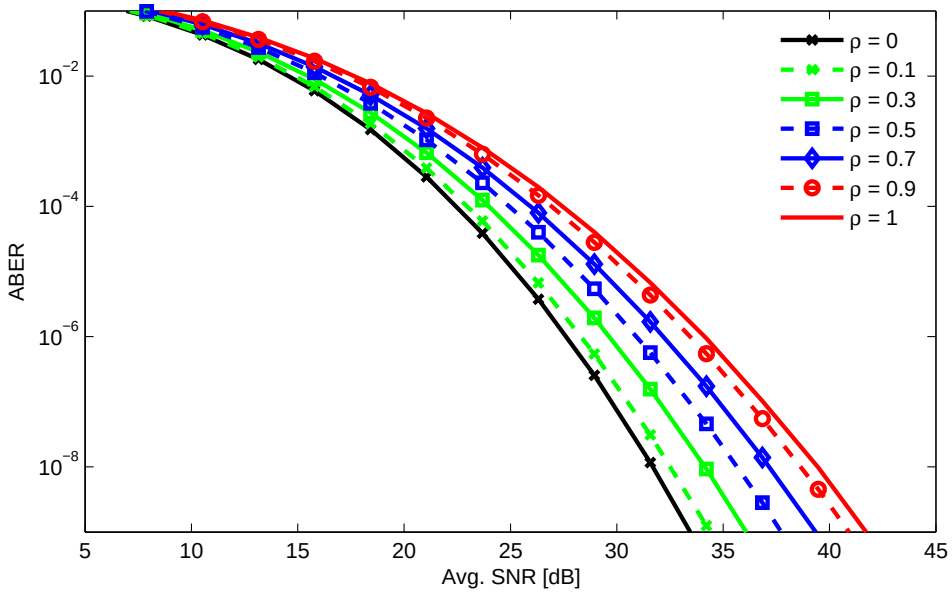


FIGURE 3.14 – RCs over correlated LN with $\sigma_x = 0.3$, $\mu_x = -\sigma_x^2$, $N_t = 2$, and clear air for different correlation coefficients.

links are studied where it is shown that fog degrades the FSO performance significantly. In Chapter 4, a high spectral efficient FSO link based on space shift keying (SSK) system is presented and compared with the state of the art of RC using multiple pulse position modulation.

4

Performance Analysis of Space Shift Keying Over Turbulent Channels

4.1 Introduction

Enhancing the spectral efficiency is the ultimate goal of all wireless techniques to cope up with the ever increasing demand of high data rate and better quality of service. To obtain high spectral efficiency, space shift keying (SSK) is considered in this chapter. We investigated the average bit error rate (ABER) performance of free-space optical (FSO) communication links for SSK over log-normal (LN) and negative exponential (NE) atmospheric turbulence channels.

SSK is compared with the state-of-the-art repetition codes (RCs) and a single-input single-output (SISO) systems using multiple pulse amplitude modulations (M-PAM). Simulation results show that the signal-to-noise ratio (SNR) gain of SSK largely increases with greater spectral efficiencies or higher turbulence effects. It is so difficult to use a probability density function (PDF) approach to obtain ABER expressions. Hence, a moment generation function (MGF) approach is used and an exact MGF for NE channel and an approximate MGF for LN channels are derived. Based on MGFs, a tight bounds for ABER expressions are derived. Finally, extensive Monte Carlo simulations have been run to validate the analytical analysis.

Table 4.1 summarizes the contribution of the most relevant works in the literature and our work by specifying the considered channel models. Figure 4.1 shows the main three axes considered in the thesis to mitigate various challenges facing FSO. The achieved contribution of the second axis, spatial modulation, is considered where a special case of spatial modulation called space shift keying is employed in this chapter.

4.2 System Model

A system with SSK modulation consisting of N_t transmitters and N_r receivers is illustrated in Figure 4.2. In our system, $\log_2(N_t)$ bits are transmitted at each particular time instant and are mapped to the spatial location, g, of one of the existing N_t transmitters. Hence, only one transmitter becomes active at any particular time instant [176]. The transmitted light propagates over a NE channel for a strong turbulence or a LN channel for a moderate turbulence. Furthermore, it is assumed that the received signal

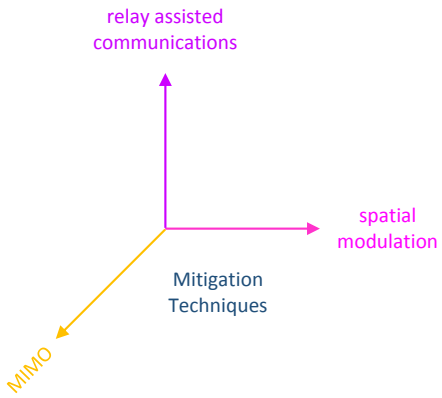


FIGURE 4.1 – The main axes of the research.

TABLE 4.1 – Comparison between our SSK scheme & the closed literature works

Reference	Channel Model	Contributions
[75]	indoor optical wireless (multipath)	applying spatial modulation (SM) for indoor optical communications
[84]		SM outperforms RCs for spectral efficiencies ≥ 4 bit/s/Hz
[85]	gamma-gamma	RCs outperforms SSK for spectral efficiency $= 1$ bit/s/Hz
[87]	LN & gamma-gamma	spatial pulse position amplitude modulation outperforms SSK for spectral efficiencies ≥ 2 bit/s/Hz
Our work	LN & NE (to model weak-to-strong turbulence)	SSK outperforms RCs over moderate-to-strong turbulence for spectral efficiencies ≥ 4 bit/s/Hz

suffers from shot, thermal and dark noises. The shot noise is assumed to dominate other noise sources [76] and it can be modeled as an Additive White Gaussian Noise (AWGN).

The received signal vector $\mathbf{r}$ is given by

$$\mathbf{r} = \eta \mathbf{H}\mathbf{s} + \mathbf{n}, \tag{4.1}$$

where $\mathbf{r} \in \mathbb{C}^{N_r \times 1}$ with the received signal at the jth branch, r_j, η is the optical to electrical conversion coefficient, $\mathbf{H} \in \mathbb{C}^{N_r \times N_t}$ is the channel irradiance matrix with channel irradiance entries, $h_{jg} \geq 0$ denoting the channel irradiance between the active transmitter $g = 2^p; 1 \leq p \leq \log_2(N_t)$ and receiver $j = 1, \cdots, N_r$, $\mathbf{s} = [s_1 \dots s_{N_t}]^T$ is the transmitted signal vector with $[.]^T$ being the transpose operator and $\mathbf{n} \in \mathbb{C}^{N_r \times 1}$ is the received AWGN vector with entries, n_j at the receiver input with zero mean and variance $\sigma_n^2 = N_o/2$ with N_o being the noise power spectral density. A RC $M-$PAM

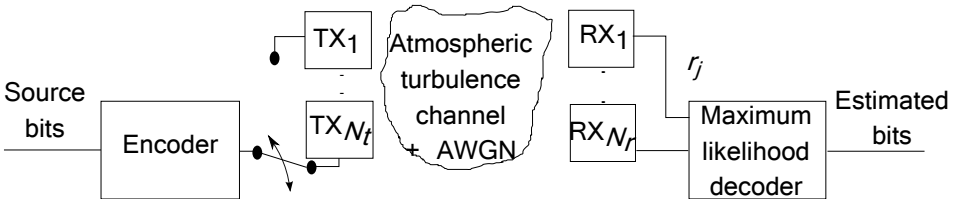


FIGURE 4.2 – Synoptic diagram of the proposed model.

signal has different intensity levels according to the symbol sequence as [84]

$$I_i^{\mathrm{PAM}} = \frac{\overline{I}}{M-1}\ (i-1), \qquad i = 1, 2, \cdots, M, \tag{4.2}$$

where $\overline{I}$ denotes the average light intensity and M is the signal constellation size.

Channel state information (CSI) is considered available at the receiver side. Therefore, the maximum likelihood (ML) decoder decides for the signal vector $\hat{\mathbf{s}}$ which minimises the Euclidean distance between the received signal vector $\mathbf{r}$ and all potential received signals leading to [84]

$$\hat{\mathbf{s}} = \underset{\mathbf{s}}{\operatorname{argmin}} ||\mathbf{r} - \eta \mathbf{H}\mathbf{s}||_{\mathrm{F}}^2, \tag{4.3}$$

where $||.||_F$ is the Frobenius norm [177].

For a **strong turbulence** condition, the channel irradiance h_{jg} can be modeled as an independent and identically distributed (i.i.d.) NE random variables (RVs) with a PDF given by [178]

$$f_{h_{jg}}(h_{jg}) = \exp(-h_{jg}). \tag{4.4}$$

However in **moderate turbulence**, h_{jg} can be modeled as i.i.d. LN RVs with a PDF given by [14]

$$f_{h_{jg}}(h_{jg}) = \frac{1}{h_{jg}\sqrt{8\pi\sigma_x^2}} \times \exp\left(-\frac{(\ln(h_{jg}) - 2\mu_x)^2}{8\sigma_x^2}\right), \tag{4.5}$$

where $h_{jg} = \exp(2x_{jg})$ with x_{jg} being modeled as an i.i.d. Gaussian RV with mean μ_x and variance σ_x^2. To ensure that the fading channel does not attenuate or amplify the average power, the fading irradiances are normalized as $\mathbf{E}[h_{jg}] = e^{2(\mu_x + \sigma_x^2)} = 1$ (i.e., $\mu_x = -\sigma_x^2$).

4.3 Performance Analysis

A tight upper bound of the bit error rate (BER) of SSK can be calculated by [84]

$$\mathrm{BER}_{\mathrm{SSK}}^{\mathrm{U}} \leq \frac{1}{N_t \log_2(N_t)} \sum_{g=1}^{N_t} \sum_{i=1}^{N_t} \mathrm{d_H}(b_g, b_i)\ Q\left(\frac{1}{N_r}\sqrt{\frac{\bar{\gamma}\log_2(N_t)}{2}\sum_{j=1}^{N_r} \mid h_{jg} - \hat{h}_{ji} \mid^2}\right), \tag{4.6}$$

where $Q(.)$ is the Gaussian-Q function as defined in Equation (3.11), with $\bar{\gamma} = (\eta \overline{I})^2/N_o$ being the average SNR [76]. The Hamming distance $\mathrm{d_H}(b_g, b_i)$ counts the number of bit errors between received symbol, b_i, and transmitted symbol, b_g [75]. Besides, the $1/N_r$ term is added to make sure that the total area of the receivers becomes the same as the single-input single-output (SISO) receiver aperture [76], and $\hat{h}_{ji}$ is the channel irradiance between the receiver j and the estimated active transmitter i.

A tight lower bound of the BER of RC $M-$PAM using maximum ratio combining (MRC) at the receiver is given by [179]

$$\mathrm{BER}_{\mathrm{RC}}^{\mathrm{L}} \geq \frac{2(M-1)}{M\log_2(M)} Q\left(\frac{1}{N_r N_t (M-1)}\sqrt{\frac{\overline{\gamma}\log_2(M) N_r}{2}\sum_{j=1}^{N_r}\left(\sum_{g=1}^{N_t} h_{jg}\right)^2}\right). \quad (4.7)$$

The term $1/N_t$ is added to ensure that the total power for the N_t transmitters is equivalent to the active transmitter of SSK system [76] and the term $\sqrt{N_r}$ is due to the use of MRC where the noise variance in each aperture is equal to $N_o/2N_r$ [76].

4.4 Average BER Probability of SSK Over Turbulent Channels

Indoor optical wireless channel is mainly affected by multi-path, while FSO communication is affected by atmospheric turbulence which causes scintillation of the laser beam due to temperature and pressure variations. As such, concluding similar behavior of SSK system [84,179] over both channels is not straightforward. Also, the derived expressions for indoor channel can not be directly used in FSO channels. For this reason, we derived an exact MGF of the absolute difference of two NE RVs and an approximated MGF of the absolute difference of two LN RVs. The derived MGFs are used to derive tight bound of the ABER of SSK over LN and NE channels.

4.4.1 Negative exponential channels

If X and Y are two independent RVs and $U = X - Y$. It is well known that the PDF of U is equal to the cross-correlation between the two PDFs as in [180, Equation (4.160)]

$$f_U(u) = \int_{-\infty}^{\infty} f_X(u+y) f_Y(y) dy. \quad (4.8)$$

Let $X \geq 0$ and $Y \geq 0$ be i.i.d. NE RVs, then it can be shown in [177, Equation (3.310)] that $f_U(u) = \exp(-|u|)/2$. If $Z = |U| = \mid h_{jg} - \hat{h}_{ji} \mid$ then $f_Z(z) = f_U(z) + f_U(-z) = \exp(-z)$. The histogram of the absolute difference of the two NE RVs and exact NE PDF are depicted in Figure 4.3. The PDF of the electrical SNR, $\gamma = z^2\bar{\gamma}$, can be obtained from the PDF of Z

$$f_\gamma(\gamma) = \frac{1}{2\sqrt{\gamma\bar{\gamma}}} \exp\left(-\sqrt{\frac{\gamma}{\bar{\gamma}}}\right), \qquad \gamma > 0. \quad (4.9)$$

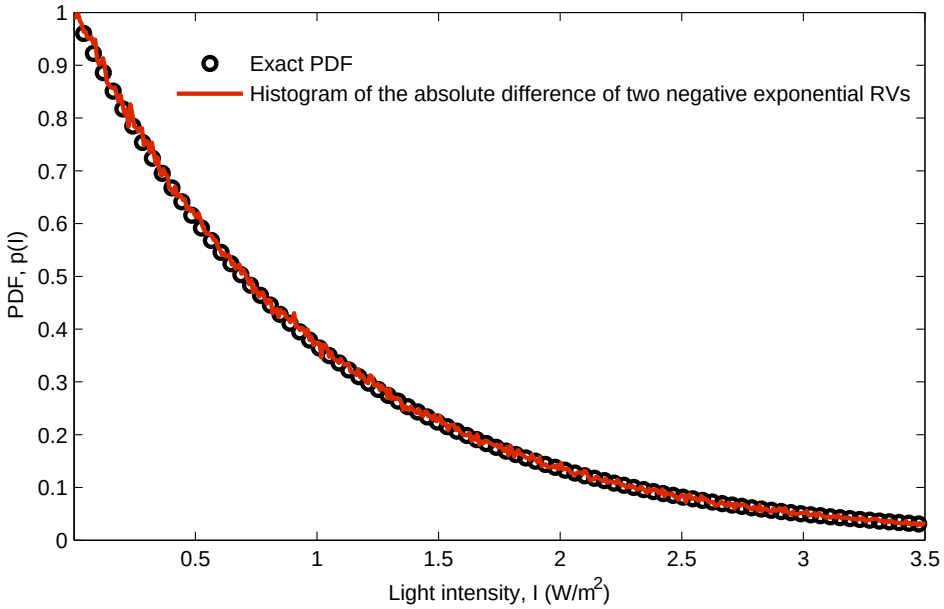


FIGURE 4.3 – Histogram of the absolute difference of the two NE RVs.

The MGF is defined by [117]

$$\Psi_\gamma(-s) = \int_0^\infty \exp(-s\gamma) f_\gamma(\gamma) d\gamma. \tag{4.10}$$

Using [177, Equation (3.322/2)], the MGF of Equation (4.10) can be derived as

$$\Psi_\gamma(-s) = \sqrt{\frac{\pi}{s\bar{\gamma}}} \exp\left(\frac{1}{4s\bar{\gamma}}\right) Q\left(\sqrt{\frac{1}{2s\bar{\gamma}}}\right), \qquad s > 0. \tag{4.11}$$

Since the RVs are i.i.d., the MGF of their difference becomes independent of the transmitter indices (i and g). Therefore, the Q function can be taken outside the summation in Equation (4.6) and the two-fold summation can be replaced by [181]

$$\frac{1}{N_t \log_2(N_t)} \sum_{g=1}^{N_t} \underbrace{\sum_{i=1}^{N_t} \mathrm{d_H}(b_g, b_i)}_{N_t \log_2(N_t)/2} = \frac{N_t}{2}. \tag{4.12}$$

with the use of $Q(x) \approx \frac{1}{12} e^{-\frac{x^2}{2}} + \frac{1}{4} e^{-\frac{2x^2}{3}}$ which is accurate for $x > 0.5$ [182] and Equation (4.12), Equation (4.6) can be rewritten as

$$\mathrm{BER}_{\mathrm{SSK}}^{\mathrm{U}} \leq \frac{N_t}{24} \exp\left(-\frac{\sum_{j=1}^{N_r} \gamma_j \log_2(N_t)}{4N_r^2}\right) + \frac{N_t}{8} \exp\left(-\frac{\sum_{j=1}^{N_r} \gamma_j \log_2(N_t)}{3N_r^2}\right). \tag{4.13}$$

The upper bound of the ABER probability of SSK over NE channels can be obtained as

$$\mathrm{ABER}_{\mathrm{SSK}}^{\mathrm{U}} = \int_0^{\infty} \cdots \int_0^{\infty} \mathrm{BER}_{\mathrm{SSK}}^{\mathrm{U}} f_{\boldsymbol{\gamma}}(\boldsymbol{\gamma}) d\boldsymbol{\gamma}, \tag{4.14}$$

where $\boldsymbol{\gamma} = \gamma_1 \cdots \gamma_{N_r}$ and since the RVs are i.i.d., the total MGF is the product of the individual MGFs as

$$\Psi_T(-s) = \prod_{j=1}^{N_r} \Psi_{\gamma_j}(-s) = \Psi_{\gamma}(-s)^{N_r}. \tag{4.15}$$

The upper bound of the ABER using Equations (4.11), (4.12) and (4.13), is derived as

$$\mathrm{ABER}_{\mathrm{SSK}}^{\mathrm{U}} \leq \frac{N_t c}{2} \left(\frac{1}{12} \Psi_{\gamma} \left(-\frac{\log_2(N_t)}{4N_r^2} \right)^{N_r} + \frac{1}{4} \Psi_{\gamma} \left(-\frac{\log_2(N_t)}{3N_r^2} \right)^{N_r} \right), \tag{4.16}$$

where c is added to improve the tight bound of the ABER of SSK over LN and NE channels. Extensive simulations and different values of N_t and N_r showed that $c = 0.8$ will improve the tight bound for $N_r > 2$. SSK uses only an active transmitter at any time instance, so it cannot provide transmit diversity.

4.4.2 LN channels (moderate turbulence)

If X and Y are i.i.d. LN RVs, there exists no closed-form expression for the PDF $f_Z(z)$ of $Z = |X - Y|$. Hence, obtaining the ABER of SSK system over LN channel is analytically not possible. However, we assume that $f_Z(z)$ for moderate turbulence can be approximately modeled by Gamma-Gamma (G-G) distribution. G-G channel represents the effective number of large-scale and small-scale eddies denoted by a and b, respectively [14]. To demonstrate the accuracy of this approximation, Figure 4.4 shows a comparison between the exact and approximate PDF of the absolute difference of two LN RVs of $\sigma_x = 0.37$. In our study, extensive simulations are used to obtain accurate estimates of a and b. Figure 4.4 shows that G-G distribution with $a = 3.3$ and $b = 1.1$ achieve accurate approximation of $f_Z(z)$.

The MGF of G-G distribution using the series representation which was originally proposed by [118], $\Psi_I(-s)$, and after a few manipulations the MGF of the SNR of G-G [117] is given by,

$$\Psi_{\gamma}(-s) = \sum_{p=0}^{\infty} \left[d_p(b,a) \Gamma\left(\frac{b+p}{2} \right) (s\bar{\gamma})^{-\frac{b+p}{2}} + d_p(a,b) \Gamma\left(\frac{a+p}{2} \right) (s\bar{\gamma})^{-\frac{a+p}{2}} \right], \tag{4.17}$$

where $\Gamma(w)$ is the gamma function defined as $\Gamma = \int_0^{\infty} t^{w-1} \exp(-t) dt$ and $d_p(f,v)$ is given as

$$d_p(f,v) = \frac{\pi (vf)^{f+p}}{2 \sin[\pi(v-f)] p! \Gamma(v) \Gamma(f) \Gamma(f-v+p+1)}. \tag{4.18}$$

By conducting many simulations, a saturation effect around 300 was observed for the infinite sum in Equation (4.17), which still has accurate numerical results. In this case, a tight bound for the ABER can be provided by substituting Equation (4.17) into Equation (4.16)..

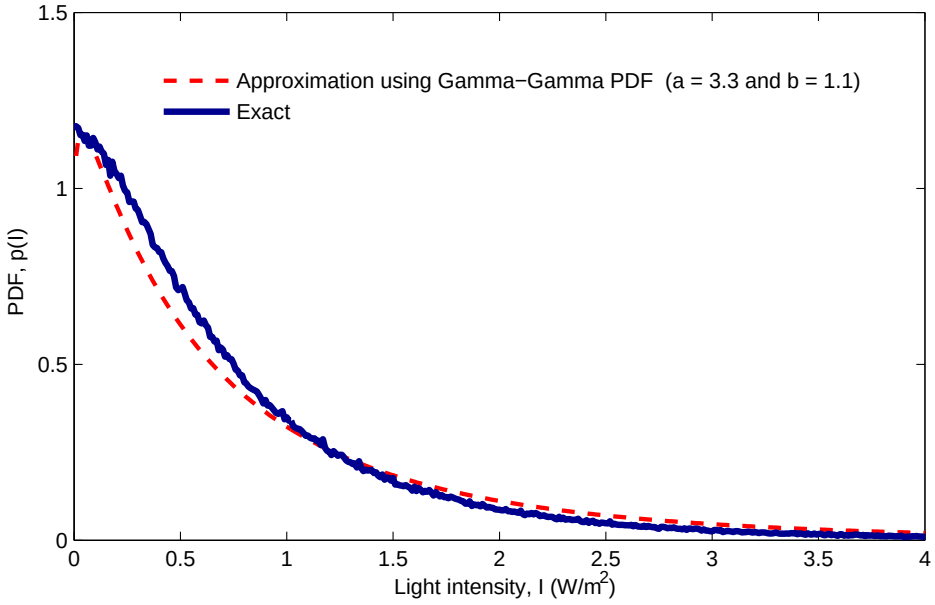


FIGURE 4.4 – Histogram of the absolute difference of two LN RVs ($\sigma_x = 0.37$ and $\mu_x = -\sigma_x^2$).

4.4.3 LN channels (weak turbulence)

As mentioned in the previous section, $f_Z(z)$ must be approximately modeled by another PDF. In the case of weak turbulence (i.e., $\sigma_x = 0.1$ and $\mu_x = -\sigma_x^2$), it is derived in [183] that $f_U(u)$ can be approximated by a normal distribution, with the addition of the variances and the difference of the means then $f_Z(z)$ can be written as

$$f_Z(z) \approx \frac{2}{\sqrt{16\pi\sigma_x^2}} \exp\left(-\frac{z^2}{16\sigma_x^2}\right) \tag{4.19}$$

The histogram of the absolute difference of two LN RVs, for the weak turbulence case, is depicted in Figure 4.5. However the derivation of ABER for weak turbulence is omitted from this chapter as the superiority of the proposed SSK is only for moderate to strong turbulence.

4.5 Numerical Results and Discussions

In the analysis, the derived ABER performance of SSK and the semi-analytical ABER of RC $M-$PAM using Equation (4.7) are compared with respect to that of SNR. Different scenarios over NE or LN channels are employed while considering similar spectral efficiency for compared systems. Hence, M-PAM and SSK provide spectral efficiency of $\log_2(M)$ and $\log_2(N_t)$ bits/s/Hz, respectively.

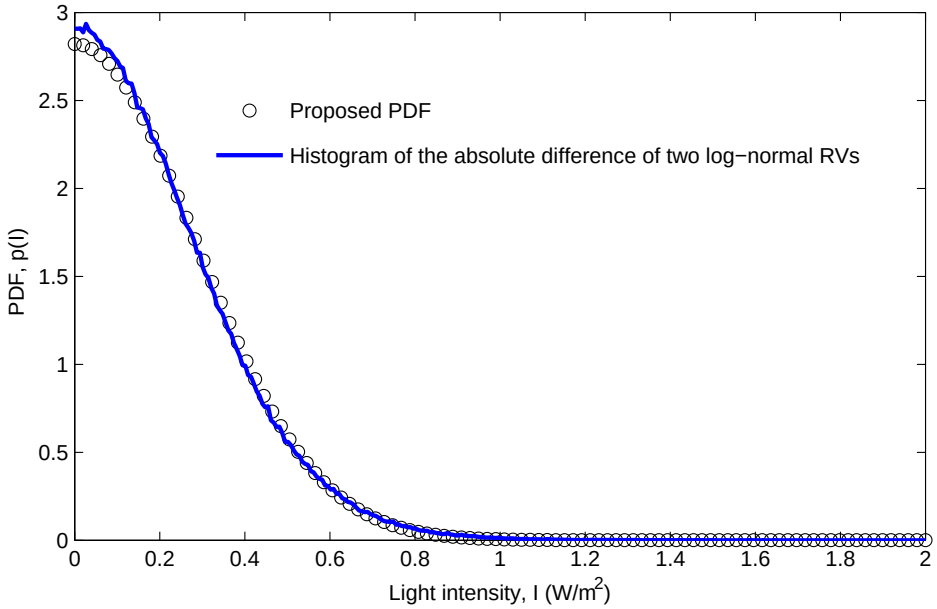


FIGURE 4.5 – Histogram of the absolute difference of two LN RVs ($\sigma_x = 0.1$ and $\mu_x = -\sigma_x^2$).

It is shown that the upper bound in Equation (4.6) is loose at low SNR values but tightens at pragmatic values. This is in accordance with other obtained results using similar bound as in [84, 179]. For NE, it is worth mentioning that the ABER of SISO is considered as a benchmark using Equation (4.7) with $N_t = N_r = 1$ as in [184]. For LN channels, the ABER of SISO is considered as in [79]. While using M-PAM for fair comparison with the same spectral efficiency of Figures 4.6-4.8.

Furthermore, the performance of commercially available MIMO systems using RCs with $N_t = N_r = 2$ and employing OOK modulation is compared with that of the proposed SSK system. For this purpose and for the sake of fair comparison, the power of OOK [1] is normalized by $\log_2(M)$.

To achieve a spectral efficiency of 3 bits/s/Hz, a 8×8 MIMO system is considered and the simulation results are reported in Figure 4.6. Analytical and simulation results show close match for a wide range of SNR values which support the analysis. Additionally, the same figure shows that SSK outperforms RC system for SNR < 28 dB.

This is due to the benefits of SSK over RC M-PAM, namely, increased SNR gain along with greater spectral efficiency or higher turbulence effects. This, while RC systems show better performance at higher SNR due to the high diversity gain. Increasing the number of receivers to 10 instead of 8 enhances the performance of SSK systems as

1. $\bar{\gamma}$ is proportional to the square of the intensity modulation and direct detection (IM/DD) optical power

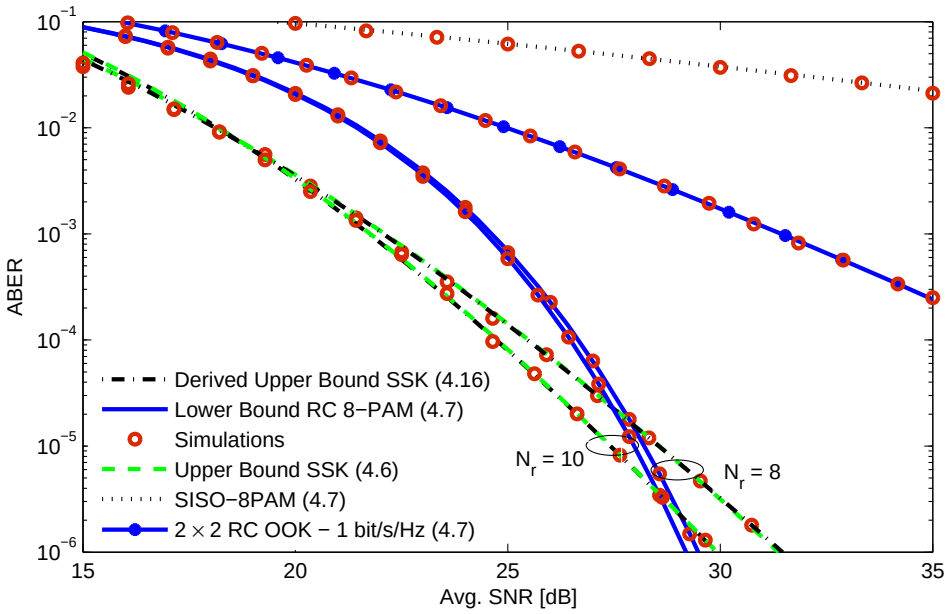


FIGURE 4.6 – Comparison of space shift keying and repetition codes with spectral efficiency = 3 bits/s/Hz in a NE channel (strong turbulence) with $N_t = 8$ and the number of receivers $N_r \, \epsilon$ [8 10].

compared to RC for high SNR. The SSK system gains about 2 dB in SNR at ABER of 10^{-6}.

Figure 4.7 shows the results of increasing the spectral efficiency to 4 bits/s/Hz. This increase is made by considering a 16×16 MIMO setup. SSK system shows superior performance as compared to RC and a gain of about 6.5 dB is achieved at ABER of 10^{-6}. Simulation results in Figure 4.7 depict the case of an ABER of 10^{-9} and shows the accuracy of the Q-function approximation [185].

Figure 4.8 shows the case of a moderate turbulence in a LN channel with $\sigma_x = 0.37$ as an example of a moderate turbulence. Based on the approximation, the results of which are shown in Figure 4.4, the MGF of G-G is used to derive a tight bound ABER for SSK over LN channel. This approximation leads to a narrow gap between the upper bound Equation (4.6) and the derived lower bound of SSK. This is unlike the results shown in Figures 4.6 and 4.7, which are based on an exact MGF of the absolute difference of NE RVs.

Obtained results show that at an ABER of 10^{-6}, SSK gains 4 dB and 7.5 dB over RC 16-PAM and RC OOK (2×2), respectively. The SNR corresponding to RC illustrated in Figure 4.8 is lower than that of the RC illustrated in Figure 4.7 by 0.3 dB, while SSK system is shown to perform better in strong turbulent channels as compared to moderate turbulent channels. This is mainly because the ABER of SSK system is not determined by the actual channel realizations as in the case of RCs and SISO, rather

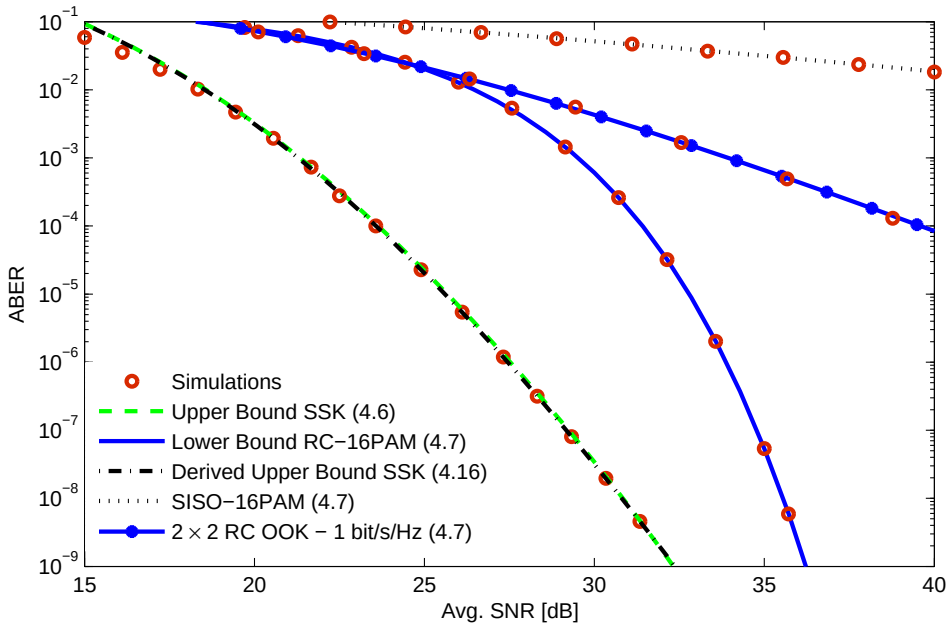


FIGURE 4.7 – Comparison of space shift keying and repetition codes with spectral efficiency = 4 bits/s/Hz in a NE channel (strong turbulence), $N_t = N_r = 16$.

by the differences among different channels associated with various transmitters. It is shown that the SSK system outperforms RC $M-$PAM system for a large number of transmitters.

Since, the SSK uses a single transmitter at each time instant and all others are off for that time. Hence, single-stream-based low-complexity ML detection is employed. As such, the synchronization and the complexity are significantly reduced ; this fact enables the use of large number of transmitters.

Figure 4.9 depicts the lack of the SNR gain of SSK system compared to RC $M-$PAM system over weak turbulence channels at the same ABER. Adaptive selection between SSK and RCs can be obtained according to the channel state information at the transmitter. In this case, the SNR gain will be enhanced at the expenses of creating a feedback link between transmitter and receiver which increases overall system complexity.

Finally, Figure 4.10 shows the accuracy of the Q approximation by comparing the conditional BER of Equation (4.6) with Equation (4.13) for parametric SNR values using spectral efficiency = 4 bits/s/Hz in a NE channel (strong turbulence), $N_t = N_r = 16$.

4.6 Summary

Data volumes in wireless multimedia applications (e.g., video on demand and interactive video gaming) is increased by a factor of ten every five years associated with an

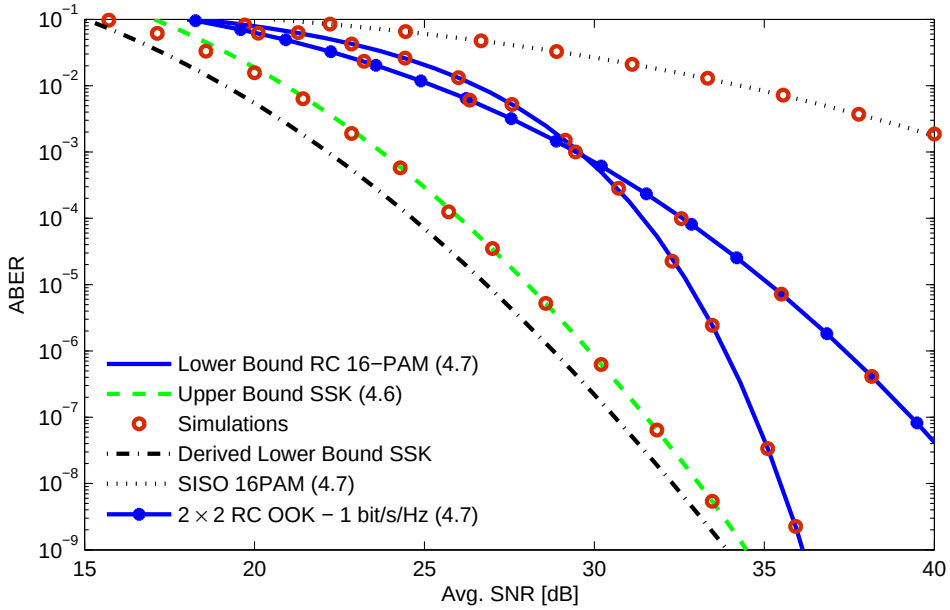


FIGURE 4.8 – Comparison of space shift keying and repetition codes with spectral efficiency = 4 bits/s/Hz in a LN channel with $\sigma_x = 0.37$ (moderate turbulence), $N_t = N_r = 16$.

increase of energy consumption [186]. Moreover, the main goal for wireless communication companies is to cut energy costs therefore our analyzed system will be important for the next generation of FSO. Our proposed link achieves triple or quadruple data rate without changing both the energy efficiency of the link and the bandwidth, increases the propagation distance and decreases the complexity of the receiver. For the current FSO companies, they already multiplied the number of apertures by four. In the next FSO generation, the companies may multiply it again by four according to the need of the market.

In this chapter, the ABER performance of FSO links with SSK over NE and LN atmospheric turbulence channels are investigated. Tight upper and lower bounds for ABER expressions corresponding to NE channels and LN channels, respectively are obtained. In comparison to SISO and RC M-PAM techniques, our results are in favor of SSK FSO links for high spectral efficiencies applications or channel high turbulence effects. Moreover, increasing the number of receivers is shown to have yield lower SNR in SSK systems as compared to RC $M-$PAM systems. In Chapter 5, MISO multi-hop decode-and-forward FSO system, considering different turbulence conditions and path loss attenuations, is proposed and compared to direct link and MISO systems.

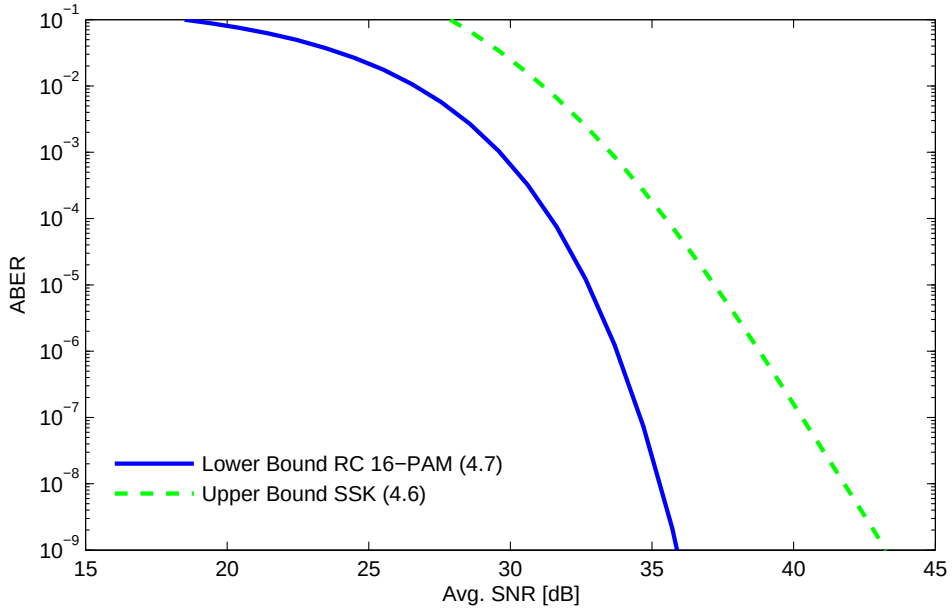


FIGURE 4.9 – Comparison of space shift keying and repetition codes with spectral efficiency = 4 bits/s/Hz in a LN channel with $\sigma_x = 0.1$ (weak turbulence), $N_t = N_r = 16$.

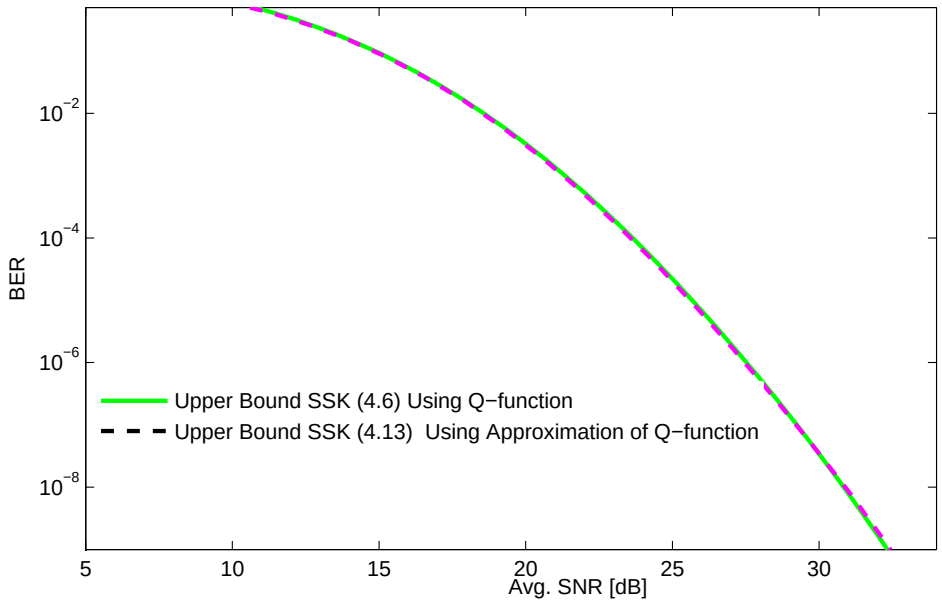


FIGURE 4.10 – A comparison between upper bound SSK using Q-function and using the approximation of Q-function on space shift keying.

5

Performance Analysis of MISO Multi-hop Over Log-normal Channels

5.1 Introduction

The performance analysis of a multiple-input single-output (MISO) multi-hop decode-and-forward (DF) relaying free-space optical (FSO) communication system is discussed in this chapter. Intensity modulation and direct detection (IM/DD) are employed for cheap and simple transmission and reception. Weak and moderate turbulence are modeled by log-normal (LN) channels. The transmitted optical signal is also affected by several challenges such as different weather attenuation effects and geometric losses. It is shown that multi-hop is a powerful mitigation technique for most challenges in FSO communication systems. MISO multi-hop is compared with a direct link and MISO systems considering correlation effects among transmitters. MISO multi-hop FSO systems have a higher signal-to-noise ratio (SNR) gain than their counterparts, especially for high attenuation links. Monte Carlo simulations corroborate the accuracy of the derived average bit error rate (ABER) expressions.

Table 5.1 summarizes the contribution of the most relevant works in the literature and our work by specifying the considered channel models. Figure 5.1 shows the main three axes considered in the thesis to mitigate various challenges facing FSO. The third axis, relay-assisted multi-hop scenario is considered in this chapter.

5.2 System Description

5.2.1 Single-Input Single-Output

A single-input single-output (SISO) scheme implementation of FSO system is depicted in Figure 5.2. On-off keying (OOK) signals are transmitted through laser over a LN channel where path losses result from different weather conditions and geometric loss are considered. The received signal at the photodetector input is given by [79]

$$r(t) = s(t)\ \eta\ I + n(t), \tag{5.1}$$

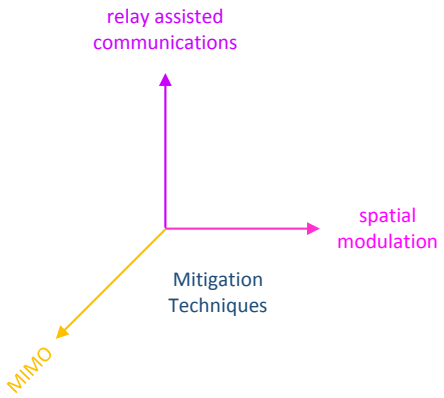


FIGURE 5.1 – The main axes of the research.

TABLE 5.1 – Comparison between our MISO multi-hop scheme & the closed literature works

Reference	Channel Model	Contributions
[140]	LN	cooperative optical amplify and forward relay outperforms MISO using repetition codes (RCs)
[137]	LN & Rayleigh	cooperative decode and forward relay outperforms MISO using RCs
[156]	gamma-gamma	cooperative decode and forward relay outperforms MISO using transmit laser selection under certain relay location
Our work	correlated LN (to model correlation among transmitters)	MISO multi-hop outperforms MISO using RCs

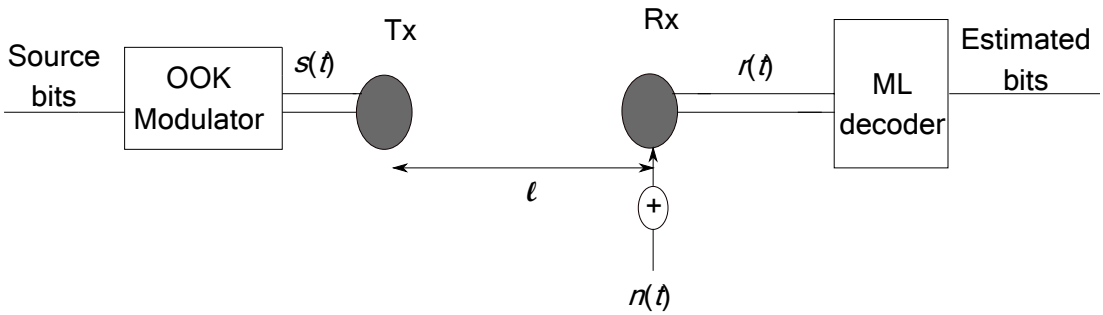


FIGURE 5.2 – FSO SISO system using OOK modulation.

where $s(t)$ represents the transmitted electrical signal, η is the optical-to-electrical conversion coefficient, I stands for the received signal light intensity given by [9, 79],

$$I = \beta_n \, \overline{I} \, h, \tag{5.2}$$

with $\overline{I}$ being the received signal light intensity without considering the channel effect, $h = e^{2x}$ is the channel irradiance from the transmitter to the receiver with x being modeled as independent and identically distributed (i.i.d.) Gaussian random variables (RVs) with a mean μ_x and a variance σ_x^2 and β_n is the normalized path loss coefficient, $\beta_n = \beta(\ell)/\beta_d(\ell)$ with $\beta(\ell)$ is the path loss coefficient and $\beta_d(\ell)$ being the path loss of direct link in clear air conditions. $n(t)$ in Equation (5.1) is an additive white Gaussian noise (AWGN), with zero mean and variance $\sigma_n^2 = N_o/2$, resulting from mainly background noise [11].

Due to beam divergence loss, the transmit beam diverges and illuminates the static receiver. Assuming a static receiver, without laser tracking methods, spherical wave propagation is considered [39]. The channel variance is calculated based on the Rytov theory as a function of the distance [79]

$$\sigma_x^2(\ell) = 0.124\ k^{7/6} C_n^2\ \ell^{11/6}, \tag{5.3}$$

with ℓ being the link distance per hop (in km), k is the wave number, C_n^2 is the refractive index constant and $\sigma_x(\ell) \leq 0.37$ for FSO communication as discussed in subsection 3.3.2. Usually C_n^2 is assumed to be independent on distance and its typical values vary from 10^{-17} to 10^{-13} $\mathrm{m}^{-2/3}$ [2].

The path losses can be calculated by combining weather attenuation [9] with geometric losses [131] as

$$\beta(\ell) = 10^{-\alpha\ell/10} \times \frac{D_R^2}{(D_T + \theta_T \ell)^2}, \tag{5.4}$$

with α is the weather-dependent attenuation coefficient (in dB/km), D_R and D_T are the receiver and transmitter aperture diameters (in m), and θ_T is the optical beam divergence angle (in mrad). The values of α, for different weather conditions, are provided in Table 2.1. Acceptable values for D_R, D_T and θ_T are given in [14, 187].

Hence, h becomes a LN RVs with probability density functions (PDF) given by [90]

$$f_h(h) = \frac{1}{h\sqrt{8\pi\sigma_x^2}} \times \exp\left(-\frac{(\ln(h) - 2\mu_x)^2}{8\sigma_x^2}\right). \qquad h > 0 \tag{5.5}$$

To ensure that the fading channel does not attenuate or amplify the average power, the fading coefficients, throughout the chapter, are normalized as $\mathbf{E}[h] = e^{2(\mu_x + \sigma_x^2)} = 1$, (i.e., $\mu_x = -\sigma_x^2$).

Using Equation (5.2), the instantaneous SNR at the receiver input [76], γ, can be obtained as

$$\gamma = \frac{(\eta I)^2}{N_o} = \frac{\eta^2 \beta_n^2\ \overline{I}^2\ h^2}{N_o} = \beta_n^2\ \bar{\gamma}\ h^2, \tag{5.6}$$

with $\bar{\gamma} = (\eta\overline{I})^2/N_o$ being the average SNR [76].

After performing a simple transformation of the RVs in Equation (5.5) and by using Equation (5.6), the PDF of the instantaneous SNR becomes (see Appendix B.3)

$$f_\gamma(\gamma) = \frac{1}{\sqrt{32\pi\sigma_x^2\gamma}} \exp\left[-\frac{\left(\ln\left(\frac{\gamma}{\beta_n^2\bar{\gamma}}\right) + 4\sigma_x^2\right)^2}{32\sigma_x^2}\right]. \tag{5.7}$$

The conditional bit error rate (BER) of a FSO communication system using OOK modulation is given [1] by [76]

$$\Pr(e|\gamma) = Q\left(\sqrt{\frac{\gamma}{2}}\right), \tag{5.8}$$

where $Q(.)$ is the Gaussian-Q function as defined in Equation (3.11). Using $Q(x) \approx \frac{1}{12}e^{-\frac{x^2}{2}} + \frac{1}{4}e^{-\frac{2x^2}{3}}$ which is accurate for $x > 0.5$ [182] to Equation (5.8) yields

$$\Pr(e|\gamma) \approx \frac{1}{12}\exp\left(-\frac{\gamma}{4}\right) + \frac{1}{4}\exp\left(-\frac{\gamma}{3}\right), \tag{5.9}$$

which is an approximated closed-form expression of the BER for FSO SISO systems using OOK modulation.

Now, to consider the impact of LN channel and path losses effects on the BER, the ABER can be obtained by averaging the BER Equation (5.9) using Equation (5.7) as

$$\text{ABER} = \int_0^\infty \Pr(e|\gamma) f_\gamma(\gamma) d\gamma. \tag{5.10}$$

The above integral can be approximated by using Hermite polynomial of Equation (3.20) yield an approximated closed-form solution given by

$$\begin{aligned}\text{ABER} \approx \frac{1}{12\sqrt{\pi}} \sum_{i=1}^{N} w_i \exp\left(-\frac{\beta_n^2 \bar{\gamma}\ e^{-4\sigma_x^2 + z_i\sqrt{32\sigma_x^2}}}{4}\right) \\ + \frac{1}{4\sqrt{\pi}} \sum_{i=1}^{N} w_i \exp\left(-\frac{\beta_n^2 \bar{\gamma}\ e^{-4\sigma_x^2 + z_i\sqrt{32\sigma_x^2}}}{3}\right),\end{aligned} \tag{5.11}$$

where z_i and w_i are the zeros and the weights of the Hermite polynomial [174, page 924] of order N, respectively. It has been shown in [15], that accurate results for LN channels can be obtained when $N \geq 20$.

At the receiver side, maximum-likelihood (ML) decoder is considered to decode the received signals [173].

5.2.2 MISO Using Repetition Codes

A FSO MISO system, with N_t transmitters and using RCs, is depicted in Figure 5.3. In RCs system, OOK signals are transmitted simultaneously through N_t lasers over correlated LN channel with similar statistics as SISO scheme. The analytical model of MISO using repetition codes is discussed in details in sections 3.2 and 3.3. However, in this subsection, normalized path loss β_n is used.

Both correlated and uncorrelated effects among the transmitters are considered in this chapter. The assumption of uncorrelated channel paths assumes the spacing between

1. Many wireless optical books such as [58] define $\Pr(e|\gamma)$ as $Q(\sqrt{\gamma})$, to be compatible with the probability of error of OOK in radio frequency digital communications system. In our work, we followed the notation adopted in [76] to compare our work with their works.

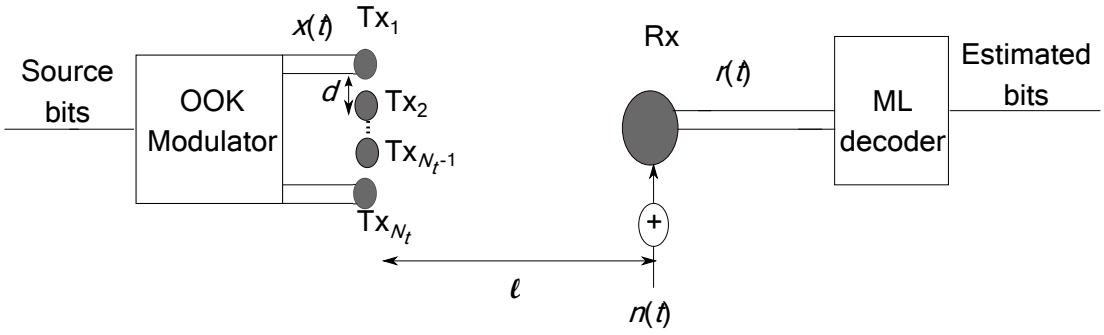


FIGURE 5.3 – MISO scheme using RCs.

each two successive transmitters, d, is larger than the fading correlation length $d_o \approx \sqrt{\lambda \ell}$ with λ being the wavelength [188]. However, in many cases the available space for the transmitters may not be sufficient for such requirement [21].

Also, the total spacing among the transmitters must be within the field of view (FOV) of the receiver to avoid serious degradation of the ABER performance as shown in [80, Figure 1]. In fact, the spacing should be less than $\theta_f \ell$ meter, where θ_f is the FOV of the receiver in milliradians. (mrad) [80]. For example, if $\ell = 2$ km and $\theta_f \cong 5$ mrad, then the length of transmitters, $(d \times (N_t - 1))$, should be less than 10 m apart [79, 90].

5.2.3 Multi-Hop DF Relaying

In this subsection, an approximate ABER closed-form expression for FSO multi-hop system using DF relays, depicted in Figure 5.4, is derived. Assuming that there are K

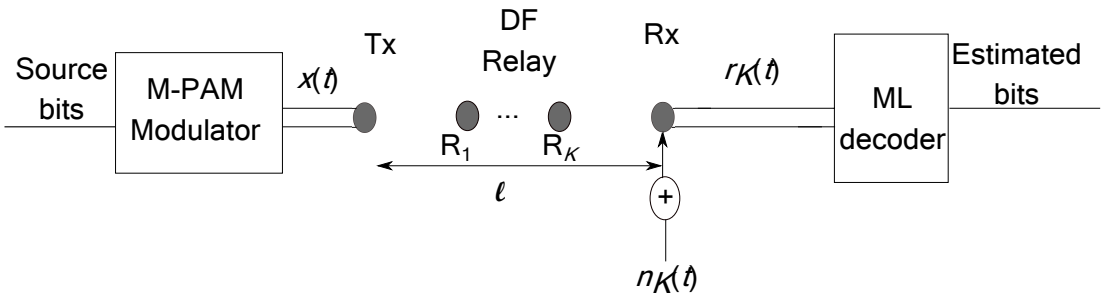


FIGURE 5.4 – Multi-hop DF relay scheme.

hops between the source and the destination and $r_k(t)$ is the received signal at the kth hop given by,

$$r_k(t) = s(t)\ \eta\ I_k + n_k(t), \qquad k = 1, \cdots, K. \tag{5.12}$$

In case of SISO and MISO schemes, one time slot is required for transmission. However, in this scheme K time slots are required. In order to achieve similar spectral efficiency

as compared to these systems, $2^{(K)}$-ary pulse amplitude modulation (PAM) modulation is considered. Besides, in DF system, every relay receives the signal, regenerates it and send it again either to the next relay or to the final destination. However, shorter communication links are created and the impact of turbulence effect σ_k and path loss β_k are significantly reduced. The calculation of σ_k and β_k are the same as given in Equation (5.3) and Equation (5.4), respectively.

The upper bound BER for multi-hop DF is given by [98]

$$\text{BER} \leq 1 - \prod_{k=1}^{K}(1 - \text{BER}_k). \tag{5.13}$$

Assuming all hops having the same statistical behavior, an approximated BER can be calculated by [189]

$$\text{BER} \approx \frac{1}{2}\left(1 - (1 - 2\text{BER}_k)^K\right). \tag{5.14}$$

The conditional BER of M-PAM modulation is derived in Appendix B.4 as

$$\Pr(e|\gamma) \approx \frac{2(M-1)}{M\log_2(M)} Q\left(\sqrt{\frac{P^2\log_2(M)}{(M-1)^2 R\sigma_n^2}}\right), \tag{5.15}$$

where P is the optical power and R is the bit rate. Following the same notation of Equation (5.8), γ is defined as

$$\gamma = \frac{2P^2}{\sigma_n^2 R}. \tag{5.16}$$

Now, applying the approximate Q function on Equation (5.15) and substituting in Equation (5.16) gives

$$\Pr(e|\gamma) \approx \frac{2(M-1)}{M\log_2(M)}\left[\frac{1}{12}\exp\left(-\frac{\gamma\log_2(M)}{4(M-1)^2}\right) + \frac{1}{4}\exp\left(-\frac{\gamma\log_2(M)}{3(M-1)^2}\right)\right]. \tag{5.17}$$

It is important to note that Equation (5.17) is a general expression of the conditional BER of FSO systems using M-PAM scheme and the expression for OOK in Equation (5.9) can be derived as a special case by setting $M = 2$.

Using Equation (5.17), the kth hop ABER of M-PAM FSO communication system under a LN channel and path loss attenuation effects can be calculated following similar steps as discussed above to obtain Equation (5.11) and is given by

$$\begin{aligned}\text{ABER}_\text{k} \approx{}& \frac{G}{12\sqrt{\pi}}\sum_{i=1}^{N} w_i \exp\left(-\frac{\log_2(M)\beta_{kn}^2\bar{\gamma}\; e^{-4\sigma_k^2 + z_i\sqrt{32\sigma_k^2}}}{4(M-1)^2}\right) \\ &+ \frac{G}{4\sqrt{\pi}}\sum_{i=1}^{N} w_i \exp\left(-\frac{\log_2(M)\beta_{kn}^2\bar{\gamma}\; e^{-4\sigma_k^2 + z_i\sqrt{32\sigma_k^2}}}{3(M-1)^2}\right),\end{aligned} \tag{5.18}$$

where $G = \frac{2(M-1)}{M\log_2(M)}$, and β_{kn} is the normalized path loss coefficient for multi-hop system with respect to the direct link in clear air conditions, $\beta_{kn} = \beta_k/\beta_d(\ell)$.

Assuming all ABER_k are equal, substituting Equation (5.18) in Equations (5.14) and (5.13), the final approximated closed form expression of the ABER of the multi-hop system and the upper bound ABER expressions are obtained, respectively.

5.2.4 MISO Multi-Hop DF Relaying

In this subsection, an approximate ABER closed-form expression for FSO MISO multi-hop system using DF relays, with N_t transmitters and using RCs, as depicted in Figure 5.5, is derived. This scheme is a hybrid MISO and multi-hop system that benefits from the advantages of both systems to mitigate the impact of FSO channel turbulence and attenuations.

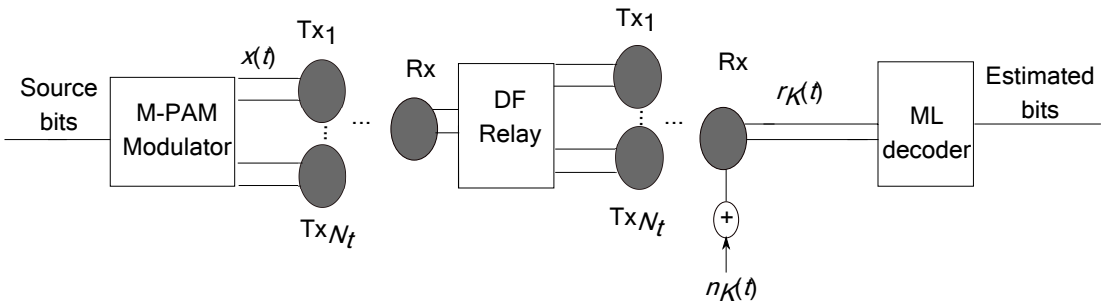


FIGURE 5.5 – MISO Multi-hop DF relay scheme.

Let us consider (K-1) relays where each relay receives the signal and re-transmits it simultaneously using N_t transmitters with RCs. The number of hops is assumed to be similar to the number of transmitters for each relay. The received signal at each hop is given by,

$$r_k(t) = s(t)\ \eta \sum_{i=1}^{N_t} I_{ki} + n_k(t), \qquad k = 1, \cdots, K. \tag{5.19}$$

Using Equation (5.18) and substitute σ_x by $c_{ij}^{'}$ which is the $(i,j)^{\text{th}}$ coefficient of $\mathbf{\Gamma}_{\text{sq}} = \mathbf{\Gamma}^{1/2}$, the kth hop ABER of M-PAM MISO multi-hop FSO communication

system is

$$\begin{aligned}
\mathrm{ABER_k} \approx & \sum_{n_1=1}^{N} \cdots \sum_{n_{N_t}=1}^{N} \left[\prod_{i=1}^{N_t} \frac{w_{n_i}}{\sqrt{\pi}} \right] \\
& \times \frac{G}{12} \exp\left(-\frac{\log_2(M)\beta_{kn}^2 \bar{\gamma}}{4(M-1)^2 N_t} \sum_{i=1}^{N_t} \left[\exp\left(\sqrt{32} \sum_{j=1}^{N_t} c_{ij}^{'} x_{n_j} - 4\sigma_k^2 \right) \right] \right) \\
& + \sum_{n_1=1}^{N} \cdots \sum_{n_{N_t}=1}^{N} \left[\prod_{i=1}^{N_t} \frac{w_{n_i}}{\sqrt{\pi}} \right] \\
& \times \frac{G}{4} \exp\left(-\frac{\log_2(M)\beta_{kn}^2 \bar{\gamma}}{3(M-1)^2 N_t} \sum_{i=1}^{N_t} \left[\exp\left(\sqrt{32} \sum_{j=1}^{N_t} c_{ij}^{'} x_{n_j} - 4\sigma_k^2 \right) \right] \right),
\end{aligned} \tag{5.20}$$

where N_t is added to Equation (5.20) to guarantee that the total power of the MISO system is equal to the power of a SISO system.

The spatial covariance matrix $\acute{\mathbf{\Gamma}}$ can be calculated as

$$\Gamma_{ij}^{'} = \sigma_k^2 \times \rho^{|i-j|}. \tag{5.21}$$

Substituting Equation (5.20) in Equation (5.14) and Equation (5.13), the final approximated closed form of ABER of the MISO multi-hop system and the upper bound ABER expressions are obtained, respectively.

5.3 Numerical Results and Discussions

In this section, numerical results are presented to validate the derived analysis in this chapter. The considered parameters are provided in Table 5.2. Derived analytical results are corroborated via Monte Carlo simulations and both results are shown to match closely for wide and pragmatic SNR values. In the obtained simulation results, 10^7 bits are transmitted for each depicted SNR value with 1000 iterations to achieve the target ABER of 10^{-9}. Throughout this chapter, relays are placed equidistant to each other to obtain the optimum performance as derived in [123].

In Figure 5.6, a clear air condition with moderate turbulence is assumed and a single relay is placed mid-distance between the source and the destination in a multi-hop system. The spectral efficiency of M-PAM is $\log_2(M)$. Hence, in order to achieve the spectral efficiency of SISO and MISO systems, 4-PAM modulation was employed. The obtained results clearly demonstrate the significant performance enhancement of SISO multi-hop system even in clear air conditions. SISO multi-hop system has SNR gains of about 11 dB and 22 dB at the target ABER as compared to uncorrelated MISO and SISO systems, respectively. A correlation of $\rho = 0.3$ is shown to degrade the performance of MISO system by about 3 dB. Moreover, correlated and uncorrelated

TABLE 5.2 – System configuration

Parameter	Symbol	Value
The target ABER		10^{-9}
Wavelength	λ	1550 nm
Receiver diameter	D_R	0.2 m
Transmitter diameter	D_T	0.2 m
The optical beam divergence angle	θ_T	2 mrad
The link distance	L	1.2 km
Refractive index constant	C_n^2	1.7×10^{-14} $m^{-2/3}$ in the morning and 5×10^{-14} $m^{-2/3}$ in strong sunlight condition
Weather-dependent attenuation coefficient	α	20 dB/km for light fog attenuation and 0.43 dB/km for clear air condition
Correlation coefficient	ρ	0 and 0.3

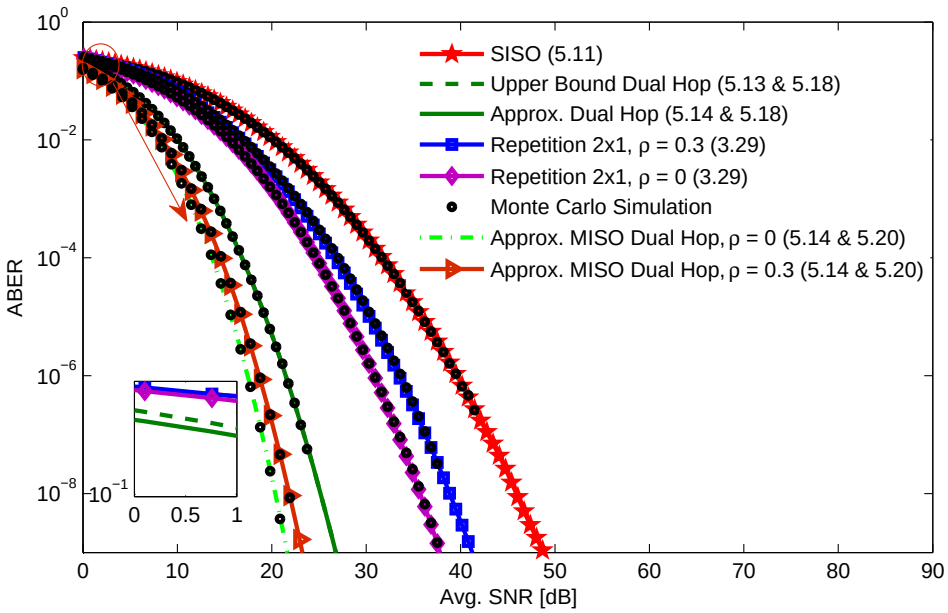


FIGURE 5.6 – ABER of single-relay multi-hop using one or two transmitters with 4-PAM modulation, two transmitters MISO using RCs and OOK, and SISO using OOK modulation FSO systems in LN fading channel and clear air conditions ($C_n^2 = 5 \times 10^{-14}$ $m^{-2/3}, \alpha = 0.43$ dB/km). From Equation (3.8), ρ in Equations (3.29) and (5.20) can be approximated as zero when $d \gg d_o$.

MISO multi-hop outperforms SISO multi-hop system by 3.4 dB and 5 dB, respectively.

There is an inversely proportional relationship between the turbulence strength and attenuation such as it is very unlikely that strong turbulence occurs during a fog event [175]. So, the impact of light fog with weak turbulence is considered in Figure 5.7. While light fog degrades the performance of all systems, it has a major impact on SISO and MISO systems as compared to multi-hop systems due to multi-hop systems have shorter hops that yields significant performance improvements. As compared to clear air condition results, shown in Figure 5.6, 35 dB and 31 dB, losses are reported at the target ABER for MISO and SISO systems, respectively. However, the losses are less than 19 dB in multi-hop systems.

Consequently, SISO multi-hop system still outperform other systems and SNR gains of about 33 dB and 37 dB can be achieved when compared to MISO and SISO systems, respectively. Results demonstrate that uncorrelated MISO multi-hop system has SNR gains of 1.75 dB and 2.5 dB compared to correlated MISO multi-hop system and SISO multi-hop system, respectively. It is worth mentioning that the very high power required by direct link and spatial diversity link can not be achieved at practice. As the behavior of the photodiode becomes non-linear then the photodiode will be damaged as the received optical power will be absorbed as heat.

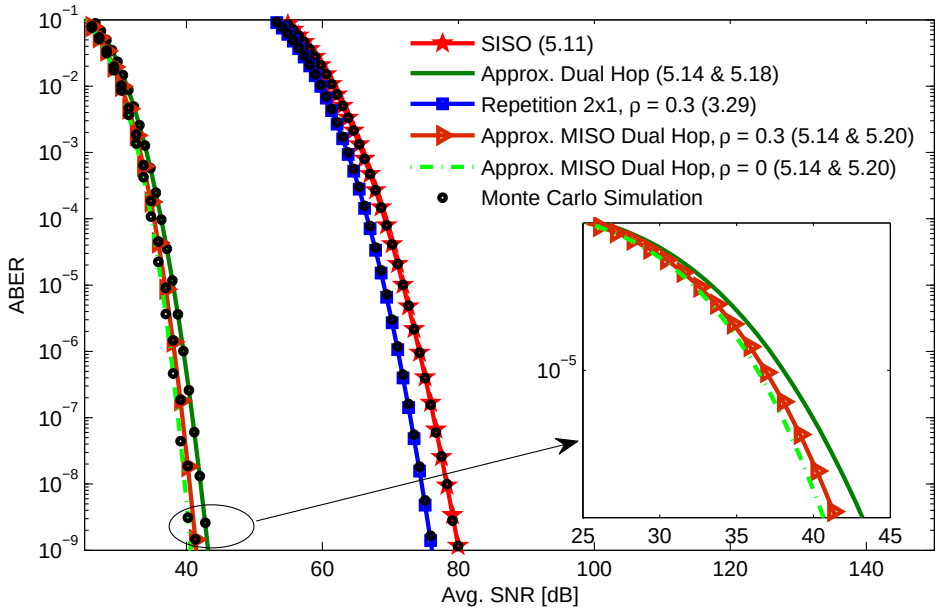


FIGURE 5.7 – ABER of single-relay multi-hop using one or two transmitters with 4-PAM modulation, two transmitters MISO using RCs and OOK, and SISO using OOK modulation FSO systems in LN fading channel and light fog ($C_n^2 = 1.7 \times 10^{-14}$ m$^{-2/3}$, $\alpha =$ 20 dB/km).

In order to achieve a fair comparison using the same number of transmitters, the number of relays is increased to two (three transmitters) in multi-hop systems and the

number of transmitters is increased to three in MISO systems as shown in Figure 5.8 for clear air and in Figure 5.9 for light fog weather. For multi-hop systems with two relays, 8-PAM modulation should be used to guarantee similar spectral efficiency as in MISO and SISO systems. Results show that multi-hop systems are still superior to MISO and SISO systems and increasing the number of relays enhances the performance significantly. In Figure 5.8, 13 dB and 27 dB SNR gains of SISO multi-hop system are obtained at the target ABER as compared to uncorrelated MISO and SISO systems, respectively. A correlation of $\rho = 0.3$ is shown to degrade the performance of MISO systems by about 4 dB. Furthermore, correlated and uncorrelated MISO multi-hop outperforms SISO multi-hop system by 3.2 dB and 4.4 dB, respectively.

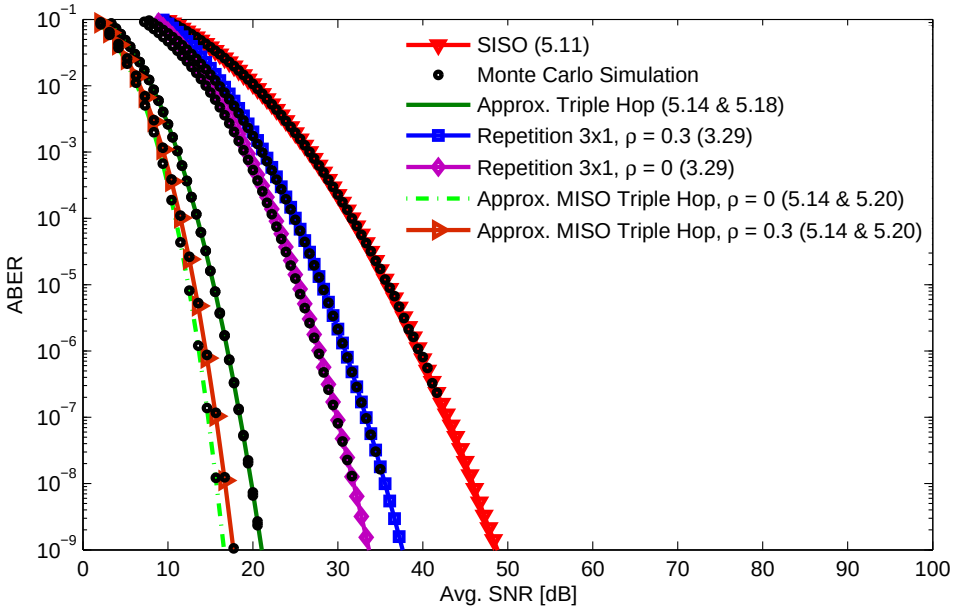


FIGURE 5.8 – ABER of two-relays multi-hop using one or three transmitters with 8-PAM modulation, three transmitters MISO using RCs and OOK, and SISO using OOK modulation FSO systems in LN fading channel and clear air ($C_n^2 = 5\times\ 10^{-14}$ m$^{-2/3}$, $\alpha =$ 0.43 dB/km).

Finally, light fog with low turbulence is considered in Figure 5.9. Results demonstrate that having two relays enhances the performance than dual-hop systems by about 10 dB. However, increasing the number of transmitters to three in MISO systems is shown to produce a gain of about 2 dB in SNR at the target ABER. As such, 41 dB and 47 dB gains are achieved in a SISO multi-hop system as compared to MISO and SISO systems, respectively. Moreover, correlated and uncorrelated MISO multi-hop outperforms SISO multi-hop system by of 1.5 dB and 2 dB, respectively. Tables 5.3 and 5.4 summarizing the SNR gains of Figures 5.6-5.9 with respect to SISO in clear air with moderate turbulence.

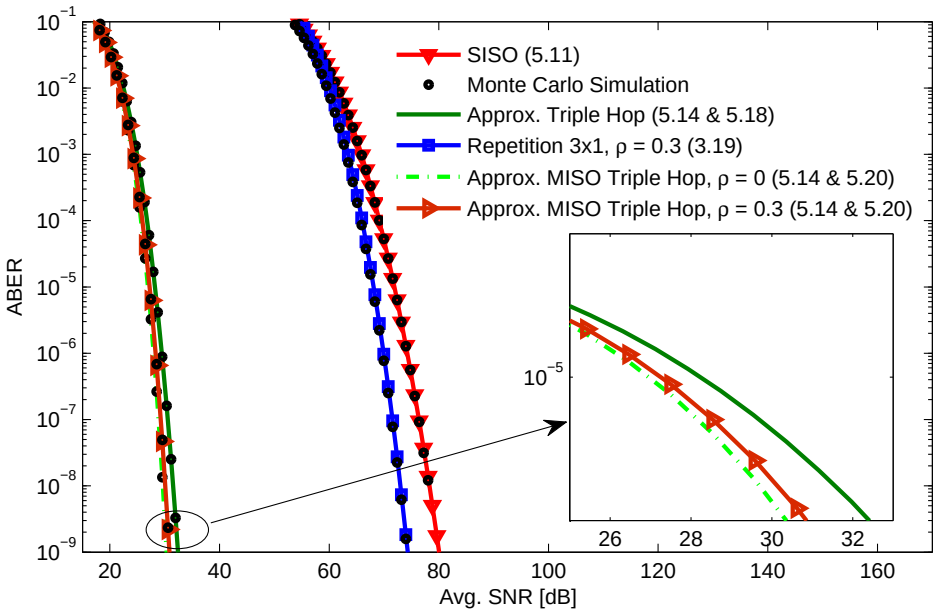


FIGURE 5.9 – ABER of two-relays multi-hop using one or three transmitters with 8-PAM modulation, three transmitters MISO using RCs and OOK, and SISO using OOK modulation FSO systems in LN fading channel and light fog ($C_n^2 = 1.7\times\ 10^{-14}$ m$^{-2/3}$, $\alpha =$ 20 dB/km).

5.4 Summary

In this chapter, MISO multi-hop DF FSO systems are considered. Results demonstrate that MISO multi-hop system using M-PAM has superior improvement than other existing systems such as SISO multi-hop system using M-PAM, SISO and MISO using OOK at the same spectral efficiency. The impact of weak turbulence with light fog and moderate turbulence with clear air conditions on the performance of considered FSO systems are analyzed. Multi-hop systems have the ability to mitigate both turbulence and path loss effects such as weather and geometric loss attenuation. However, MISO systems can only mitigate turbulence effect.

Consequently, increasing the number of relays is shown to significantly enhance the overall system performance. This is while increasing the number of transmitters in MISO systems is shown to lead to small enhancements in SNRs. In Chapter 6, full-duplex (FD) relays are analyzed under different turbulence conditions, misalignment error and path loss effects. FD relays are compared with the direct link and half-duplex relays. Our results show that FD relays have lowest ABER as well as the outage probability.

TABLE 5.3 – Summary of SNR gains of Figures 5.6-5.7

Weather condition	**SISO**	2×1 **MISO** $\rho = 0.3$	2×1 **MISO** $\rho = 0$	**Dual-hop relay**	2×1 **MISO** $\rho = 0.3$ **dual-hop relay**	2×1 **MISO** $\rho = 0$ **dual-hop relay**
Clear air + moderate turbulence	0 dB	8 dB	11 dB	22 dB	25.4 dB	27 dB
Light fog + weak turbulence	-31 dB	-27 dB		6 dB	7.75 dB	8.5 dB

TABLE 5.4 – Summary of SNR gains of Figures 5.8-5.9

Weather condition	**SISO**	3×1 **MISO** $\rho = 0.3$	3×1 **MISO** $\rho = 0$	**Triple-hop relay**	3×1 **MISO** $\rho = 0.3$ **triple-hop relay**	3×1 **MISO** $\rho = 0$ **triple-hop relay**
Clear air + moderate turbulence	0 dB	9 dB	13 dB	27 dB	30.2 dB	31.4 dB
Light fog + weak turbulence	-31 dB	-25 dB		16 dB	17.5 dB	18 dB

6

Relay Selection For Full-Duplex FSO Relays Over Turbulent Channels

6.1 Introduction

This chapter investigates the performance of a best relay selection, based on the max-min signal-to-noise ratio criterion for dual-hop free-space optical (FSO) full-duplex (FD) relays communication system. Decode-and-forward (DF) relays over log-normal (LN) channels for weak-to-moderate turbulence and gamma-gamma (G-G) channels for strong turbulence are considered. We assume that the relays have full channel knowledge and the channel is symmetrical. Considering path loss effects and misalignment errors, the outage probability (OP) of the selection is obtained for both half-duplex (HD) and FD relays using the cumulative distribution function (CDF) of the best selection for LN and G-G random variables. Moreover, the average bit error rate (ABER) expressions for FSO communication system over LN channels are derived with the help of Gauss-Laguerre's quadrature rule for HD relays, FD relays and direct link. Our results show that FD relays have lowest ABER and OP compared with the direct link and HD relays. Monte Carlo simulations corroborate the correctness of the obtained analytical results.

Table 6.1 summarizes the contribution of the most relevant works in the literature and our work by specifying the considered channel models. Figure 6.1 shows the main three axes considered in the thesis to mitigate various challenges facing FSO. The third axis, a relay-assisted cooperative relays scenario is considered in this chapter.

6.2 System And Channel Models

6.2.1 System Model

The considered system is depicted in Figure 6.2, where two users communicate through N_{re} relay nodes. Only a single relay, with index j, among existing N_{re} relays participates in the communication process. The selected relay should have the highest receive end-to-end SNR and that is known to both users [131,135,151,153]. The selection process is achieved according to Equation (2.1).

In the first time slot, t_1, each user transmits his data to the preselected relay. The user's transceiver steers the signal in the direction of the selected relay. The relay has

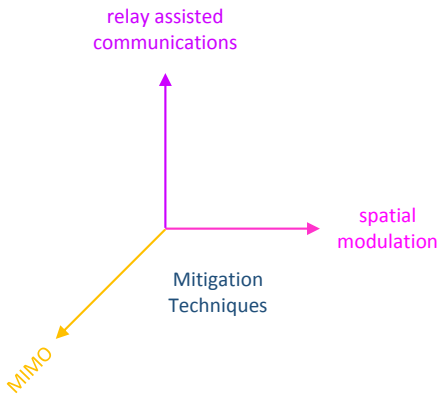


FIGURE 6.1 – The main axes of the research.

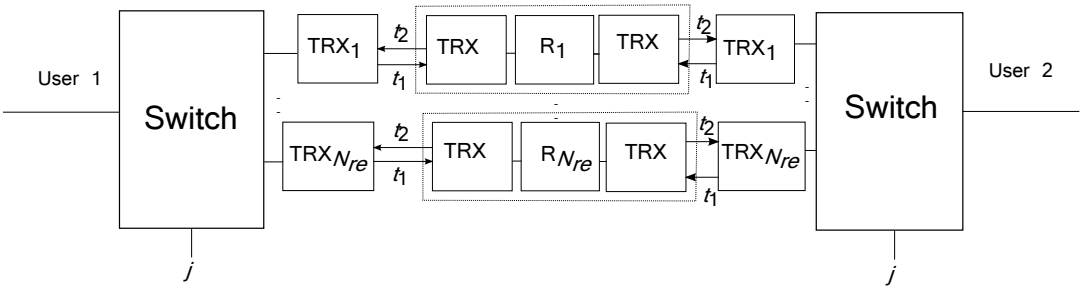


FIGURE 6.2 – Block diagram of the proposed FD FSO communication system.

two transceivers, each of which is directed towards one user. The relay decodes the received signals and in the second time slot, t_2, forwards the received signal to both users.

It is assumed that all relays have full channel knowledge and the channel is symmetrical [164]. The received signals are affected by an additive white Gaussian noise (AWGN) with zero mean and variance $\sigma_n^2 = N_o/2$ resulting mainly from background noise [11].

The normalized channel coefficient of the considered system can be formulated as follows [14]:

$$h = h_a \; h_p \; \beta, \tag{6.1}$$

where h_a and h_p are the channel fading coefficients due to atmospheric turbulence and misalignment error, respectively. The path losses, β, can be calculated by combining weather attenuation [9] with geometric losses [131] as Equation (5.4).

The general model of misalignment fading proposed in [14] is considered hereinafter

$$h_p \approx A_o \exp\left(\frac{-2r^2}{w_{\text{zeq}}^2}\right), \tag{6.2}$$

where r is the radial displacement which is modeled by Rayleigh distribution, the equi-

TABLE 6.1 – Comparison between our FD best relay selection & the closed literature works

Reference	Channel Model	Contributions
[131]	gamma-gamma (G-G)	derive the OP of an asynchronous low-complexity cooperative relaying
[149]		the ABER expression is derived using the power series expansion
[190]		the ABER of DF relays using Gauss- Laguerre quadrature rule is derived
[150]		the ABER and the diversity order of DF relays considering misalignment error are derived
[168]		partial relay selection for FD coherent system is employed while considering the effects of path loss and misalignment error
[148]	LN & Rayleigh	the ABER expressions are derived
[166]	$\mathcal{M}$-distribution	FD DF relays re employed and the ABER and the OP are derived considering misalignment error
Our work	LN & GG (to model weak-to-strong turbulence)	the ABER and OP are derived while considering the effects of path loss and misalignment error for FD and HD relays

valent beam width (in m), w_{zeq}, is calculated as $w_{\text{zeq}}^2 = (w_z^2\sqrt{\pi}\text{erf}(v))/(2v\exp(-v^2))$, $v = (\sqrt{\pi}D_R)/(2\sqrt{2}w_z)$, $A_o = [\text{erf}(v)]^2$, erf(.) is the error function (see Appendix C.1), w_z is the beam waist (in m) (radius calculated at e^{-2}) and D_R is the receiver aperture diameters (in m).

The radial displacement can be modeled as

$$f_r(r) = \frac{r}{\sigma_s^2}\exp\left(-\frac{r}{2\sigma_s^2}\right), \qquad r > 0 \tag{6.3}$$

where σ_s^2 is the jitter variance at the receiver.

6.2.2 LN Channels

The probability density function (PDF) of LN channels considering path loss effects and misalignment errors is given by [14]

$$f_h(h) = \frac{\xi^2 h^{(\xi^2-1)}}{2(A_o\beta_n)^{\xi^2}}\text{erfc}\left(\frac{\ln\left(\frac{h}{A_o\beta_n}\right)+q}{\sqrt{8}\sigma_x}\right)\exp\left(2\sigma_x^2\xi^2(1+\xi^2)\right), \tag{6.4}$$

where erfc(.) is the complementary error function (see Appendix C.1), β_n denotes the normalized path loss coefficient, $\beta_n = \beta/\beta_k$ with β_k being the path loss for a single hop,

$q = 2\sigma_x^2(1+2\xi^2)$ and $\xi = \frac{w_{\text{zeq}}^2}{2\sigma_s^2}$ is the ratio between the equivalent beam width at the receiver and the pointing error displacement standard deviation at the receiver.

The channel fading coefficient $h_a = \exp(2x)$, with x being an independent and identically distributed (i.i.d.) Gaussian random variable (RV) with a mean μ_x and a variance σ_x^2. To ensure that the fading channel does not attenuate or amplify the average power, the fading coefficients are normalized by considering $\mathbb{E}[h_a] = e^{2(\mu_x+\sigma_x^2)} = 1$ (i.e., $\mu_x = -\sigma_x^2$) [76]. Hence, a plane wave propagation is assumed and the log-amplitude variance is calculated based on the Rytov theory as a function of the distance [14]

$$\sigma_x^2 = 0.30545\ k^{7/6} C_n^2\ \ell^{11/6}, \tag{6.5}$$

with $k = 2\pi/\lambda$ is the wave number, λ is the wavelength and C_n^2 is the refractive index constant ($\text{m}^{-2/3}$).

6.2.3 G-G Channels

The PDF of G-G channels is given by [191]

$$f_h(h) = \frac{ab\xi^2}{A_o \beta_n \Gamma(a)\Gamma(b)} G_{1,3}^{3,0}\left[\frac{abh}{\beta_n A_o}\middle| \begin{matrix}\xi^2 \\ \xi^2-1, a-1, b-1\end{matrix}\right], \tag{6.6}$$

where $G_{p,w}^{m,o}[.]$ is the Meijer's G-function (see Appendix C.1), $\Gamma(.)$ is the Gamma function (see Equation 4.17), a and b are the effective number of large-scale and small-scale eddies of scattering environment, respectively. Their values for plane wave are given as [38]

$$a = \left[\exp\left(\frac{0.49\sigma_R^2}{(1+1.11\sigma_R^{\frac{12}{5}})^{\frac{7}{6}}}\right) - 1\right]^{-1}, \tag{6.7}$$

$$b = \left[\exp\left(\frac{0.51\sigma_R^2}{(1+0.69\sigma_R^{\frac{12}{5}})^{\frac{7}{6}}}\right) - 1\right]^{-1}, \tag{6.8}$$

and the Rytov variance, σ_R^2, is given as [38]

$$\sigma_R^2 = 1.23\ k^{7/6} C_n^2\ \ell^{11/6}. \tag{6.9}$$

6.3 Outage Performance Analysis

6.3.1 LN Channels

The OP at each node can be obtained directly from the CDF of SNR, $F_\gamma(\gamma)$, [131]

$$P_{\text{out,direct}} = \Pr(\gamma < \gamma_{th}) = F_\gamma(\gamma_{th}), \tag{6.10}$$

where $\gamma = h^2\bar{\gamma}$ is the SNR, $\bar{\gamma}$ is the average SNR. If SNR exceeds γ_{th}, no outage occurs and the signal can be decoded with an arbitrarily low error probability at the receiver. For LN channels, the OP is derived as [14]

$$\begin{aligned} P_{\text{out,direct}} &= \Pr\left(h < \frac{1}{\acute{\rho} P_M}\right) = F_\gamma(\gamma_{th}) \\ &= \frac{1}{2}\exp\left(\xi^2\psi - 2\sigma_x^2\xi^4\right)\operatorname{erfc}\left(\frac{\psi}{\sqrt{8}\sigma_x}\right) + \frac{1}{2}\operatorname{erfc}\left(\frac{4\sigma_x^2\xi^2 - \psi}{\sqrt{8}\sigma_x}\right), \end{aligned} \tag{6.11}$$

where $P_M = \sqrt{\frac{\bar{\gamma}}{\gamma_{th}}}$ is the power margin and $\psi = \ln\left(\frac{1}{A_o\beta_n\acute{\rho}P_M}\right) + 2\sigma_x^2(1+2\xi^2)$.

The power of HD systems, such as direct link and HD relays, are assumed to be half the power of FD systems in order to achieve a fair comparison using the same equipment of Figure 6.2 [192]. Hence, the power margin is multiplied by a constant, $\acute{\rho}$. The value of $\acute{\rho}$ is unity for FD systems and one-half for HD systems.

Since the SNRs for the two hops are independent and without loss of generality, the relay is assumed being located at equidistant from the source and the destination, and equal average SNRs per hop are also assumed, the OP for a dual-hop system is given by [131]

$$P_{\text{out}} = 1 - \left[1 - P_{\text{out,direct}}\right]^2. \tag{6.12}$$

Due to the assumption that the relays have full channel knowledge and the network is symmetrical [164], Equation (6.12) can be used for both FD and HD relays taking into consideration the power constraint.

The values of β_n and σ_x^2 in dual-hop scheme can be decreased as the distance can be divided by two which enhances the performance of multi-hop systems. If multiple branches of dual-hop exist, as in Figure 6.2, the OP for the best relay selection as in Equation (2.1) can be calculated as [131]

$$P_{\text{out}} = \left[1 - \left[1 - P_{\text{out,direct}}\right]^2\right]^{N_{re}} = F_\gamma(\gamma_{th}). \tag{6.13}$$

It is evident that a diversity gain of N_{re} is achieved for a dual-hop system with the best relay selection.

6.3.2 G-G Channels

For G-G channels, the OP at each node is derived as [117]

$$P_{\text{out,direct}} = \frac{\xi^2}{\Gamma(a)\Gamma(b)} \times G_{2,4}^{3,1}\left[\frac{ab}{\beta_n\acute{\rho}P_M}\middle|\begin{matrix}1, \xi^2+1\\ \xi^2, a, b, 0\end{matrix}\right] = F_\gamma(\gamma_{th}), \tag{6.14}$$

The OP for the best relay selection can be calculated as [131]

$$P_{\text{out}} = \left[1 - \left[1 - (P_{\text{out,direct}})\right]^2\right]^{N_{re}} = F_\gamma(\gamma_{th}). \tag{6.15}$$

For dual-hop system, the values of a, b and β_n should be changed as the link distance is divided by two.

6.4 Performance Analysis

The ABER can be calculated directly using the CDF approach as [193]

$$\text{ABER} = e\,\mathbb{E}\left[Q(\sqrt{c\gamma}\,)\right] = \frac{e}{\sqrt{2\pi}}\int_0^\infty F_\gamma\left(\frac{y^2}{c}\right)\exp\left(-\frac{y^2}{2}\right)dy, \tag{6.16}$$

where $Q(.)$ is the Gaussian-Q function as defined in Equation (3.11), $\mathbb{E}[.]$ denotes the average over channel fading distributions, and c and e are constants determined by the modulation format. In this study, multiple pulse amplitude modulation ($M-$PAM) using intensity modulation with direct detection (IM/DD) is considered as in [194]. The spectral efficiency of $M-$PAM is equal to $\log_2(M)$ bits/s/Hz [194]. Hence, 2-PAM is considered for direct link (1 bit per slot) and FD relays (2 bits from two users per 2 slots), while 4-PAM is considered for HD relays (2 bits per 2 slots) to maintain similar spectral efficiency [195].

The conditional bit error probability (BEP) of M-PAM is given by [58]

$$\Pr(e|\gamma) \approx \frac{2(M-1)}{M\log_2(M)}Q\left(\sqrt{\frac{\gamma\log_2(M)}{2(M-1)^2}}\right). \tag{6.17}$$

The values of e and c can be calculated using Eq. (6.17) as $(e, c) = (1,\, 0.5)$ for 2-PAM and $(e, c) = (0.75,\, 0.1111)$ for 4-PAM.

It is worth mentioning that $M-$PAM has different intensity levels as in Equation (4.2). Channel state information (CSI) is assumed available at the receiver side and a maximum likelihood (ML) decoder is used to decode the received signals as Equation (4.3).

The ABER of the direct link over LN channels can be derived by substituting Equation (6.11) into Equation (6.16) as

$$\begin{aligned}\text{ABER}_\text{d} =& \frac{e}{\sqrt{2\pi}}\int_0^\infty \frac{1}{2}\exp\left(\xi^2\grave{\psi} - 2\sigma_x^2\xi^4\right)\text{erfc}\left(\frac{\grave{\psi}}{\sqrt{8}\sigma_x}\right)\exp\left(-\frac{y^2}{2}\right)dy \\ &+ \frac{e}{\sqrt{2\pi}}\int_0^\infty \frac{1}{2}\,\text{erfc}\left(\frac{4\sigma_x^2\xi^2 - \grave{\psi}}{\sqrt{8}\sigma_x}\right)\exp\left(-\frac{y^2}{2}\right)dy,\end{aligned} \tag{6.18}$$

where $\grave{\psi} = \ln\left(\frac{y}{A_o\beta_n\rho\sqrt{\bar{\gamma}c}}\right) + 2\sigma_x^2(1+2\xi^2)$.

After performing a simple transformation of $x = \frac{y^2}{2}$, Equation (6.18) is easily obtained as

$$\begin{aligned}\text{ABER}_\text{d} =& \frac{e}{2\sqrt{\pi}}\int_0^\infty \frac{1}{2\sqrt{x}}\exp\left(\xi^2\tilde{\psi} - 2\sigma_x^2\xi^4\right)\text{erfc}\left(\frac{\tilde{\psi}}{\sqrt{8}\sigma_x}\right)\exp\left(-x\right)dx \\ &+ \frac{e}{2\sqrt{\pi}}\int_0^\infty \frac{1}{2\sqrt{x}}\,\text{erfc}\left(\frac{4\sigma_x^2\xi^2 - \tilde{\psi}}{\sqrt{8}\sigma_x}\right)\exp\left(-x\right)dx,\end{aligned} \tag{6.19}$$

where $\tilde{\psi} = \ln\left(\frac{\sqrt{2x}}{A_o \beta_n \rho \sqrt{\bar{\gamma}c}}\right) + 2\sigma_x^2(1+2\xi^2)$.

The integration in Equation (6.19) can be computed using the generalized Gauss-Laguerre quadrature function as [196]

$$\int_0^\infty z^f \exp(-z) g(z) dz \approx \sum_{i=1}^{N} \grave{w}_i g(\grave{z}_i), \tag{6.20}$$

where N is the order of the approximation and $\grave{z}_i$ and $\grave{w}_i$ are the roots and the weights of the generalized Laguerre polynomial of degree f, respectively. The first hundred values of $\grave{z}_i$ and $\grave{w}_i$ are well tabulated in [197]. Thus Equation (6.19) can be expressed by truncated series as

$$\begin{aligned} \text{ABER}_\text{d} \approx & \frac{e}{2\sqrt{\pi}} \sum_{i=1}^{N} \frac{\grave{w}_i}{2} \exp\left(\xi^2 \bar{\psi} - 2\sigma_x^2 \xi^4\right) \text{erfc}\left(\frac{\bar{\psi}}{\sqrt{8}\sigma_x}\right) \\ & + \frac{e}{2\sqrt{\pi}} \sum_{i=1}^{N} \frac{\grave{w}_i}{2} \text{ erfc}\left(\frac{4\sigma_x^2\xi^2 - \bar{\psi}}{\sqrt{8}\sigma_x}\right) \approx \frac{e}{2\sqrt{\pi}} \sum_{i=1}^{N} \grave{w}_i \grave{I}, \end{aligned} \tag{6.21}$$

where $\bar{\psi} = \ln\left(\frac{\sqrt{2\grave{z}_i}}{A_o \beta_n \rho \sqrt{\bar{\gamma}c}}\right) + 2\sigma_x^2(1+2\xi^2)$ and $\grave{I} = \frac{1}{2}\exp\left(\xi^2\bar{\psi} - 2\sigma_x^2\xi^4\right)\text{erfc}\left(\frac{\bar{\psi}}{\sqrt{8}\sigma_x}\right) + \frac{1}{2}\text{erfc}\left(\frac{4\sigma_x^2\xi^2 - \bar{\psi}}{\sqrt{8}\sigma_x}\right)$.

For a dual-hop system, assuming equal average SNRs per hop, an approximated ABER can be calculated by [189]

$$\text{ABER} \approx \frac{1}{2}\left(1 - (1 - 2\ \text{ABER}_\text{d})^2\right). \tag{6.22}$$

Following the same steps of Equation (6.21), an approximated ABER expression of the best relay selection for LN channels can be calculated by substituting the CDF, $F_\gamma(\gamma_{th})$, of Equation (6.13) into Equation (6.16) and using Equation (6.20) as

$$\text{ABER} \approx \frac{e}{2\sqrt{\pi}} \sum_{i=1}^{N} \grave{w}_i \left[1 - \left(1 - \grave{I}\right)^2\right]^{N_{re}}. \tag{6.23}$$

6.5 Numerical Results and Discussions

In the presented results, a target ABER of 10^{-9}, OP for 10^{-15} and equal hop distance are considered. Derived analytical results are corroborated via Monte Carlo simulations. In the obtained simulation results, 10^7 bits are transmitted for each depicted SNR value and the Gauss-Laguerre quadrature approximation order is $N \leq 50$. Table 6.2 shows the system parameters under investigation which are used in various FSO communication systems [14,131,198]. Using Table 6.2, atmospheric turbulence conditions are calculated by Equations (6.5), (6.7), (6.8) and (6.9) and are presented in Table 6.3.

The OP for HD relays, FD relays and direct link for FSO links over weak, moderate and strong turbulence channels are depicted in Figures 6.3, 6.4 and 6.5 respectively.

TABLE 6.2 – System configuration

Parameter	Symbol	Value
Wavelength	λ	1550 nm
Receiver diameter	D_R	0.2 m
Transmitter diameter	D_T	0.2 m
Divergence angle	θ_T	2 mrad
Distance between the source and the destination	L	1 km
Attenuation coefficient	α	0.43 dB
Jitter standard deviation	σ_s	0.3 m
Beam waist	w_z	2 m
Pointing error parameter	ξ	3.3377
Refractive index constant (weak-to-strong turbulence)	C_n^2	0.5×10^{-14} m$^{-2/3}$, 2×10^{-14} m$^{-2/3}$, 5×10^{-14} m$^{-2/3}$

TABLE 6.3 – Atmospheric conditions

Atmospheric turbulence	Link type	σ_x	a	b	σ_R^2
Weak turbulence	Direct link	0.16			
	Dual-hop	0.08			
Moderate turbulence	Direct link	0.31			
	Dual-hop	0.17			
Strong turbulence	Direct link		4.4	3.15	1
	Dual-hop		8.9	7.77	0.28

Figure 6.3 shows that FD relays, with a single relay or multiple relays, outperforms their counterparts HD relays and direct link systems. Furthermore, it can be noticed that the performance of FD relays with the best relay selection is enhanced by increasing the number of relays. Performance gains of about 3 dB can be noticed as compared to HD relays.

Similar behaviors can be noticed as well in Figures 6.4 and 6.5, where FD relays are shown to outperform HD relays and direct link systems. It is worth mentioning that the performance of FD relays degrades by about 2 dB for moderate turbulence and by more than 7 dB for strong turbulence. HD relays performance is shown to degrade as well. FD relays outperform HD relays by about 3 dB for moderate and strong turbulence. Moreover, Figures 6.3 and 6.5 show that misalignment error effect is more sensitive to weak turbulence than moderate and strong turbulence.

For the negligible misalignment error case when ($\xi \to \infty$), Equation (6.11) matches with the formula obtained in [101, Equation 21] and Equation (6.14) is consistent with the formula obtained in [131, Equation 54].

The ABER of FD relays, HD relays and direct link for FSO links over weak and moderate turbulent channels with respect to the average SNR are shown in Figures 6.6

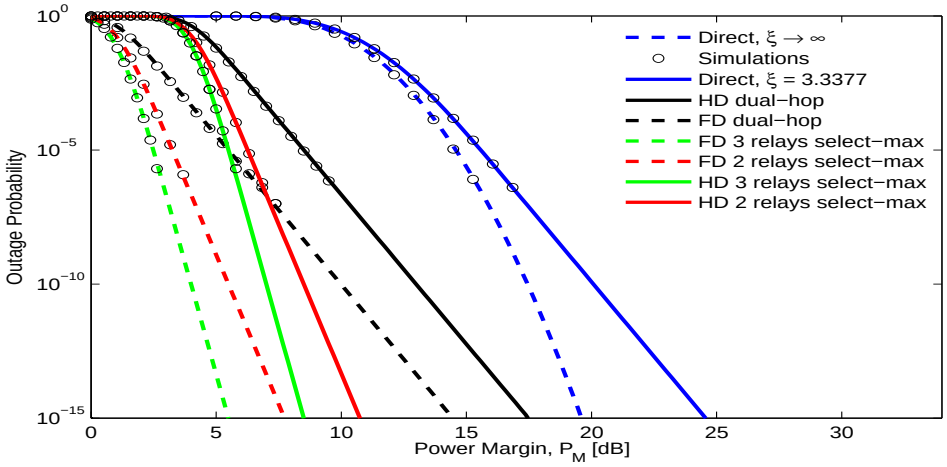


FIGURE 6.3 – OP for FSO over weak fading channel and clear air conditions ($C_n^2 = 0.5 \times 10^{-14}$ m$^{-2/3}$, $\alpha = 0.43$ dB/km).

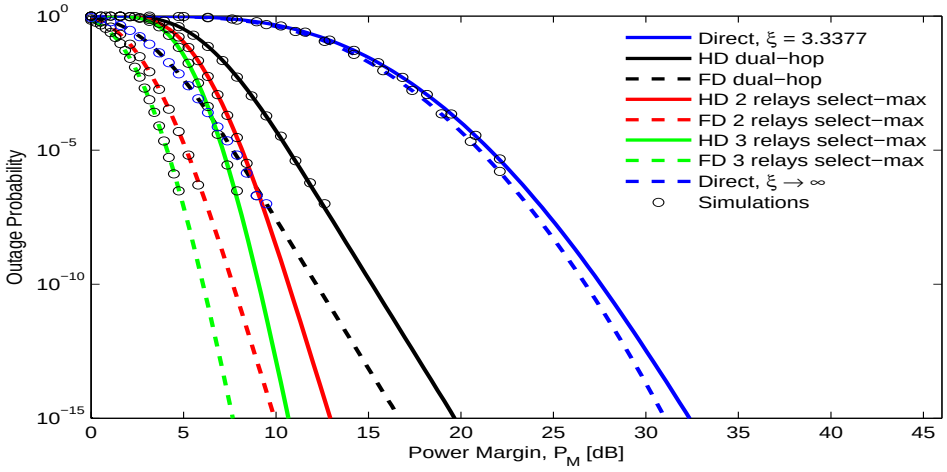


FIGURE 6.4 – OP for FSO over moderate fading channel and clear air conditions ($C_n^2 = 2 \times 10^{-14}$ m$^{-2/3}$, $\alpha = 0.43$ dB/km).

and 6.7, respectively. To guarantee consistent spectral efficiency for all compared systems, 2-PAM is considered for direct and FD relays while 4-PAM is used for HD relays. The significant enhancement of FD relays as compared to HD relays and direct link are clearly shown in Figures 6.6 and 6.7. Performance gains of more than 12 dB can be clearly noticed in Figures 6.6 and 6.7.

Additionally, for negligible misalignment error case when ($\xi \to \infty$), Equation (6.21) is consistent with the formula obtained in [79, Equation 12]. The ABER expression of the best of relay selection shown in Equation (6.23) is obtained as approximated and

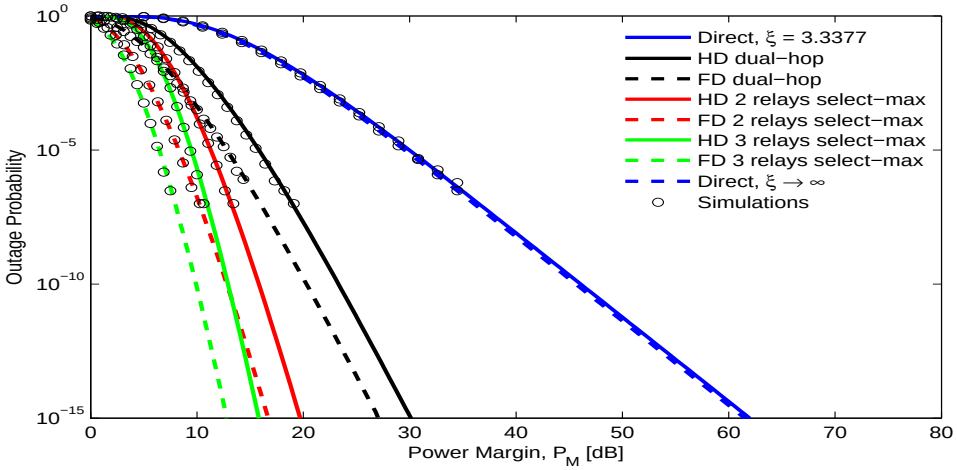


FIGURE 6.5 – OP for FSO over strong fading channel and clear air conditions ($C_n^2 = 5 \times 10^{-14}$ m$^{-2/3}$, $\alpha = 0.43$ dB/km).

series based analytical expressions. Thus, the truncation errors of Equation (6.23) lead to a narrow gap between Equation (6.23) and Monte Carlo simulations at high ABER.

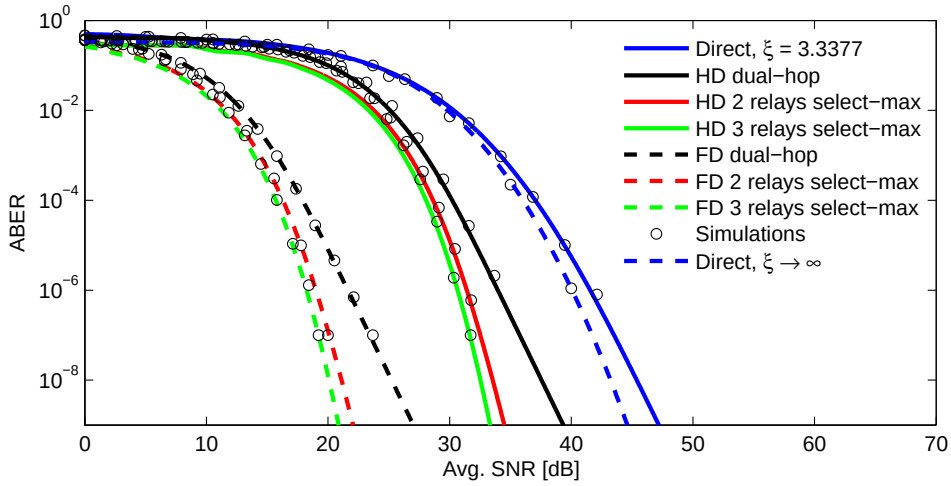


FIGURE 6.6 – ABER of FSO over weak fading channel and clear air conditions ($C_n^2 = 0.5 \times 10^{-14}$ m$^{-2/3}$, $\alpha = 0.43$ dB/km).

6.6 Summary

In this chapter, we investigated the selection of a single relay based on the max-min SNR criterion for FSO communication systems. Dual-hop DF relaying system over

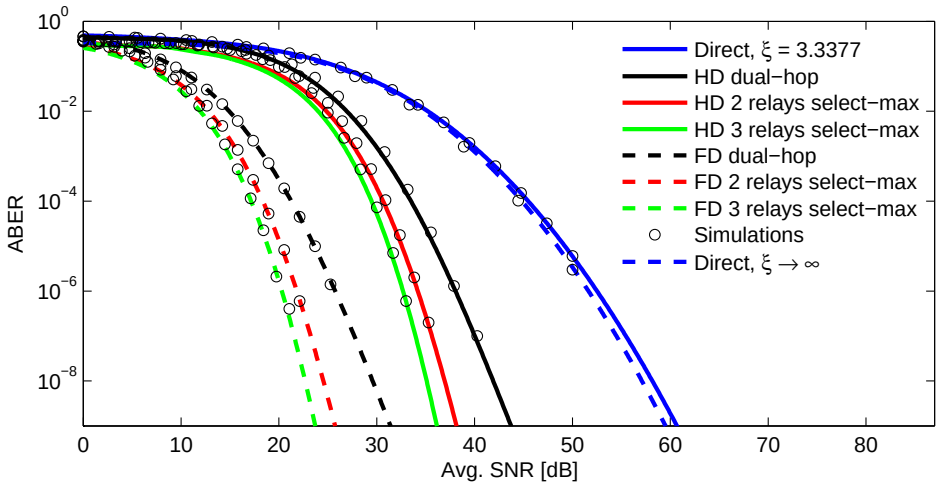


FIGURE 6.7 – ABER of FSO over moderate fading channel and clear air conditions ($C_n^2 = 2 \times 10^{-14}$ m$^{-2/3}$, $\alpha = 0.43$ dB/km).

different atmospheric turbulence channels affected with path losses and misalignment errors are employed. OP are obtained for LN and G-G channels under the considered challenges. Moreover, approximated ABER expressions for FD relays, HD relays and direct link are derived using Gauss-Laguerre quadrature rule assuming full CSI. Our simulation results show the superiority of FD relays systems as compared to their counterparts in terms of ABER and OP especially for strong turbulence.

7 Conclusions and Future Work

7.1 Conclusions

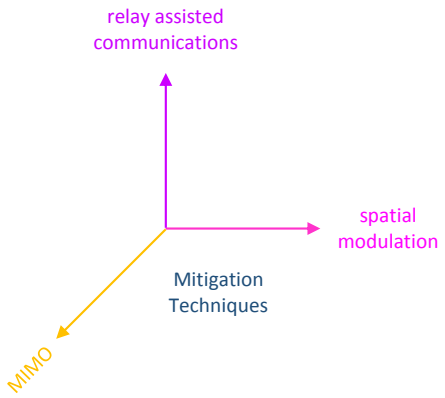


FIGURE 7.1 – The main axes of the research.

Free-space optical (FSO) systems are gaining significant popularity due to their ability to provide high bandwidth and cost-effectiveness for a variety of applications in wireless communication systems. While promising, FSO communication systems still face challenges including atmospheric turbulence, misalignment error, and harsh weather conditions that degrade their performance.

Atmospheric turbulence results from the variations of the index of refraction due to inhomogeneities in temperature and pressure causes fluctuation of the received signal. Several statistical models of atmospheric turbulence are available in the literature. The most common models are log-normal (LN) channels for weak-to-moderate turbulence, gamma-gamma (G-G) channels for moderate-to-strong turbulence and negative exponential (NE) channels for saturated strong turbulence.

To mitigate the severe effect of atmospheric turbulence, many promising solutions such as multiple-input multiple-output (MIMO), spatial modulation and relay assisted technique have been proposed in the literature as shown in Figure 7.1 and these three axis are considered in the thesis as follows.

In this study, special spatial correlation for multiple-input single-output (MISO)

FSO systems with on-off keying (OOK) modulation using intensity modulation and direct detection (IM/DD) is considered. In the case of spatial correlation, signal-to-noise ratio (SNR) gain decreases with decreasing the separation distance among transmitter units or receiver units. Hence, the importance of spatial correlation appears when there is a spacing limitation in the transmitter or in the receiver side. LN channels are considered for weak-to-moderate turbulence and the probability density function (PDF) of correlated LN channels is expressed according to an approach based on moment generating functions. In our approach, approximated average bit error rate (ABER) expressions for both orthogonal space-time block codes (OSTBCs) and repetition codes (RCs) in correlated LN channels with different path loss effects are obtained.

Our results show that RCs always have better SNR gain than OSTBCs by at least 3 dB. In addition, increasing the number of transmitters for RCs always enhances the SNR. On the other hand, increasing the number of transmitters for OSTBCs in weak turbulence degrades the SNR gain.

The demand for higher data rates in wireless systems is essential to sustain the increasing demand for bandwidth-hungry applications, such as for video applications. Our results show that space shift keying (SSK) is a good candidate for FSO communication systems for the next generation of FSO in order to keep pace with progress of wireless devices and simultaneously decrease the energy cost as well as the receiver complexity.

Tight upper and lower bounds for ABER expressions corresponding to NE and LN channels respectively are obtained for SSK FSO communication systems. Our results demonstrate that SSK has more SNR gain than the single-input single-output (SISO) system as well as recent RC multi-pulse amplitude modulation (M-PAM) techniques, especially for strong turbulence and high spectral efficiency. In addition, the diversity order of SSK system depends on the receiver diversity order. Therefore, by increasing the number of receivers we can enhance the SNR gain compared to RC $M-$PAM systems.

The relay-assisted technique, in particular, has recently attracted attention for overcoming several challenges such as atmospheric turbulence, path loss attenuation, and line-of-sight propagation. MISO multi-hop decode-and-forward (DF) FSO system is proposed and the analytical model is derived. Our results show the superior performance of the proposed system as compared with SISO multi-hop system using M-PAM, SISO or MISO using OOK at the same spectral efficiency. Our results also show that the proposed system can mitigate turbulence effects, weather attenuation effects and beam divergence loss. It is worth mentioning that MISO systems mitigate only turbulence effects as they do not have the advantage of shorter hops. In addition, increasing the number of relays leads to more SNR gain as compared with the increasing number of transmitters in MISO systems.

The selection of a single relay based on the max-min SNR criterion of FSO communication systems is investigated for both full-duplex (FD) and half-duplex (HD) relays. The outage probability (OP) of the considered system, using dual-hop DF for both LN and G-G channels, takes into consideration that path loss and misalignment errors are obtained. In addition, approximated ABER expressions using Gauss-Laguerre quadrature rule and assuming full channel state information (CSI) are derived for FD relays, HD relays, and direct link. FD relays have better spectral efficiency as compared to

HD relays. Therefore, FD relays can be considered as a good candidate for the next generation of FSO communication systems due to its superiority in outage probability and in ABER compared to HD relays.

7.2 Recommendations for Future Work

The results of this dissertation point to several intriguing paths, which can be pursued in future work.

1. **Massive MIMO Systems**: Extending the basic work presented in Chapter 3 by employing massive MIMO systems as in 5G radio frequency (RF) systems. This needs a study of the correlation effects among transmit and receive units. Our approximation in Equation (3.28) to calculate the ABER expression for correlated LN channels will not be applicable for massive MIMO systems. The alternative analytical model worth investigating for massive MIMO future systems in order to achieve both higher spectral efficiency and high a SNR gain.
2. **Optimum Relay Number**: The optimum number of relays given the maximum diversity should be investigated. The analytical model for that optimum number should be developed under different turbulence channels, a different configuration of relays and different misalignment error cases.
3. **Blind and Semi-Blind Channel Estimation**: At present the FSO systems in this thesis are losing some of their capacity using CSI. To overcome this issue, blind and semi-blind channel estimation may be considered. That may increase the spectral efficiency of FSO systems at the expenses of SNR gain.
4. **Light-Emitting Diodes (LEDs) Communications**: Extensive research and measurement should be carried out on outdoor LEDs communications in order to increase the data rate from just a few Mbps to several Gbps. Furthermore, non line of sight (LOS) wireless optical communications should be also considered.
5. **Mixed FSO and Indoor Wireless Optical Communications**: We can also investigate mixed systems using both advantages of FSO and indoor wireless optical communications. FSO can be used for last mile high data rate applications instead of heavy infrastructure required by optical fiber. In addition, indoor wireless optical communications can be applied for both illuminations and high date rate green applications.

Appendix A

A.1 List of Publications

Some of our works have been published and other are still under review for possible publications.

- International Journal Papers

1. **M. Abaza**, R. Mesleh, A. Mansour, and e.-H. M. Aggoune, "Diversity techniques for a free-space optical communication system in correlated log-normal channels," ***SPIE Optical Engineering***, vol. 53, no. 1, pp. 1–6, Jan. 2014. (**Impact Factor = 0.954**)
2. **M. Abaza**, R. Mesleh, A. Mansour, and e.-H. M. Aggoune, "Performance analysis of MISO multi-hop FSO links over log-normal channels with fog and beam divergence attenuations," ***Elsevier Optics Communications***, vol. 334, pp. 247–252, Jan. 2015. (**Impact Factor = 1.449**)
3. **M. Abaza**, R. Mesleh, A. Mansour, and e.-H. M. Aggoune, "Performance analysis of space-shift keying over negative-exponential and log-normal FSO channels," ***Chinese Optics Letters***, vol. 13, no. 5, May 2015. (**Impact Factor = 1.851**)
4. **M. Abaza**, R. Mesleh, A. Mansour, and e.-H. M. Aggoune, "Relay selection for full-duplex FSO relays over turbulent channels," ***Chinese Optics Letters***, submitted in 2015. (**Impact Factor = 1.851**)

- Conference Papers

1. **M. Abaza**, R. Mesleh, A. Mansour, and A. Alfalou, "MIMO techniques for high data rate free space optical communication system in log-normal channel," ***in Proceedings of International Conference on Technological Advances in Electrical, Electronics and Computer Engineering***, Konya, Turkey, May 9-11, 2013, pp. 1-5.
2. **M. Abaza**, R. Mesleh, A. Mansour, and e.-H. M. Aggoune, "Spatial diversity and multi hop in FSO communication over turbulence channels," ***in Proceedings of Second Symposium on Wireless Sensor and Cellular Networks***, Jeddah, Saudi Arabia, Dec. 13–16, 2013, pp. 111-118.
3. **M. Abaza**, R. Mesleh, A. Mansour, and e.-H. M. Aggoune, "Spatial diversity for FSO communication systems over atmospheric turbulence channels," ***in Proceedings of IEEE Wireless Communications and Networking Conference***, Istanbul, Turkey, Apr. 6–9, 2014, pp. 382-387.
4. **M. Abaza**, R. Mesleh, A. Mansour, and e.-H. M. Aggoune, "The performance of space shift keying for free-space optical communications over turbulent channels," ***in Proceedings of SPIE 9387***, San Francisco, USA, Feb. 7–12, 2015, pp. 1-8.
5. **M. Abaza**, R. Mesleh, A. Mansour, and e.-H. M. Aggoune, "Relay selection in two-way relays free-space optical communications," ***in Proceedings of IEEE Wireless Communications and Networking Conference***, submitted.

Appendix B

B.1 Approximation of Equation (3.27)

Here, we would like to investigate the proposed approximation of Equation (3.28)

$$\left(\sum_{i=1}^{N_t}\sqrt{\gamma_i}\right)^2 \approx N_t\sum_{i=1}^{N_t}\gamma_i. \tag{B.1}$$

The instantaneous signal-to-noise ratio (SNR) γ_i is given by [76],

$$\gamma_i = \frac{(\eta I_i)^2}{N_o} \tag{B.2}$$

The received signal light intensity from the i^{th} transmitter to the receiver after channel effect which can be evaluated according to [9,79] as follows

$$I_i = \beta\ I_o\ h_i \tag{B.3}$$

Substituting Equation (B.3) into Equation (B.2) gets

$$\gamma_i = \frac{(\eta\beta\ I_o\ h_i)^2}{N_o} \tag{B.4}$$

where $h_i = e^{2x_i}$ is the channel irradiance from transmitter i to the receiver with x_i being modeled as spatially correlated identically distributed (c.i.d.) Gaussian random variables (RVs) with mean μ_x and variance σ_x^2.
Based on Equation (B.4), γ_i can be written as

$$\gamma_i = ch_i^2 \tag{B.5}$$

where c is a constant. Substituting Equation (B.5) on Equation (B.1) yields

$$E_1 = \left(\sum_{i=1}^{N_t} h_i\sqrt{c}\right)^2 = c\left(\sum_{i=1}^{N_t} h_i\right)^2 \tag{B.6}$$

$$E_2 = N_t c\sum_{i=1}^{N_t} h_i^2 \tag{B.7}$$

we can simplify c from E_1 and E_2 as

$$E_1 = \left(\sum_{i=1}^{N_t} h_i\right)^2 = \sum_{i=1}^{N_t} h_i^2 + \sum_{i=1}^{N_t}\sum_{\substack{j=1\\ j\neq i}}^{N_t} h_i h_j \tag{B.8}$$

$$E_2 = N_t\sum_{i=1}^{N_t} h_i^2 \tag{B.9}$$

To see the impact of σ_x on this approximation, we assume that h_i can be modeled as an independent and identically distributed (i.i.d.) log-normal RVs, the mean of the fading coefficients is

$$\mathbf{E}[h_i] = e^{2(\mu_x+\sigma_x^2)} \tag{B.10}$$

We assume that log-normal parameters are equal for all channels. To ensure that the fading channel does not attenuate or amplify the average power, the fading coefficients are normalized as $\mathbf{E}[h_i] = e^{2(\mu_x+\sigma_x^2)} = 1$ (i.e., $\mu_x = -\sigma_x^2$).

The second moment of log-normal channel is

$$\mathbf{E}[h_i^2] = e^{4(\mu_x+2\sigma_x^2)} = e^{4\sigma_x^2} \tag{B.11}$$

The mean of Equation (B.8) is

$$\mathbf{E}[E1] = N_t\mathbf{E}[h_i^2] + (N_t(N_t-1))\underbrace{\left(\rho e^{4\sigma_x^2} - \rho + \mathbf{E}[h_i]^2\right)}_{\mathbf{E}[h_ih_j]} \tag{B.12}$$

Substituting Equation (B.11) and $\mathbf{E}[h_i] = 1$ on Equation (B.12), yields

$$\mathbf{E}[E1] = N_t e^{4\sigma_x^2} + (N_t(N_t-1))\left(\rho e^{4\sigma_x^2} - \rho + 1\right) \tag{B.13}$$

The mean of Equation (B.9) is

$$\mathbf{E}[E2] = N_t^2\mathbf{E}[h_i^2] = N_t^2 e^{4\sigma_x^2} \tag{B.14}$$

For correlated and uncorrelated cases, if $\sigma_x^2 \ll 1$, which is the case for FSO communications, then $e^{4\sigma_x^2} \approx 1$. Please note that the maximum value of σ_x for FSO LN channels corresponds to the maximum scintillation index (SI) value for LN channels, which is $\leq$ 0.75 [15]. The relation between SI and σ_x is defined in [90] as $\sigma_x = \left(\frac{\sqrt{\ln(\text{SI}+1)}}{2}\right)$. Hence, σ_x should be ≤ 0.374. In this case, $\mathbf{E}[E1] \approx \mathbf{E}[E2]$ that explain the impact of σ_x on the proposed approximation of Equation (3.27).

B.2 Matlab Code of Equation (3.27)

B.2.1 Introduction

Using Monte Carlo simulations with 10^6 realizations, the results show that the proposed approximation of Equation (3.27) can be applied with acceptance error percentage as shown in Figure B.2. In addition, Figure B.3, shows the effect of increasing the number of realizations on the proposed approximation. In this code, correlated normal RVs are obtained by multiplying the transpose of Cholesky factorization of the correlation matrix (U') by the uncorrelated normal RVs (Ra).

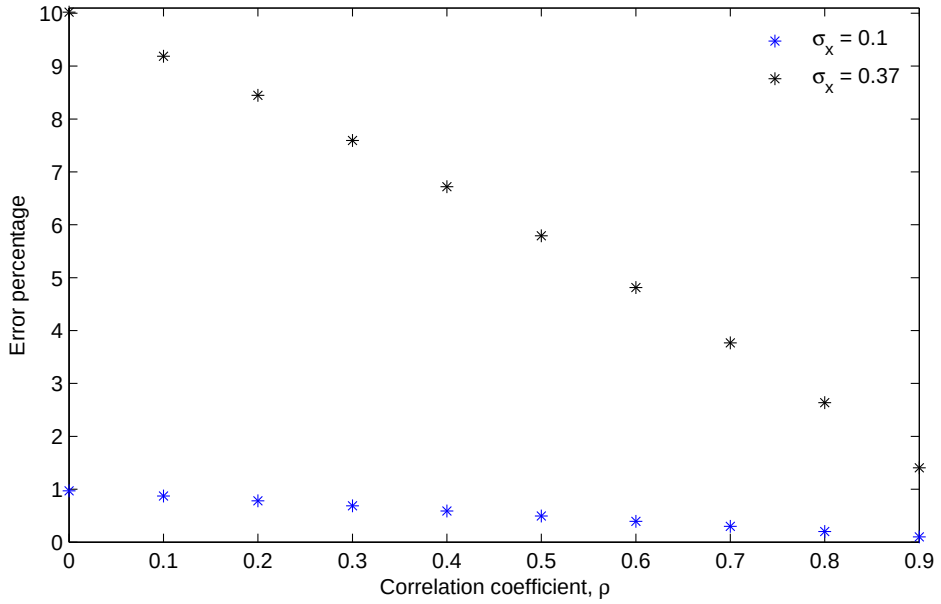


FIGURE B.2 – Impact of the correlation coefficient on the proposed approximation.

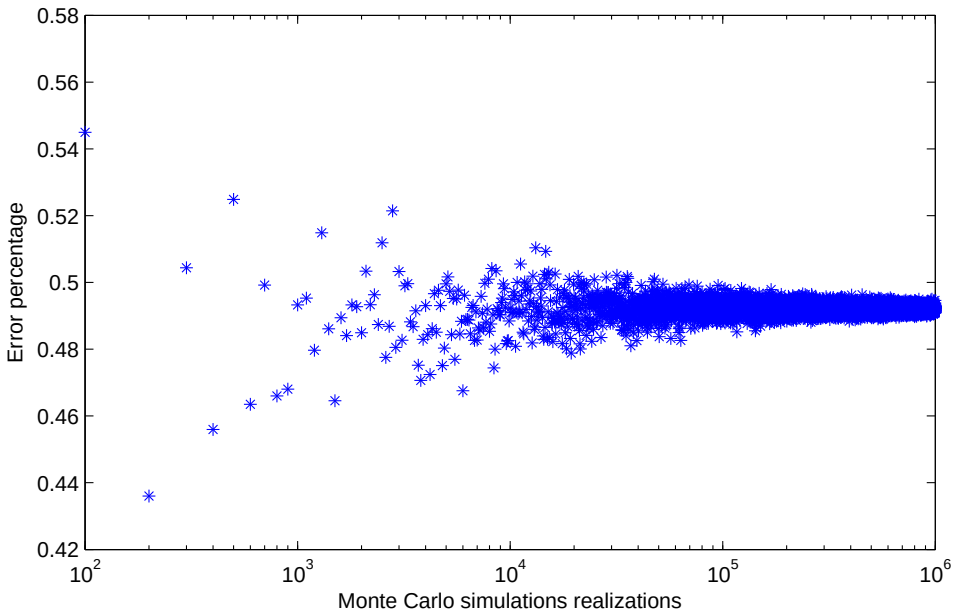


FIGURE B.3 – Impact of Monte Carlo simulations realizations on the proposed approximation for $\rho = 0.5$ and $\sigma_x = 0.1$.

B.2.2 The Matlab code

```
%Impact of the correlation coefficient on the proposed approximation
clc;clear;close all;
figure(1);
%standard deviation of normal distribution where the case for
%FSO communications is that sigma is less than 0.37
sigma=0.1;
sigma2=sigma^2; %variance of normal distribution
for i=1:10 %10 times to employ different rho values
    rho=0.1*(i-1); %correlation coefficient
    RHO(i)=rho; %correlation coefficient vector
    M=10^6; %simulations realizations
    U = chol([1 rho; rho 1]);  %cholesky factorization
    Ra =  normrnd(-sigma2,sigma,2,M);
    Xa = U' * Ra; % generates correlated normal RVs
    Za =exp(2*Xa); %generates correlated log-normal RVs
    ya=sum(sum(Za))/M; %Left hand side of Equation (3.27)
    Zb = Za.^2;
    yb = sum(sqrt(2*sum(Zb)))/M ; %Right hand side of Equation (3.27)
    percentage_paper(i) =abs(100*((ya-yb)/(ya))); %calculates the error
end
plot(RHO,percentage_paper,'*');
xlabel('Correlation coefficient, \rho');
ylabel('Error percentage');

%Impact of simulations realizations on the proposed approximation
figure(2);
for i=1:10:10000 %9991 times to emply different simulations realizations
    rho=0.5; %correlation coefficient
    M=10^2*i; %simulations realizations
    MA(i)=M; %simulations realizations vector
    U = chol([1 rho; rho 1]); %cholesky factorization
    Ra =  normrnd(-sigma2,sigma,2,M);
    Xa = U' * Ra; %generates correlated normal RVs
    Za =exp(2*Xa); %generates correlated log-normal RVs
    ya=sum(sum(Za))/M; %Left hand side of Equation (3.27)
    Zb = Za.^2;
    yb = sum(sqrt(2*sum(Zb)))/M ; %Right hand side of Equation (3.27)
    percentage_paper(i) =abs(100*((ya-yb)/(ya))); %calculates the error
end
semilogx(MA,percentage_paper,'*'); %logarithmic scales for the x-axis
xlabel('Monte Carlo simulations realizations');
ylabel('Error percentage');
axis([-inf inf 0.42 0.58]);
```

B.3 Proof of Equation (5.7)

In this section, the probability density functions (PDF) of the instantaneous SNR is derived as

$$f_\gamma(\gamma) = \frac{1}{\sqrt{32\pi\sigma_x^2\gamma}} \exp\left[-\frac{\left(\ln\left(\frac{\gamma}{\beta_n^2\bar{\gamma}}\right) + 4\sigma_x^2\right)^2}{32\sigma_x^2}\right]. \tag{B.15}$$

The PDF of log-normal (LN) RVs h is given by [90]

$$f_h(h) = \frac{1}{h\sqrt{8\pi\sigma_x^2}} \times \exp\left(-\frac{(\ln(h) - 2\mu_x)^2}{8\sigma_x^2}\right). \qquad h > 0 \tag{B.16}$$

To ensure that the fading channel does not attenuate or amplify the average power, the fading coefficients are normalized as $\mathbf{E}[h] = e^{2(\mu_x+\sigma_x^2)} = 1$, (i.e., $\mu_x = -\sigma_x^2$).

The instantaneous SNR at the receiver input, γ, is given by [76],

$$\gamma = \frac{(\eta I)^2}{N_o}, \tag{B.17}$$

where I stands for the received signal light intensity and is given by [9, 79],

$$I = \beta_n \, \overline{I} \, h, \tag{B.18}$$

Substituting Equation (B.18) in Equation (B.17), yields

$$\gamma = \frac{\eta^2\beta_n^2 \, \overline{I}^2 \, h^2}{N_o} = \beta_n^2 \, \bar{\gamma} \, h^2, \tag{B.19}$$

with $\bar{\gamma} = (\eta\overline{I})^2/N_o$ being the average SNR [76].

Using Equation (B.19), we can conclude:

$$h = \sqrt{\frac{\gamma}{\beta_n^2\bar{\gamma}}} \tag{B.20}$$

Equation (B.20) is a bijective function as $h > 0$; in this case, we know [199] that

$$f_h|h|\left|\frac{dh}{d\gamma}\right| = f_\gamma|\gamma| \tag{B.21}$$

and

$$\left|\frac{dh}{d\gamma}\right| = \frac{1}{2\sqrt{\beta_n^2\gamma\bar{\gamma}}} \tag{B.22}$$

Substituting Equations (B.20) and (B.22) in Equation (B.21) and using $\mu_x = -\sigma_x^2$, we can obtain Equation (B.15).

B.4 Proof of Equation (5.15)

In this section, the conditional bit error rate (BER) of M-ary pulse amplitude modulation (PAM) modulation is derived as

$$\Pr(e|\gamma) \approx \frac{2(M-1)}{M\log_2(M)} Q\left(\sqrt{\frac{P^2\log_2(M)}{(M-1)^2 R\sigma_n^2}}\right). \tag{B.23}$$

The symbol probability of error using a union bound approximation is given by [200]

$$\Pr_{\text{sym}} \approx \bar{N} Q\left(\frac{d_{\min}}{2\sigma_n}\right). \tag{B.24}$$

where $\bar{N}$ is the average number of constellation points away from any constellation point and $d_{\min}$ is the minimum Euclidean distance between two points in the signal constellation.

In the case of M-ary PAM, $\bar{N} = M-1$ and M-ary PAM has one dimensional basis function where M constellation points are equally spaced on the axis, $d_{\min} = \frac{2P\sqrt{T_s}}{M-1}$ [58].

where T_s is the symbol duration and P is the optical power. In addition, $(2/M)$ is multiplied with Equation (B.24) to ensure that the average optical power of each symbol is fixed at P.

Now, Equation (B.24) becomes

$$\Pr_{\text{sym}} \approx \frac{2(M-1)}{M} Q\left(\sqrt{\frac{P^2 T_s}{(M-1)^2\sigma_n^2}}\right). \tag{B.25}$$

The probability of symbol error, $\Pr_{\text{sym}}$, can be converted to a probability of bit error, $\Pr(e|\gamma)$, by multiplying $\Pr_{\text{sym}}$ by a factor of $(1/\log_2 M)$ as in [201]

The probability of bit error becomes

$$\Pr(e|\gamma) \approx \frac{2(M-1)}{M\log_2 M} Q\left(\sqrt{\frac{P^2 T_s}{(M-1)^2\sigma_n^2}}\right), \tag{B.26}$$

Substituting $T_s = \frac{\log_2(M)}{R}$, we gets

$$\Pr(e|\gamma) \approx \frac{2(M-1)}{M\log_2(M)} Q\left(\sqrt{\frac{P^2\log_2(M)}{(M-1)^2 R\sigma_n^2}}\right). \tag{B.27}$$

where R is the bit rate.

Appendix C

The definitions of commonly used special functions are given.

C.1 The error function

This function is defined in the first equation in section 8.250 in [177]

$$\operatorname{erf}(x) = \frac{2}{\sqrt{\pi}} \int_0^x \exp(-t^2) \mathrm{d}t. \tag{C.1}$$

C.2 The complementary error function

This function is defined in the fourth equation in section 8.250 in [177]

$$\operatorname{erfc}(x) = 1 - \operatorname{erf}(x). \tag{C.2}$$

C.3 Meijer's G-function

This function is defined in Equation (9.301) in [177]. Meijer's G-function introduced by C. S. Meijer in 1936. Many special functions can be written as G functions such as logarithms, exponentials, trigonometric functions, hypergeometric functions and Bessel functions [202].

$$G_{p,w}^{m,o}\left[x \,\middle|\, \begin{matrix} a_1, \ldots, a_p \\ b_1, \ldots, b_w \end{matrix}\right] = \frac{1}{2\pi i} \int_L \frac{\prod_{j=1}^{m} \Gamma(b_j - s) \prod_{j=1}^{o} \Gamma\left(1 - a_j + s\right)}{\prod_{j=m+1}^{w} \Gamma(1 - b_j + s) \prod_{j=o+1}^{p} \Gamma\left(a_j - s\right)} x^s \, ds. \tag{C.3}$$

where this integration is called line integration, an empty product is interpreted as 1 and i is a complex number.
Special cases include:

$$G_{2,2}^{1,2}\left[x \,\middle|\, \begin{matrix} 1, 1 \\ 1, 0 \end{matrix}\right] = \ln(x + 1). \tag{C.4}$$

$$G_{2,2}^{1,2}\left[x \,\middle|\, \begin{matrix} 1, 1 \\ 1, 1 \end{matrix}\right] = \frac{x}{x + 1}. \tag{C.5}$$

$$G_{0,2}^{1,0}\left[\frac{x}{2} \,\middle|\, \begin{matrix} - \\ 0, \frac{1}{2} \end{matrix}\right] = \frac{\cos(\sqrt{2x}\,)}{\sqrt{\pi}}. \tag{C.6}$$

$$G_{1,0}^{0,1}\left[x \,\middle|\, \begin{matrix} 1 - a \\ - \end{matrix}\right] = \exp\left(-\frac{1}{x}\right) x^{-a}. \tag{C.7}$$

References

[1] A. A. Huurdeman, *The Worldwide History of Telecommunications*. Wiley Interscience, Aug. 2003.

[2] M. A. Khalighi and M. Uysal, "Survey on free space optical communication : a communication theory perspective," *IEEE Communications Surveys and Tutorials*, vol. 16, no. 4, pp. 2231–2258, Jun. 2014.

[3] S. Randel, F. Breyer, S. C. J. Lee, and J. W. Walewski, "Advanced modulation schemes for short-range optical communications," *IEEE Journal of Selected Topics in Quantum Electronics*, vol. 16, no. 5, pp. 1280–1289, Sep.–Oct. 2010.

[4] A. M. Street, P. N. Stavrinou, D. C. O'brien, and D. J. Edwards, "Indoor optical wireless systems–a review," *Optical and Quantum Electronics*, vol. 29, no. 3, pp. 349–378, Mar. 1997.

[5] H. Elgala, R. Mesleh, and H. Haas, "Indoor optical wireless communication : potential and state-of-the-art," *IEEE Communications Magazine*, vol. 49, no. 9, pp. 56–62, Sep. 2011.

[6] Y. Tanaka, T. Komine, S. Haruyama, and M. Nakagawa, "Indoor visible communication utilizing plural white LEDs as lighting," in *Proceedings of IEEE International Symposium on Personal, Indoor and Mobile Radio Communications*, San Diego, CA, USA, Sep. 30– Oct. 3, 2001, pp. 81–85.

[7] D. Kedar and S. Arnon, "Urban optical wireless communication networks : The main challenges and possible solutions," *IEEE Communications Magazine*, vol. 42, no. 5, pp. 2–7, May 2004.

[8] G. Parca, A. Shahpari, V. Carrozzo, G. M. T. Beleffi, and A. L. J. Teixeira, "Optical wireless transmission at 1.6-Tbit/s (16×100 Gbit/s) for next-generation convergent urban infrastructure," *SPIE Optical Engineering*, vol. 52, no. 11, pp. 1–5, Nov. 2013.

[9] E. Bayaki, D. S. Michalopoulos, and R. Schober, "EDFA-based all-optical relaying in free-space optical systems," *IEEE Transactions on Communications*, vol. 60, no. 12, pp. 3797–3807, Dec. 2012.

[10] C. K. Datsikas, K. P. Peppas, N. C. Sagias, and G. S. Tombras, "Serial free-space optical relaying communications over gamma-gamma atmospheric turbulence channels," *IEEE/OSA Journal of Optical Communications and Networking*, vol. 2, no. 8, pp. 576–586, Aug. 2010.

[11] M. Safari and M. Uysal, "Do we really need OSTBC for free-space optical communication with direct detection ?" *IEEE Transactions on Wireless Communications*, vol. 7, no. 11, pp. 4445–4448, Nov. 2008.

[12] E. Wainright, H. Refai, and J. S. Jr., "Wavelength diversity in free-space optics to alleviate fog effects," *Proceedings of SPIE*, vol. 5712, no. 16, pp. 110–118, Apr. 2005.

[13] S. Bloom, E. Korevaar, J. Schuster, and H. Willebrand, "Understanding the performance of free-space optics," *IEEE/OSA Journal of Optical Communications and Networking*, vol. 2, no. 6, pp. 178–200, Jan. 2003.

[14] A. A. Farid and S. Hranilovic, "Outage capacity optimization for free-space optical links with pointing errors," *IEEE/OSA Journal of Lightwave Technology*, vol. 25, no. 7, pp. 1702–1710, Jul. 2007.

[15] K. Kiasaleh, "Performance of APD-based, PPM free-space optical communication systems in atmospheric turbulence," *IEEE Transactions on Communications*, vol. 53, no. 9, pp. 1455–1461, Sep. 2005.

[16] B. He and R. Schober, "Bit-interleaved coded modulation for hybrid RF/FSO systems," *IEEE Transactions on Communications*, vol. 57, no. 12, pp. 3753–3763, Dec. 2009.

[17] M. Abaza, R. Mesleh, A. Mansour, and E.-H. M. Aggoune, "Diversity techniques for a free-space optical communication system in correlated log-normal channels," *SPIE Optical Engineering*, vol. 53, no. 1, pp. 1–6, Jan. 2014.

[18] M. R. Abaza, N. A. Mohammed, and M. H. Aly, "BER performance of M-ary PPM free-space optical communications with channel fading," in *Proceedings of International Conference on High Capacity Optical Networks and Enabling Technologies*, Riyadh, Saudi Arabia, Dec. 19–21, 2011, pp. 111–115.

[19] R. Barrios and F. Dios, "Exponentiated Weibull distribution family under aperture averaging for Gaussian beam waves," *Optics Express*, vol. 20, no. 12, pp. 13 055–13 064, Jun. 2012.

[20] A. Jurado-Navas, J. Garrido-Balsells, J. Paris, M. Castillo-Vzquez, and A. Puerta-Notario, "Impact of pointing errors on the performance of generalized atmospheric optical channels," *Optics Express*, vol. 20, no. 11, pp. 12 550–12 562, May 2012.

[21] X. Zhu and J. M. Kahn, "Maximum-likelihood spatial-diversity reception on correlated turbulent free-space optical channels," in *Proceedings of IEEE Global Communications Conference*, vol. 2, San Francisco, California, USA, 27 Nov. - 1 Dec., 2000, pp. 1237–1241.

[22] S. Hranilovic, L. Lampe, and S. Hosur, "Visible light communications : the road to standardization and commercialization (Part 1) ," *IEEE Communications Magazine*, vol. 51, no. 12, pp. 24–25, Dec. 2013.

[23] L. Grobe, A. Paraskevopoulos, J. Hilt, D. Schulz, F. Lassak, F. Hartlieb, C. Kottke, V. Jungnickel, and K.-D. Langer, "High-speed visible light communication systems," *IEEE Communications Magazine*, vol. 51, no. 12, pp. 60–66, Dec. 2013.

[24] A. Jovicic, J. Li, and T. Richardson, "Visible light communication : opportunities, challenges and the path to market," *IEEE Communications Magazine*, vol. 51, no. 12, pp. 26–32, Dec. 2013.

[25] S.-K. Lim, K. G. Ruling, I. Kim, and I. S. Jang, "Entertainment lighting control network standardization to support VLC services," *IEEE Communications Magazine*, vol. 51, no. 12, pp. 42–48, Dec. 2013.

[26] S.-H. Yu, O. Shih, H.-M. Tsai, and R. D. Roberts, "Smart automotive lighting for vehicle safety," *IEEE Communications Magazine*, vol. 51, no. 12, pp. 50–59, Dec. 2013.

[27] D. Karunatilaka, F. Zafar, V. Kalavally, and R. Parthiban, "LED based indoor visible light communications : state of the art," *IEEE Communications Surveys and Tutorials*, vol. 17, no. 3, pp. 1649–1678, Aug. 2015.

[28] J. H. Burroughes, D. D. C. Bradley, A. R. Brown, R. N. Marks, K. Mackay, R. H. Friend, P. L. Burns, and A. B. Holmes, "Light-emitting diodes based on conjugated polymers," *Nature*, vol. 347, pp. 539–541, Oct. 1990.

[29] P. A. Haigh, Z. Ghassemlooy, S. Rajbhandari, and I. Papakonstantinou, "Visible light communications using organic light emitting diodes," *IEEE Communications Magazine*, vol. 51, no. 8, pp. 148–154, Aug. 2013.

[30] B. Tian, F. Zhang, and X. Tan, "Design and development of an LED-based optical communication system for autonomous underwater robots," in *Proceedings of IEEE/ASME International Conference on Advanced Intelligent Mechatronics*, Wollongong, Australia, Jul. 9–12, 2013, pp. 1558–1563.

[31] D. M. Boroson, J. J. Scozzafava, D. V. Murphy, B. S. Robinson, and H. Shaw, "The lunar laser communications demonstration," in *Proceedings of IEEE International Conference on Space Mission Challenges for Information Technology*, California, USA, Jul. 19–23, 2009, pp. 23–28.

[32] B. Gutlich, R. Meyer, S. Philipp-May, and A. Pagels-Kerp, "German roadmap on optical communication in space," in *Proceedings of International Conference on Space Optical Systems and Applications*, Kobe, Japan, May 7–9, 2014.

[33] "Optical Interorbit Communications Engineering Test Satellite," https://directory.eoportal.org/web/eoportal/satellite-missions/o/oicets, May 2015.

[34] W. D. Williams, M. Collins, D. M. Boroson, J. Lesh, A. Biswas, R. Orr, L. Schuchman, and O. S. Sands, "RF and optical communications: A comparison of high data rate returns from deep space in the 2020 timeframe," NASA/TM, Tech. Rep. 214459, 2007.

[35] I. S. Ansari, F. Yilmaz, and M.-S. Alouini, "Impact of pointing errors on the performance of mixed RF/FSO dual-hop transmission systems," *IEEE Wireless Communications Letters*, vol. 2, no. 3, pp. 351–354, Jun. 2013.

[36] J. Zhang, L. Dai, Y. Zhang, and Z. Wang, "Unified performance analysis of mixed radio frequency/free-space optical dual-hop transmission systems," *IEEE/OSA Journal of Lightwave Technology*, vol. 33, no. 11, pp. 2286–2293, Jun. 2015.

[37] W. R. Leeb, "Applied optics," *Degradation of signal to noise ratio in optical free space data links due to background illumination*, vol. 28, no. 15, pp. 3443–3449, Aug. 1989.

[38] L. C. Andrews, R. L. Phillips, and C. Y. Hopen, *Laser Beam Scintillation with Applications*. Bellingham, WA : SPIE Press, 2001.

[39] H. Henniger and O. Wilfert, "An introduction to free-space optical communications," *Radioengineering*, vol. 19, no. 2, pp. 203–212, Jun. 2010.

[40] R. L. Phillips and L. C. Andrews, "Measured statistics of laser-light scattering in atmospheric turbulence," *Journal of the Optical Society of America*, vol. 71, no. 12, pp. 1440–1445, Dec. 1981.

[41] J. H. Churnside and R. J. Hill, "Probability density of irradiance scintillations for strong path-integrated refractive turbulence," *Journal of the Optical Society of America A*, vol. 4, no. 4, pp. 727–733, Apr. 1987.

[42] S. M. F. C. Bracher and G.-Y. Wang, "Probability-density functions of irradiance for waves in atmospheric turbulence calculated by numerical simulation," *Journal of the Optical Society of America A*, vol. 11, no. 7, pp. 2080–2092, Jul. 1994.

[43] R. J. Hill and R. G. Frehlich, "Probability distribution of irradiance for the onset of strong scintillation," *Journal of the Optical Society of America A*, vol. 14, no. 7, pp. 1530–1540, Jul. 1997.

[44] M. A. Al-Habash, L. C. Andrews, and R. L. Philips, "Mathematical model for the irradiance probability density function of a laser beam propagating through turbulent media," *SPIE Optical Engineering*, vol. 40, pp. 1554–1562, Aug. 2001.

[45] N. D. Chatzidiamantis, H. G. Sandalidis, G. K. Karagiannidis, S. A. Kotsopoulos, and M. Matthaiou, "New results on turbulence modeling for free-space optical systems," in *Proceeding of IEEE International Conference on Telecommunications*, Doha, Qatar, Apr. 4–7, 2010, pp. 487–492.

[46] M. A. Kashani, M. Uysal, and M. Kavehrad, "A novel statistical channel model for turbulence-induced fading in free-space optical systems," *IEEE/OSA Journal of Lightwave Technology*, vol. 33, no. 11, pp. 2303–2312, Jun. 2015.

[47] K. P. Peppas and P. T. Mathiopoulos, "Free space optical communication with spatial modulation and coherent detection over H-K atmospheric turbulence channels," *IEEE/OSA Journal of Lightwave Technology*, accepted in 2015.

[48] C. H. Cox, *Analog Optic Links : Theory and Practice*. Cambridge, UK : Cambridge University Press, 2004.

[49] Z. Ghassemlooy and W. O. Popoola, *Mobile and Wireless Communications Network Layer and Circuit Level Design*. InTech, Jan. 2010, ch. Terrestrial Free-Space Optical Communications, pp. 355–392.

[50] J. Karout and E. A. M. Karlsson, "Power efficient subcarrier modulation for intensity modulated channels," *Optics Express*, vol. 18, no. 17, pp. 17913–17921, Aug. 2010.

[51] S. G. Wilson, M. Brandt-Pearce, Q. Cao, and J. H. Leveque, "Freespace optical mimo transmission with q-ary ppm," *IEEE Transactions on Communications*, vol. 53, no. 8, pp. 1402–1412, Aug. 2005.

[52] H. Sugiyama and K. Nosu, "MPPM : A method for improving the bandutilization efficency in optical PPM," *IEEE/OSA Journal of Lightwave Technology*, vol. 7, no. 3, pp. 465–471, Mar. 1989.

[53] F. Xu, M. A. Khalighi, and S. Bourennane, "Coded PPM and multipulse PPM and iterative detection for Free-Space optical links," *IEEE/OSA Journal of Optical Communications and Networking*, vol. 1, no. 5, pp. 404–415, Oct. 2009.

[54] Y. Fan and R. J. Green, "Comparison of pulse position modulation and pulse width modulation for application in optical communications," *SPIE Optical Engineering*, vol. 46, no. 6, Jun. 2007, doi :10.1117/1.2746010.

[55] Z. Ghassemlooy, A. R. Hayes, N. L. Seed, and E. D. Kaluarachchi, "Digital pulse interval modulation for optical communications," *IEEE Communications Magazine*, vol. 36, no. 12, pp. 95–99, Dec. 1998.

[56] Z. Ghassemlooy, W. Popoola, and S. Rajbhandari, *Optical Wireless Communications : System and Channel Modelling with MATLAB.* CRC Press, 2013.

[57] H. Hemmati, *Deep Space Optical Communications.* Wiley-Interscience, 2006.

[58] S. Hranilovic, *Wireless Optical Communication Systems.* Springer, 2005.

[59] S.-H. Hwang and Y. Cheng, "SIM/SM-aided free-space optical communication with receiver diversity," *IEEE/OSA Journal of Lightwave Technology*, vol. 32, no. 14, pp. 2443–2450, Jul. 2014.

[60] W. Popoola, Z. Ghassemlooy, and V. Ahmadi, "Performance of sub-carrier modulated free-space optical communication link in negative exponential atmospheric turbulence environment," *International Journal of Autonomous and Adaptive Communications Systems*, vol. 1, no. 3, pp. 342–355, 2008.

[61] M. M. Karbassian and H. Ghafouri-Shiraz, "Transceiver architecture for incoherent optical CDMA network based on polarization modulation," *IEEE/OSA Journal of Lightwave Technology*, vol. 26, no. Dec., pp. 3820–3828, 12 2008.

[62] X. Zhao, Y. Yao, Y. Sun, and C. Liu, "Circle polarization shift keying with direct detection for free-space optical communication," *IEEE/OSA Journal of Optical Communications and Networking*, vol. 1, no. 9, pp. 307–312, Sep. 2009.

[63] Y. Wang, F. Du, J. Ma, and L. Tan, "Employing circle polarization shift keying in free space optical communication with gamma-gamma atmospheric turbulence channel," *Elsevier Optics Communications*, vol. 333, pp. 167–174, Dec. 2014.

[64] A. Belmonte and J. M. Kahn, "Capacity of coherent free-space optical links using diversity combining techniques," *Optics Express*, vol. 17, no. 15, pp. 12 601–12 611, Jul. 2009.

[65] M. Kuschnerov, F. N. Hauske, K. Piyawanno, B. Spinnler, M. S. Alfiad, A. Napoli, and B. Lankl, "DSP for coherent single-carrier receivers," *IEEE/OSA Journal of Lightwave Technology*, vol. 27, no. 16, pp. 3614–3622, Aug. 2009.

[66] R. Lange, B. Smutny, B. Wandernoth, R. Czichy, and D. Giggenbach, "142 km, 5.625 Gbps free-space optical link based on homodyne BPSK modulation," in *Proceedings of SPIE 6105*, Mar. 2006, doi :10.1117/12.673749.

[67] J. Yan, Z. Zheng, W. Hu, and A. Xu, "Improved performance of M-ary PPM free-space optical communication systems in atmospheric turbulence due to forward error correction," in *Proceeding of the International Conference on Commununication Technology*, Guilin, China, Nov. 27–30, 2006, pp. 1–4.

[68] S. S. Muhammad, T. Javornik, I. Jelovcan, E. Leitgeb, and O. Koudelka, "Reed Solomon coded PPM for terristal FSO links," in *Proceeding of the International Conference on Electrical Engineering*, Lahore, Pakistan, Apr. 11–12, 2007, pp. 1–5.

[69] S. S. Muhammad, T. Javornik, I. Jelovcan, Z. Ghassemlooy, and E. Leitgeb, "Comparison of hard-decision and soft-decision channel coded M-ary PPM performance over free space optical links," *European Transactions on Telecommunications*, vol. 20, no. 8, pp. 746–757, Dec. 2009.

[70] O. A. Sab and J. Fang, "Concatenated forward error correction schemes for long-haul DWDM optical transmission systems," in *Proceeding of the European Conference on Optical Communications*, Nice, France, Dec. 26–30, 1999, pp. 290–291.

[71] I. B. Djordjevic, S. Denic, J. Anguita, B. Vasic, and M. A. Neifeld, "LDPC-coded MIMO optical communication over the atmospheric turbulence channel," *IEEE/OSA Journal of Lightwave Technology*, vol. 26, no. 5, pp. 478–487, Mar. 2008.

[72] H. T. T. Pham, N. T. Dang, L. T. Vu, and H. T. Bui, "A survey of performance improvement methods for free-space optical communication systems," in *Proceedings of International Conference on Advanced Technologies for Communications*, Hanoi, Vietnam, Oct. 15–17, 2014.

[73] M.-A. Khalighi, N. Schwartz, N. Aitamer, and S. Bourennane, "Fading reduction by aperture averaging and spatial diversity in optical wireless systems," *IEEE/OSA Journal of Optical Communications and Networking*, vol. 1, no. 6, pp. 580–593, Nov. 2009.

[74] G. Abbas, E. Ahmed, W. Aziz, S. Saleem, and Q. ul Islam, "Performance enhancement of multi-input multi-output (MIMO) system with diversity," *International Journal of Multidisciplinary Sciences and Engineering*, vol. 3, no. 5, pp. 8–12, May 2012.

[75] R. Mesleh, R. Mehmood, H. Elgala, and H. Haas, "Indoor MIMO optical wireless communication using spatial modulation," in *Proceedings of IEEE International Conference on Communications*, Cape Town, South Africa, May 22–27, 2010, pp. 1–5.

[76] T. A. Tsiftsis, H. G. Sandalidis, G. K. Karagiannidis, and M. Uysal, "Optical wireless links with spatial diversity over strong atmospheric turbulence channels," *IEEE Transactions on Wireless Communications*, vol. 8, no. 2, pp. 951–957, Feb. 2009.

[77] M. Safari and S. Hranilovic, "Diversity gain for near-field MISO atmospheric optical communications," in *Proceedings of International Conference on Communications*, Ottawa, Canada, Jun. 10–15, 2012, pp. 3128–3132.

[78] M. R. Abaza, R. Mesleh, A. Mansour, and A. Alfalou, "MIMO techniques for high data rate free space optical communication system in log-normal channel," in *Proceedings of International Conference on Technological Advances in Electrical, Electronics and Computer Engineering*, Konya, Turkey, May 9–11, 2013, pp. 1–5.

[79] S. M. Navidpour, M. Uysal, and M. Kavehrad, "BER performance of free-space optical transmission with spatial diversity," *IEEE Transactions on Wireless Communications*, vol. 6, no. 8, pp. 2813–2819, Aug. 2007.

[80] M. K. Simon and V. Vilnrotter, "Alamouti-type space-time coding for free-space optical communication with direct detection," *IEEE Transactions on Wireless Communications*, vol. 4, no. 1, pp. 35–39, Jan. 2005.

[81] M. Premaratne and F.-C. Zheng, "Orthogonal space-time block codes for free-space IM/DD optical links," *Electronics Letters*, vol. 43, no. 15, pp. 822–823, Jul. 2007.

[82] E. Bayaki and R. Schober, "Performance and design of coherent and differential space-time coded FSO systems," *IEEE/OSA Journal of Lightwave Technology*, vol. 30, no. 11, pp. 1569–1577, Jun. 2012.

[83] A. Garcia-Zambrana, C. Castillo-Vazquez, B. Castillo-Vazquez, and A. Hiniesta-Gomez, "Selection transmit diversity for FSO links over strong atmospheric turbulence channels," *IEEE Photonics Technology Letters*, vol. 21, no. 14, pp. 1017–1019, Jul. 2009.

[84] T. Fath, H. Haas, Marco Di Renzo, and R. Mesleh, "Spatial modulation applied to optical wireless communications in indoor LOS environments," in *Proceedings of IEEE Global Communications Conference*, Houston, Texas, USA, Dec. 5–9, 2011, pp. 1–5.

[85] G. Yang, M.-A. Khalighi, T. Virieu, S. Bourennane, and Z. Ghassemlooy, "Contrasting space-time schemes for MIMO FSO systems with non-coherent modulation," in *Proceedings of International Workshop on Optical Wireless Communications*, Pisa, Italy, Oct. 22, 2012, pp. 1–3.

[86] M. D. Renzo, H. Haas, A. Ghrayeb, S. Sugiura, and L. Hanzo, "Spatial modulation for generalized mimo : challenges, opportunities, and implementation," *Proceedings of the IEEE*, vol. 102, no. 1, pp. 56–103, Jan. 2014.

[87] T. Ozbilgin and M. Koca, "Optical Spatial Pulse Position Amplitude Modulation over Atmospheric Turbulence Channels," in *Proceedings of International Conference on Communications*, Sydney, Australia, Jun. 10-14, 2014, pp. 3412–3417.

[88] J.-H. Lee and S.-H. Hwang, "Selection diversity-aided subcarrier intensity modulation/spatial modulation for free-space optical communication," *IET Optoelectronics*, vol. 9, no. 2, pp. 116–124, Apr. 2015.

[89] G. K. Karagiannidis, D. A. Zogas, and S. A. Kotsopoulos, "An efficient approach to multivariate Nakagami-m distribution using green's matrix approximation," *IEEE Transactions on Wireless Communications*, vol. 2, no. 5, pp. 883–889, Sep. 2003.

[90] H. Moradi, H. H. Refai, and P. G. LoPresti, "A switched diversity approach for multi-receiving optical wireless systems," *Applied Optics*, vol. 50, no. 29, pp. 5606–5614, Oct. 2011.

[91] N. B. Mehta, A. F. Molisch, J. Wu, and J. Zhang, "Approximating the sum of correlated lognormal or lognormal-Rice random variables," *IEEE Transactions on Wireless Communications*, vol. 6, no. 7, pp. 2690–2699, Jul. 2007.

[92] T. Ozbilgin and M. Koca, "Inter-aperturecorrelationinMIMOfreespaceopticalsystems," *Elsevier Optics Communications*, vol. 353, pp. 139–146, Oct. 2015.

[93] G. Yang, M.-A. Khalighi, S. Bourennane, and Z. Ghassemlooy, "Approximation to the sum of two correlated gamma-gamma variates and its applications in free-space optical communications," *IEEE Wireless Communications Letters*, vol. 1, no. 6, pp. 621–624, Dec. 2012.

[94] M. D. Yacoub, "The $\alpha - \mu$ distribution : a physical fading model for the Stacy distribution," *IEEE Transactions on Vehicular Technology*, vol. 56, no. 1, pp. 27–34, Jan. 2007.

[95] G. Yang, M. A. Khalighi, S. Bourennane, and Z. Ghassemlooy, "Fading correlation and analytical performance evaluation of the space-diversity free-space optical communications system," *IOP Journal of Optics*, vol. 16, no. 3, pp. 1–10, Feb. 2014.

[96] G. K. Karagiannidis, "Moments-based approach to the performance analysis of equal gain diversity in Nakagami-m fading," *IEEE Transactions on Communications*, vol. 52, no. 5, pp. 685–690, May 2004.

[97] G. Yang, M. A. Khalighi, Z. Ghassemlooy, and S. Bourennane, "Iet communications," *Performance analysis of space-diversity FSO systems over the correlated Gamma-Gamma fading channel using Pade approximation method*, vol. 8, no. 13, pp. 2246–2255, Sep. 2014.

[98] J. Akella, M. Yuksel, and S. Kalyanaraman, "Error analysis of multihop free-space optical communication," in *Proceedings of International Conference on Communications*, Seoul, Korea, May 16–20, 2005, pp. 1777–1781.

[99] G. Karagiannidis, T. Tsiftsis, and H. Sandalidis, "Outage probability of relayed free space optical communication systems," *Electronics Letters*, vol. 42, no. 17, pp. 994–995, Aug. 2006.

[100] T. A. Tsiftsis, H. G. Sandalidis, G. K. Karagiannidis, and N. C. Sagias, "Multihop free-space optical communications over strong turbulence channels," in *Proceedings of International Conference on Communications*, Istanbul, Turkey, Jun. 11–15, 2006, pp. 2755–2759.

[101] M. Safari and M. Uysal, "Relay-assisted free-space optical communication," *IEEE Transactions on Wireless Communications*, vol. 7, no. 12, pp. 5441–5449, Dec. 2008.

[102] ——, "Diversity gain analysis of free-space optical communication systems," in *Proceedings of Canadian Conference on Electrical and Computer Engineering*, Niagara Falls, Ontario, May 4–7, 2008, pp. 1239–1244.

[103] Y. Jiao, J. B. Wang, X. Dang, M. Chen, W. Hu, and Y. H. Huang, "Performance analysis of multi-hop free space optical communications with pointing errors," in *Proceedings of International Conference on Optical Communications and Networks*, Colombo, Sri Lanka, Sep. 6–8, 2010, pp. 290–293.

[104] M. Safari, M. M. Rad, and M. Uysal, "Multi-hop relaying over the atmospheric poisson channel : outage analysis and optimization," *IEEE Transactions on Communications*, vol. 60, no. 3, pp. 817–829, Mar. 2012.

[105] A. Vavoulas, H. G. Sandalidis, and D. Varoutas, "Weather effects on FSO network connectivity," *IEEE/OSA Journal of Optical Communications and Networking*, vol. 4, no. 10, pp. 734–740, Oct. 2012.

[106] C. Abou-Rjeily, "Power allocation for quantum-limited multihop free-space optical communication systems," *IEEE Communications Letters*, vol. 16, no. 12, pp. 2068–2071, Dec. 2012.

[107] N. T. Dang, H. T. T. Pham, and A. T. Pham, "Average BER analysis of multihop FSO systems over strong turbulence and misalignment fading Channels," in *Proceedings of International Conference on Communications in China*, Xi'an, China, Aug. 12–14, 2013, pp. 153–157.

[108] Q.-S. Hu, J.-B. Wang, J.-Y. Wang, M. Chen, and X. Song, "Outage probability analysis of multi-hop free space optical communications over strong turbulence channels," in *Proceedings of International Conference on Wireless Communications and Signal Processing*, Hangzhou, China, Oct. 24–26, 2013, pp. 1–6.

[109] S. Kazemlou, S. Hranilovic, and S. Kumar, "All-optical multihop free-space optical communication systems," *IEEE/OSA Journal of Lightwave Technology*, vol. 29, no. 18, pp. 2663–2669, Sep. 2011.

[110] P. V. Trinh, N. T. Dang, and A. T. Pham, "All-optical AF relaying FSO systems using EDFA combined with OHL over gamma-gamma channels," in *Proceedings of International Conference on Communications*, London, UK, Jun. 8–12, 2015.

[111] S. M. Aghajanzadeh and M. Uysal, "Multi-hop coherent free-space optical communications over atmospheric turbulence channels," *IEEE Transactions on Communications*, vol. 59, no. 6, pp. 1657–1663, Jun. 2011.

[112] T. V. Pham, T. C. Thang, and A. T. Pham, "Performance analysis of multihop FSO systems using APD receivers over log-normal channels," in *Proceedings of International Conference on Communications in China*, Xi'an, China, Aug. 12–14, 2013, pp. 165–170.

[113] T. V. Pham and A. T. Pham, "Performance of APD-based amplify-and forward multihop FSO systems over turbulence channels," in *Proceedings of IEEE Global Communications Conference*, Atlanta, US, Dec. 9–13, 2013, pp. 1046–1051.

[114] K. P. Peppas, A. N. Stassinakis, H. E. Nistazakis, and G. S. Tombras, "Capacity analysis of dual amplify-and-forward relayed free-space optical communication systems over turbulence channels with pointing errors," *IEEE/OSA Journal of Optical Communications and Networking*, vol. 5, no. 9, pp. 1032–1042, Sep. 2013.

[115] M. Aggarwal, P. Garg, and P. Puri, "A novel MGF-based approach to analyze SIM-based relayed FSO systems," in *Proceedings of International Conference on Advances in Computing, Communications and Informatic*, Greater Noida, India, Sep. 24–27, 2014, pp. 2526–2530.

[116] X. Tang, Z. Wang, Z. Xu, and Z. Ghassemlooy, "Multihop free-space optical communications over turbulence channels with pointing errors using heterodyne detection," *IEEE/OSA Journal of Lightwave Technology*, vol. 32, no. 15, pp. 2597–2604, Aug. 2014.

[117] M. Aggarwal, P. Garg, P. Puri, and P. K. Sharma, "Performance analysis of optical wireless communication system with a decode and forward relay," in *Proceedings of International Conference on Signal Processing and Integrated Networks*, Noida, India, Feb. 20–21, 2014, pp. 333–337.

[118] E. Bayaki, R. Schober, and R. K. Mallik, "Performance analysis of MIMO free-space optical systems in Gamma-Gamma fading," *IEEE Transactions on Communications*, vol. 57, no. 11, pp. 3415–3424, Nov. 2009.

[119] C.-B. Chae and G. Yoon, "Outage probability analysis of a coherent FSO amplify-and-forward relaying system," *IEEE Photonics Technology Letters*, vol. 27, no. 11, pp. 1204–1207, Jun. 2015.

[120] E. Zedini and M.-S. Alouini, "On the performance of multihop heterodyne FSO systems with pointing errors," *IEEE Photonics Journal*, vol. 7, no. 2, Apr. 2015, doi :10.1109/JPHOT.2015.2417867.

[121] M. Aggarwal, P. Garg, and P. Puri, "Ergodic capacity of SIM based DF relayed optical wireless communication systems," *IEEE Photonics Technology Letters*, vol. 27, no. 10, pp. 1104–1107, May 2015.

[122] ——, "Exact capacity of amplify-and-forward relayed optical wireless communication systems," *IEEE Photonics Technology Letters*, vol. 27, no. 8, pp. 903–906, Apr. 2015.

[123] M. A. Kashani, M. Safari, and M. Uysal, "Optimal relay placement and diversity analysis of relay-assisted free-space optical communication systems," *IEEE/OSA Journal of Optical Communications and Networking*, vol. 5, no. 1, pp. 37–47, Jan. 2013.

[124] B. Zhu, J. Cheng, and L. Wu, "Optimal FSO relay nodes placement with link obstacles and infeasible regions," in *Proceedings of IEEE Global Communications Conference*, Austin, USA, Dec. 8–12, 2014, pp. 2137–2142.

[125] C. Gong and Z. Xu, "Non-line of sight optical wireless relaying with the photon counting receiver : a count-and-forward protocol," *IEEE Transactions on Wireless Communications*, vol. 14, no. 1, pp. 376–388, Jan. 2015.

[126] H. T. T. Pham, N. T. Dang, and A. T. Pham, "Effects of atmospheric turbulence and misalignment fading on performance of serial-relaying M-ary pulse-position modulation free-space optical systems with partially coherent Gaussian beam," *IET Communications*, vol. 8, no. 10, pp. 1762–1768, Jul. 2014.

[127] A. T. Pham and D. A. Luong, "Optical wireless communications over fading channels : spatial diversity or multihop relaying ?" in *Proceedings of International Conference on Advanced Technologies for Communications*, Hanoi, Vietnam, Oct. 15–17, 2014, pp. 760–765.

[128] C. Abou-Rjeily and A. Abdo, "Serial relaying over gamma-gamma MIMO FSO links : diversity order and aperture allocation," *IEEE Communications Letters*, vol. 19, no. 4, pp. 553–556, Apr. 2015.

[129] S. Anees and M. R. Bhatnagar, "Performance of an amplify-and-forward dual-hop asymmetric RF-FSO communication system," *IEEE/OSA Journal of Optical Communications and Networking*, vol. 7, no. 2, pp. 124–135, Feb. 2015.

[130] E. Zedini, I. S. Ansari, and M.-S. Alouini, "On the performance of hybrid line of sight RF and RF-FSO fixed gain dual-hop transmission systems," in *Proceedings of IEEE Global Communications Conference*, Austin, USA, Dec. 8–12, 2014, pp. 2119–2124.

[131] N. D. Chatzidiamantis, D. S. Michalopoulos, E. E. Kriezis, G. K. Karagiannidis, and R. Schober, "Relay selection protocols for relay-assisted free-space optical systems," *IEEE/OSA Journal of Optical Communications and Networking*, vol. 5, no. 1, pp. 92–103, Jan. 2013.

[132] H. Cui, M. Ma, L. Song, and B. Jiao, "Relay selection for two-way full duplex relay networks with amplify-and-forward protocol," *IEEE Transactions on Wireless Communications*, vol. 13, no. 7, pp. 3768–3777, Jul. 2014.

[133] M. Karimi and M. Nasiri-Kenari, "BER analysis of cooperative systems in free-space optical networks," *IEEE/OSA Journal of Lightwave Technology*, vol. 27, no. 24, pp. 5639–5647, Dec. 2009.

[134] C. Abou-Rjeily and S. Haddad, *Communications in Computer and Information Science*. Springer Berlin Heidelberg, 2011, ch. Novel cooperation strategies for free-space optical communication systems in the absence and presence of feedback.

[135] C. Abou-Rjeily, "Simple-DF versus selective-DF relaying over Rayleigh turbulence-induced FSO fading channels," in *Proceedings of International Symposium on Personal, Indoor and Mobile Radio Communications*, London, UK, Sep. 8–11, 2013, pp. 1082–1086.

[136] B. Zhu, J. Cheng, and L. Wu, "A distance-dependent free-space optical cooperative communication system," *IEEE Communications Letters*, vol. 19, no. 6, pp. 969–972, Jun. 2015.

[137] C. Abou-Rjeily and A. Slim, "Cooperative diversity for free-space optical communications : transceiver design and performance analysis," *IEEE Transactions on Communications*, vol. 59, no. 3, pp. 658–664, Mar. 2011.

[138] J.-Y. Wang, J.-B. Wang, M. Chen, Y. Tang, and Y. Zhang, "Outage analysis for relay-aided free-space optical communications over turbulence channels with nonzero boresight pointing errors," *IEEE Photonics Journal*, vol. 6, no. 4, Aug. 2014, doi :10.1109/JPHOT.2014.2332554.

[139] C. Castillo-Vazquez, R. Boluda-Ruiz, B. Castillo-Vazquez, and A. Garcia-Zambrana, "Outage performance of DF relay-assisted FSO communications using time-diversity," *IEEE Photonics Technology Letters*, vol. 27, no. 11, pp. 1149–1152, Jun. 2015.

[140] M. Karimi and M. Nasiri-Kenari, "Free space optical communications via optical amplify-and-forward relaying," *IEEE/OSA Journal of Lightwave Technology*, vol. 29, no. 2, pp. 242–248, Jan. 2011.

[141] J.-Y. Wang, J.-B. Wang, M. Chen, Q.-S. Hu, N. Huang, R. Guan, and L. Jia, "Free-space optical communications using all-optical relays over weak turbulence channels with pointing errors," in *Proceedings of International Conference on Wireless Communications and Signal Processing*, Hangzhou, China, Oct. 24–26, 2013, pp. 1–6.

[142] Z. Mostaani and M. Uysal, "Relay selection in FSO systems with all-optical relaying over Gamma-Gamma turbulence channels," in *Proceedings of IEEE Signal Processing and Communications Applications Conference*, Trabzon, Turkey, Apr. 23–25, 2014, pp. 710–713.

[143] M. R. Bhatnagar, "Average BER analysis of differential modulation in DF cooperative communication system over gamma-gamma fading FSO links," *IEEE Communications Letters*, vol. 16, no. 8, pp. 1228–1231, Aug. 2012.

[144] K. Prabu and D. S. Kumar, "Outage analysis of relay-assisted BPSK-SIM based FSO systems over strong atmospheric turbulence with pointing errors," *International Journal ofComputer and Communication Engineering*, vol. 3, no. 5, pp. 317–320, Sep. 2014.

[145] Y. Celik and N. Odabasioglu, "On relay selection for cooperative free-space optical communication," in *Proceedings of European Conference on Networks and Optical Communications*, Vilanova i la Geltru, Spain, Jun. 20–22, 2012, pp. 1–5.

[146] S. M. Aghajanzadeh and M. Uysal, "Outage performance and DMT analysis of DF parallel relaying in FSO IM/DD communications," in *Proceedings of IEEE Vehicular Technology Conference*, Quebec City, Canada, Sep. 3–6, 2012, pp. 1–5.

[147] Q. He and Z. Xu, "Opportunistic cooperation for FSO links aided by decode and forward relay," in *Proceedings of IEEE Workshop on Optical Wireless Communications*, Anaheim CA, USA, Dec. 3, 2012, pp. 1193–1197.

[148] C. Abou-Rjeily, "Performance analysis of selective relaying in cooperative free-space optical systems," *IEEE/OSA Journal of Lightwave Technology*, vol. 31, no. 18, pp. 2965–2973, Sep. 2013.

[149] M. R. Bhatnagar, "Average BER analysis of relay selection based decode-and-forward cooperative communication over gamma-gamma fading FSO links," in *Proceedings of International Conference on Communications*, Budapest, Hungary, Jun. 9–13, 2013, pp. 3142–3147.

[150] R. Boluda-Ruiz, A. Garcia-Zambrana, C. Castillo-Vazquez, and B. Castillo-Vazquez, "Adaptive selective relaying in cooperative free-space optical systems over atmospheric turbulence and misalignment fading channels," *Optics Express*, vol. 22, no. 13, pp. 16 629–16 644, Jun. 2014.

[151] B. T. Vu, T. C. Thang, and A. T. Pham, "Selection decode-and-forward cooperative FSO systems with adaptive rate strategy over gamma-gamma fading chan-

nels," in *Proceedings of IEEE Global Communications Conference*, Austin, TX, USA, Dec. 8–12, 2014, pp. 3585–3590.

[152] N. Sharma, A. Bansal, and P. Garg, "On the performance of selective transmission based DF FSO system with generalized $\mathcal{M}$-distributed turbulence," in *Proceedings of Annual IEEE India Conference*, Pune, India, Dec. 11–13, 2014, pp. 1–5.

[153] P. Wang, T. Cao, L. Guo, R. Wang, and Y. Yang, "Performance analysis of multi-hop parallel free-space optical systems over exponentiated Weibull fading channels," *IEEE Photonics Journal*, vol. 7, no. 1, Feb. 2015, doi : 10.1109/J-PHOT.2015.2396115.

[154] C. Abou-Rjeily and S. Haddad, "Cooperative FSO systems : performance analysis and optimal power allocation," *IEEE/OSA Journal of Lightwave Technology*, vol. 29, no. 7, pp. 1058–1065, Apr. 2011.

[155] X. Zhou, D. Zhang, Y. Yang, and M. S. Obaidat, "Network-coded multiple-source cooperation aided relaying for free-space optical transmission," *International Journal of Communication Systems*, vol. 25, no. 11, pp. 1465–1478, Nov. 2012.

[156] A. Garcia-Zambrana, C. Castillo-Vazquez, B. Castillo-Vazquez, and R. Boluda-Ruiz, "Bit detect and forward relaying for FSO links using equal gain combining over gamma-gamma atmospheric turbulence channels with pointing errors," *Optics Express*, vol. 20, no. 15, pp. 16 394–16 409, Jun. 2012.

[157] R. Boluda-Ruiz, A. Garcia-Zambrana, B. Castillo-Vazquez, and C. Castillo-Vazquez, "Impact of relay placement on diversity order in adaptive selective DF relay-assisted FSO communications," *Optics Express*, vol. 23, no. 3, pp. 2600–2617, Feb. 2015.

[158] M. A. Kashani and M. Uysal, "Outage performance and diversity gain analysis of free-space optical multi-hop parallel relaying," *IEEE/OSA Journal of Optical Communications and Networking*, vol. 5, no. 8, pp. 901–909, Aug. 2013.

[159] S. Zhalehpour and M. Uysal, "Outage performance analysis of mth best path selection protocol in FSO communications," in *Proceedings of International Conference on Transparent Optical Networks*, Graz, Austria, Jul. 6–10, 2014, pp. 1–4.

[160] V. Dubey, D. Chadha, and V. Chandra, "Bit error rate and reliability analysis of cooperative communication in free-space optical systems," *Photonic Network Communications*, vol. 28, no. 1, pp. 92–101, Aug. 2014.

[161] C. Abou-Rjeily, "All-active and selective FSO relaying : do we need inter-relay cooperation ?" *IEEE/OSA Journal of Lightwave Technology*, vol. 32, no. 10, pp. 1899–1906, May 2014, doi : 10.1109/JPHOT.2014.2332554.

[162] C. Abou-Rjeily and S. Haddad, "Inter-relay cooperation : a new paradigm for enhanced relay-assisted FSO communications," *IEEE Transactions on Communications*, vol. 62, no. 6, pp. 1970–1982, Jun. 2014.

[163] Y. Tang, X. Zhou, Z. Zhang, and Q. Tian, "Performance analysis of a two-way network-coded free space optical relay scheme over strong turbulence channels," in *Proceedings of IEEE Vehicular Technology Conference*, San Francisco, CA, Sep. 5–8, 2011, pp. 1–5.

[164] P. K. Sharma and P. Garg, "Bi-directional decode-XOR-forward relaying over $\mathcal{M}$-distributed free space optical links," *IEEE Photonics Technology Letters*, vol. 26, no. 19, pp. 1916–1919, Oct. 2014.

[165] P. Puri, P. Garg, and M. Aggarwal, "Analysis of spectrally efficient two-way relay assisted free space optical systems in atmospheric turbulence with path loss," *International Journal of Communication Systems*, May 2014, doi : 10.1002/dac.2801.

[166] P. K. Sharma, A. Bansal, and P. Garg, "Relay assisted bi-directional communication in generalized turbulence fading," *IEEE/OSA Journal of Lightwave Technology*, vol. 33, no. 1, pp. 133–139, Jan. 2015.

[167] P. Puri, P. Garg, M. Aggarwal, and P. K. Sharma, "Multiple user pair scheduling in TWR-FSO systems in presence of building sway," in *Proceedings of International Conference on Signal Processing and Communications*, Bangalore, India, Jul. 22–25, 2014, pp. 1–5.

[168] P. Puri, P. Garg, and M. Aggarwal, "Asymptotic analysis of TWR assisted FSO links with partial dual-relay selection," *IEEE Communications Letters*, vol. 19, no. 5, pp. 879–882, May 2015.

[169] "FSONA Provides Crédit Agricole With Innovative 10 Gigabit FSO Link," http://fsona.com/company.php?sec=pr_oct162013, May 2015.

[170] "FSONA Networks And Touch Team Up To Deliver 4G LTE Services To Mobile Customers In Lebanon," http://www.fsona.com/company.php?sec=pr_feb262013, May 2015.

[171] "Dispensing Dynamics," http://www.northernstormdirect.com/case-studies/dispensing-dynamics/, May 2015.

[172] J. Libich, M. Komanec, S. Zvanovec, P. Pesek, W. O. Popoola, and Z. Ghassemlooy, "Experimental verification of an all-optical dual-hop 10 Gbit/s free-space optics link under turbulence regimes," *Optics Letters*, vol. 40, no. 3, pp. 391–394, Feb. 2015.

[173] V. Tarokh, H. Jafarkhani, and A. R. Calderbank, "Space-time block codes from orthogonal designs," *IEEE Transactions on Information Theory*, vol. 45, no. 5, pp. 1456–1467, Jul. 1999.

[174] M. Abramowitz and I. A. Stegun, *Handbook of Mathematical Functions with Fomulas, Graphs, and Mathematical Tables*, 9th ed. New York, USA : Dover Publications, 1972.

[175] D. Bushuev and S. Arnon, "Analysis of the performance of a wireless optical multi-input to multi-output communication system," *Journal of the Optical Society of America A*, vol. 23, no. 7, pp. 1722–1730, Jul. 2006.

[176] R. Mesleh, H. Haas, S. Sinanović, C. W. Ahn, and S. Yun, "Spatial modulation," *IEEE Transactions on Vehicular Technology*, vol. 57, no. 4, pp. 2228–2241, Jul. 2008.

[177] I. S. Gradshteyn and I. M. Ryzhik, *Table of Integrals, Series, and Products*, A. Jeffrey and D. Zwillinger, Eds. New York, USA : Academic Press, 2007.

[178] W. O. Popoola and Z. Ghassemlooy, "BPSK subcarrier intensity modulated free-space optical communications in atmospheric turbulence," *IEEE/OSA Journal of Lightwave Technology*, vol. 27, no. 8, pp. 967–973, Apr. 2009.

[179] T. Fath and H. Haas, "Performance comparison of MIMO techniques for optical wireless communications in indoor environments," *IEEE Transactions on Communication*, vol. 61, no. 2, pp. 733–742, Feb. 2013.

[180] J. J. Shynk, *Probability, Random Variables, and Random Processes : Theory and Signal Processing Applications*. Somerset, NJ, USA : Wiley, 2012.

[181] M. D. Renzo and H. Haas, "Bit error probability of SM-MIMO over generalized fading channels," *IEEE Transactions on Vehicular Communications*, vol. 61, no. 3, pp. 1124–1144, Mar. 2012.

[182] M. Chiani, D. Dardari, and M. K. Simon, "New exponential bounds and approximations for the computation of error probability in fading channels," *IEEE Transactions on Wireless Communications*, vol. 2, no. 4, pp. 840–845, Jul. 2003.

[183] R. Carmona and V. Durrleman, "Pricing and hedging spread options," *SIAM Review*, vol. 45, no. 4, pp. 627–685, 2003.

[184] H. Nistazakis, V. Assimakopoulos, and G. Tombras, "Performance estimation of free space optical links over negative exponential atmospheric turbulence channels," *Optik*, vol. 122, no. 24, pp. 2191–2194, Dec. 2011.

[185] Q. Zhang, J. Cheng, and G. K. Karagiannidis, "Block error rate of optical wireless communication systems over atmospheric turbulence channels," *IET Communications*, vol. 8, no. 5, pp. 616–625, Mar. 2014.

[186] M. Elkashlan, Z. Ma, Y. Wang, M. Guizani, L. Shu, G. K. Karagiannidis, and T. Q. Duong, "Green media : the future of wireless multimedia networks," *IEEE Wireless Communications*, vol. 24, no. 4, pp. 10–12, Aug. 2014.

[187] N. D. Chatzidiamantis, D. S. Michalopoulos, E. E. Kriezis, G. K. Karagiannidis, and R. Schober, "Relay selection in relay-assisted free space optical systems," in *Proceedings of IEEE Global Communications Conference*, Houston, USA, Dec. 5–9, 2011, pp. 1–6.

[188] J. A. Anguita, M. A. Neifeld, and B. V. Vasic, "Spatial correlation and irradiance statistics in a multiple-beam terrestrial free-space optical communication link," *Applied Optics*, vol. 46, no. 26, pp. 6561–6571, Sep. 2007.

[189] E. Morgado, I. Mora-Jimenez, J. J. Vinagre, J. Ramos, and A. J. Caamano, "End-to-end average BER in multihop wireless networks over fading channels," *IEEE Transactions on Wireless Communications*, vol. 9, no. 8, pp. 2478–2487, Aug. 2010.

[190] T. Cao, P. Wang, L. Guo, B. Yang, J. Li, and Y. Yang, "Average bit error rate of multi-hop parallel decode-and-forward-based FSO cooperative system with the max-min criterion under the gamma-gamma distribution," *Chinese Optics Letters*, vol. 13, no. 8, Aug. 2015.

[191] M. Feng, J.-B. Wang, M. Sheng, L.-L. Cao, X.-X. Xie, and M. Chen, "Outage performance for parallel relay-assisted free-space optical communications in strong turbulence with pointing errors," in *Proceedings of International Conference on Wireless Communications and Signal Processing*, Nanjing, China, Nov. 9–11, 2011, pp. 1–5.

[192] T. Riihonen, S. Werner, and R. Wichman, "Rate-interference trade-off between duplex modes in decode-and-forward relaying," in *Proceedings of IEEE International Symposium on Personal, Indoor and Mobile Radio Communications*, Istanbul, Turkey, Sep. 26–29, 2010, pp. 690–695.

[193] Y. Zhao, R. Adve, and T. J. Lim, "Symbol error rate of selection amplify-and-forward relay systems," *IEEE Communications Letters*, vol. 10, no. 11, pp. 757–759, Nov. 2006.

[194] T. Fath and H. Haas, "Performance comparison of MIMO techniques for optical wireless communications in indoor environments," *IEEE Transactions on Communication*, vol. 61, no. 2, pp. 733–742, Feb. 2013.

[195] R. H. Y. Louie, Y. Li, and B. Vucetic, "Practical physical layer network coding for two-way relay channels : performance analysis and comparison," *IEEE Transactions on Wireless Communications*, vol. 9, no. 2, pp. 764–777, Feb. 2010.

[196] P. Concus, D. Cassatt, G. Jaehnig, and E. Melby, "Tables for the evaluation of $\int_0^\infty x^\beta e^{-x} f(x)dx$ by Gauss-Laguerre quadrature," *Mathematics of Computation*, vol. 17, no. 83, pp. 245–256, Oct. 1963.

[197] "Nodes and Weights of Gauss-Laguerre Calculator," http://keisan.casio.com/exec/system/1281279441, Jul. 2015.

[198] G. Soni and J. S. Malhotra, "Impact of beam divergence on the performance of free space optical system," *International Journal of Scientific Research Publication*, vol. 2, no. 2, pp. 1–5, Feb. 2012.

[199] A. Mansour, *Probabilités et statistiques pour les ingénieurs : cours, exercices et programmation.* Hermes Science, 2007.

[200] S. Haykin, *Digital Communications.* New York, USA : John Wiley & Sons, 1988.

[201] J. G. Proakis, *Digital Communications.* McGraw-Hill, 1983.

[202] A. P. Prudnikov, Y. A. Brychkov, and O. I. Marichev, *Integrals and Series, Volume 3: More special functions.* Gordon and Breach Science Publishers, 1990.

RESUME

Au cours de la dernière décennie, les communications optiques en espace libre (FSO) ont pris de l'ampleur dans les deux domaines académiques et industriels. L'importance de FSO s'appuie sur la possibilité de faire un système de transmission économique et écologique avec un débit élevé et sans licence à l'opposition des systèmes de transmission radiofréquences (RF). Dans la plupart des travaux antécédents sur les systèmes multi-émetteurs, seulement les canaux décorrélés ont été considérés. Un canal décorrélé nécessite un espace suffisant entre les émetteurs. Cette condition devient difficile et non-réalisable dans certaines applications. Pour cette raison, nos études se focalisent sur les performances des codes à répétition RC (Repitition Codes) et les codes OSTBC (Orthogonal Space-Time Block Codes) dans des canaux log-normaux corrélés en utilisant une modulation d'intensité et une détection directe (IM/DD). En addition, les effets des différentes conditions météorologiques sur le taux d'erreur moyen (ABER) sont étudiés. Les systèmes FSO à multi-entrées/ multi-sorties MIMO (Multiple-Input Multiple-Output) avec une modulation SSK (Space Shift Keying) ont été abordés. Les résultats obtenus montrent que la SSK est supérieure aux RC avec une modulation d'impulsion (Multiple Pulse Amplitude Modulation) pour toute efficacité spectrale égale ou supérieure à 4 bit/s/Hz. Nous avons aussi analysé les performances d'un système à sauts multiples (Multi-Hop) et des relais à transmission directe (forward relays). Nos simulations montrent que le système ainsi considéré est efficace pour atténuer les effets météorologiques et les pertes géométriques dans les systèmes de communication FSO. Nous avons montré qu'un tel système avec plusieurs entrées et une sortie (MISO, i.e. multiple-input single-output) à sauts multiples est supérieur à un système MISO avec un lien direct (direct link) avec une forte atténuation. Pour satisfaire la demande croissante des réseaux de communication à débits élevés, la communauté scientifique s'intéresse de plus en plus aux systèmes FSO avec des relais full-duplex (FD). Pour ces derniers systèmes, nous avons étudié la probabilité d'erreur moyenne (ABER) et nous avons analysé leurs performances. En considérant des différentes conditions de transmission, les performances de relais FD ont été comparées à celles d'un système avec un lien direct ou des relais half-duplex. Les résultats obtenus montrent que les relais FD ont le minimum ABER. En conséquence, les résultats obtenus dans cette thèse sont très prometteurs pour la prochaine génération de FSO.

ABSTRACT

Free-space optical (FSO) communication has been the subject of ongoing research activities and commercial attention in the past few years. Such attention is driven by the promise of high data rate, license-free operation, and cheap and ecological friendly means of communications alternative to congested radio frequency communications. In most previous work considering multiple transmitters, uncorrelated channel conditions have been considered. An uncorrelated channel requires sufficient spacing between transmitters. However, this can be difficult and may not be always feasible in some applications. Thereby, this thesis studies repetition codes (RCs) and orthogonal space-time block codes performance in correlated log-normal FSO channels using intensity modulation and direct detection (IM/DD). Furthermore, the effect of different weather conditions on the average bit error rate (ABER) performance of the FSO links is studied. Multiple-input multiple-output (MIMO) FSO communication systems using space shift keying (SSK) modulation have been also analyzed. Obtained results show that SSK is a potential technique for spectral efficiencies equal or greater than 4 bits/s/Hz as compared to RCs with multiple pulse amplitude modulations. The performance analysis of a multi-hop decode and forward relays for FSO communication system using IM/DD is also considered in this thesis. It is shown that multi-hop is an efficient technique to mitigate atmospheric turbulence and different weather attenuation effects and geometric losses in FSO communication systems. Our simulation results show that multiple-input single-output (MISO) multi-hop FSO systems are superior to direct link and MISO systems over links exhibiting high attenuation. Meeting the growing demand for higher data rates communication networks, a system with full-duplex (FD) relays is considered. For such a system, the outage probability and the ABER performance are analyzed under different turbulence conditions, misalignment error and path loss effects. FD relays are compared with the direct link and half-duplex relays. Obtained results show that FD relays have the lowest ABER and the outage probability as compared to the two other systems. Finally, the obtained results in this thesis are very promising towards the next generation of FSO systems.